5-14-2017

Bacterial polymertropism, the response to strain-induced alignment of polymers

David James Lemon
Syracuse University

ABSTRACT

In nature, bacteria often live in surface-associated communities known as biofilms. Biofilm-forming bacteria deposit a layer of polysaccharide on the surfaces they inhabit; hence, polysaccharide is their immediate environment on any surface. In this study, we examined how the physical characteristics of polysaccharide substrates influence the behavior of the biofilm-forming bacterium *Myxococcus xanthus*. *M. xanthus* colonies, and indeed those of the majority of biofilm-forming species tested, respond to the compression-induced deformation of polysaccharide substrates by preferentially spreading across the surface perpendicular to the axis of compression. This response is conserved across multiple distantly related phyla and is found in species with an array of distinct motility apparatuses. The birefringence and small angle X-ray scattering patterns of compressed polysaccharide substrates indicate that the directed surface movements of these bacteria consistently match the orientation of the long axes of aligned and tightly packed polysaccharide fibers in compressed substrates. Therefore, we refer to this behavior as polymertropism to denote that the directed movements are a response to the physical arrangement of the change in packing and alignment of the polymers in the substrate. In addition to altering the colony morphology we find the behavior of groups of cells, called flares, is also affected in several species resulting in increased flare speed, duration, and displacement on compressed gel substrates. We suggest that polymertropism, which requires a downward-facing motility apparatus in *M. xanthus*, may be responsible for the observed tendency of bacterial cells to follow trails of extruded and presumably aligned polysaccharides, which their neighbors secrete and deposit on the substrate as they move across it. Polymertropism may also play a role in the organization of bacteria in a biofilm, as the iterative process of polysaccharide trail deposition and following is proposed to yield aggregates of cells.

Bacterial polymertropism, the response to strain-induced alignment of polymers

by

David J. Lemon

Dissertation
Submitted in partial fulfillment of the requirements for the degree of
Doctor of Philosophy in Biology

Syracuse University
June 2017

TABLE OF CONTENTS

LIST OF FIGURES

LIST OF TABLES

Chapter 1- *Myxococcus xanthus* background and review

1.1 Multicellular life cycle of *M. xanthus*

Myxococcus xanthus, the gram-negative soil bacterium, lives a complex and varied lifestyle belied by its slow growth and long generational time of 200 to 250 minutes[1]. The individual cells which make up the *M. xanthus* colony, aptly described as a wolf pack[2] because of the group motion of its component cells, are motile on both hard and semi-solid materials[3] and are bathed in an exopolysaccharide (EPS) matrix secreted from nozzles embedded in the cell surface[4,5]. This EPS or "slime" helps to adhere the cells to their neighbors[6] as well as to their substrate, and these communities of microorganisms attached to their surface are known as biofilms[7].

M. xanthus biofilms, when experiencing environments with low or depleted nutrient content[8], undergo cooperative development[9] (for review see[10]). During development[11] cells dispersed throughout the biofilm begin to aggregate toward common centers in mounds[1,12], eventually forming large, three-dimensional structures known as fruiting bodies[13,14] which contain round, differentiated[15,16] spores morphologically distinct[11,17] from the rod-shaped, cylindrical cells typical of *M. xanthus*.

These fruiting bodies eventually become swollen with so many individual cells they become opaque and visible to the naked eye (≥ 1 mm) as more and more cells continue to move into the fruiting bodies[18]. During this process fruiting body sizes and positions are unstable, initially a large number of small fruiting bodies or aggregates is present, but as cells flow out of smaller fruiting bodies and into nearby larger ones, eventually the landscape

becomes dominated by a smaller number of bigger fruiting bodies, similar to the physical process of coarsening[19]. Stress resistant myxospores contained within these fruiting bodies can germinate to restart this process when they encounter more favorable conditions, thus protecting the swarm's future from temporary nutrient depletion.

1.2 Motility

Without the ability to move across the surface of their substrate, *M. xanthus* cells would be incapable of the complex collective behaviors described above. *M. xanthus* employs two distinct types of movement with separate motility mechanisms[20]. The first, and more historically understood of these two motility systems is Social (S) motility[21].

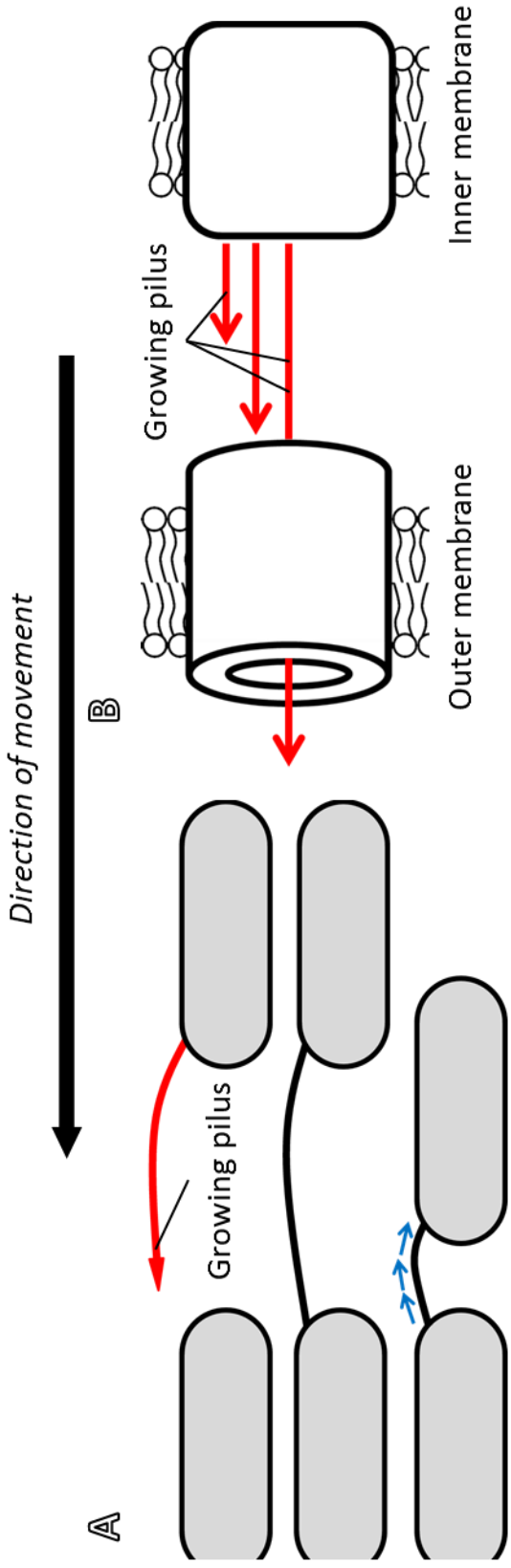

Figure 1.1. Type IV pili model of *M. xanthus* Social motility. Growing type IV pili (TFP, red arrows) emerge from the front of the cell (grey), attach to the a cell in front of them (black line), and are retracted, pulling the cell forward (blue arrows) shown in A. The growing TFP extends out through a nozzle in the outer membrane (cylinder, B) from an assembly of proteins on the inner membrane (rectangle, B).

1.2.1 Social motility

S motility is driven by the extension and retraction of type-IV pili (T4P)[22-25]. The pilus is extended from the leading end of the cell until it encounters and binds to another cell ahead, when the pilus is then retracted the following cell is pulled forward toward the leading cell[26] as shown in Figure 1.1. This method requires multiple cells to function, hence the name Social motility; solitary cells cannot move by this process effectively.

The T4P is assembled at a complex of several proteins anchored in *M. xanthus*' inner membrane[27] (IM), and extends through a nozzle or pore in the outer membrane (OM) just above the IM complex [28]. Continuous addition of subunits at the base of the growing pilus cause the entire fibril to extend away from the leading pole of the cell until it encounters another cell, at which point reversal of this process draws the pilus-producing cell toward the cell in front of it. This process is fairly well conserved[26] across bacterial phylogeny and in *M. xanthus* dominates on softer, wetter substrates[3]. In other species this process is often referred to as "twitching" motility [29,30], and has been associated with virulence or pathogenesis in both mammalian[31,32] and plant[33] hosts.

1.2.2 Adventurous motility

M. xanthus also uses Adventurous (A) motility to move across surfaces and A motility typically dominates on stiffer, drier substrates [3]. Differing from S motility, A motility does not require multiple cells to function, but rather is most prominently observed in individual cells moving in advance of groups, hence the name Adventurous. While the exact molecular mechanism which powers A motility in *M. xanthus* is still the subject of some debate, there are

three models: slime secretion[34], helical tracks[35], and focal adhesions, of which the focal adhesion model is the best supported by experimental observations[36].

The slime secretion or "slime gun" model of propulsion asserts that EPS of slime is being secreted from the lagging pole of the cell, which encounters water in the environment once it exits the slime secreting nozzle which causes the slime to swell, pushing the cell forward[34]. Experimental and model-

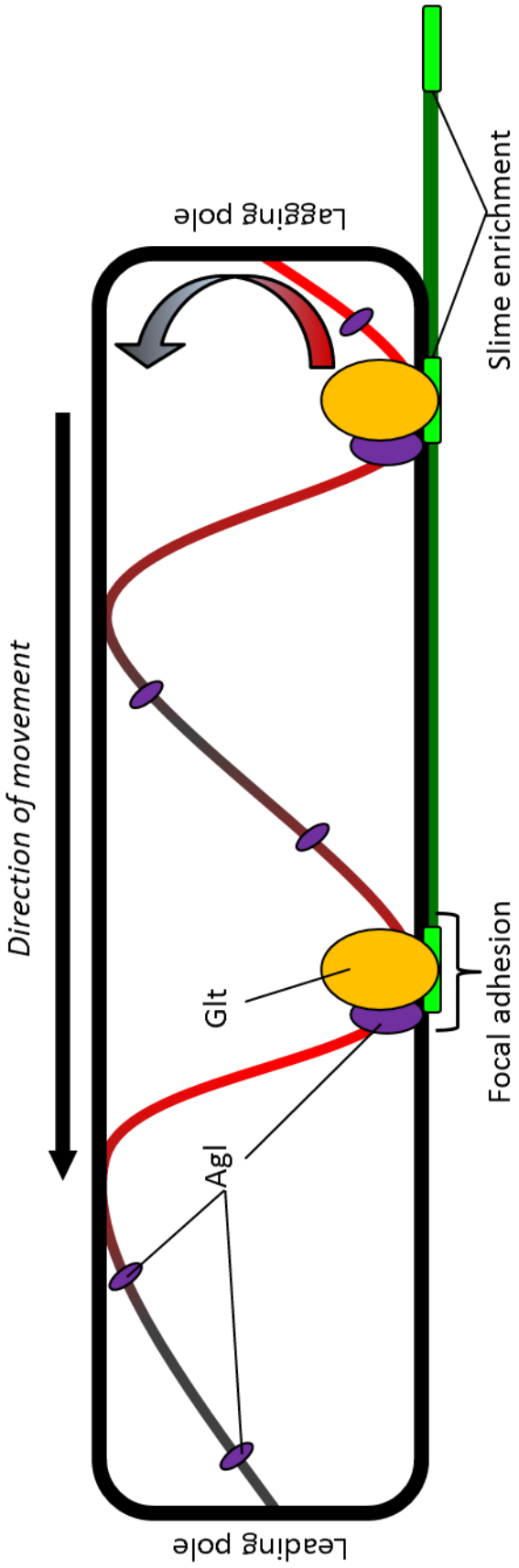

Figure 1.2. Focal adhesion model of *M. xanthus* Adventurous motility. Cells rotate about their longitudinal axis, spinning their cytoskeleton (red (foreground) and grey (background)). Adventurous gliding proteins (Agl, purple) bound to the cytoskeleton recruit Gliding transducer proteins (Glt, orange) to assemble a focal adhesion. Focal adhesions assemble at the leading pole and remain fixed relative to the substrate, driving the cell forward as the cell and cytoskeleton continue to rotate, until the focal adhesions reach the lagging pole where they disassociate. Slime trails (dark green) and slime enrichments (bright green) associated with focal adhesion complexes persist after the cell moves away.

based evidence show that when a flexible, cylindrical *M. xanthus* cell is anchored at its leading pole it appears to wriggle or flail, intimating that there is some engine at the very rear of the cell which directs its impulse through the longitudinal axis of the cell[37]. While the *M. xanthus* cell does have many slime secretion nozzles on its surface, and a large proportion of these nozzles are clustered at the ends of the cell[38] where they would be expected if they are used to propel the cell forward, they may serve another purpose than powering cell motility. That slime production is required for A motility[5,39] does not necessarily imply that slime production is itself the motor. Notably this model of motility, as is also true for S motility, does not contain or require a downward-facing motor or any direct interaction with the substrate to produce forward motion. Slime may simply be required for adhering the cell to its substrate[40], rather than itself directly propelling the cell.

A second model in which that bacteria spin around their long axis and propel themselves forward by applying drag between the cell and the substrate as cargoes on a helical cytoskeleton track are propelled toward the rear of the cell has also been proposed[35]. The helical tracks model proposes that there is a helical cytoskeleton[41] which runs around the inside of the IM and that the motor is trafficked around on this corkscrew-shaped skeleton as it rotates along with the cell[42]. This motor must pass through the peptidoglycan layer and cause a protrusion in the OM, which encounters the substrate, generating drag while the cytoskeleton continues to rotate and forces them backward, producing forward thrust[35]. This model does require a downward-facing motor and direct interaction with the substrate unlike in the slime secretion model, but the precise nature of the interaction between the cell and substrate is not well understood or explained by this model.

The third and most comprehensive model of A motility, shown in Fig. 1.2, incorporates aspects of the previous two and couples them with the addition of a focal adhesion complex which interacts directly with the cell's substrate[36,43]. The focal adhesion complex, which includes components on both the IM and OM, spans the gap between the two membranes, as well as attaches to the cytoskeletal framework of the cell[44]. This complex includes 17 different proteins, three which form the AglRQS motor which drives the complex toward the lagging pole propelling the cell forward, the 5 protein Glt core, 6 additional Glt proteins, AglZ which links the IM complex to the cytoskeletal framework, and the framework itself[44]. By combining the longitudinal rotation and helical cytoskeleton of the helical track model with the necessity of slime secretion and a recently characterized focal adhesion complex (FAC)[44,45], the focal adhesion model incorporates the best of the other two models. The FAC faces downward and, along with secreted slime, interfaces directly with the substrate, anchoring the cytoskeleton to the environment through the FAC[46,47]. As the cell rotates along its longitudinal axis[42], the FAC remains in fixed position relative to the substrate, propelling the cell forward[44]. This is presently the most complete and evidence-based model for A motility, and will be referred to throughout the remainder of this text.

1.3 Other complex, multicellular behaviors

M. xanthus exhibits other multicellular behaviors beyond development or fruiting body formation which also require motility. In addition to utilizing nutrients it is provided with in the lab setting *M. xanthus* is also able to prey upon other bacterial cells[2,48]. During predation large numbers of *M. xanthus* cells sometimes move back and forth over the same region in travelling

waves[49-51]. This rippling has also been observed in situations which do not involve predator-prey interactions [52], and these waves appear to pass through each other[53]. *M. xanthus*[40,54], among other species[55,56], has been shown to re-orient in response to and follow trails of secreted exopolysaccharide (slime-trails) laid down by cells which have previously moved across the same surface[57]. Finally, *M. xanthus*[14,58,59], as well as a small group of other species[60,61], has been shown to be responsive to changes in the physical state of its environment, a property that has been historically, and we now know erroneously, called "elasticotaxis"[14].

1.3.1 Predation

Because of its tendency toward swarming to and surrounding prey bacteria in groups of cells also called flares, *M. xanthus'* hunting behavior has been referred to as a wolfpack[2]. This unusual predation pattern requires close proximity to the prey cells, where degradative enzymes secreted from the predator's cells cause the prey's to lyse without requiring engulfment (phagocytosis) or invasion of the prey cell. The nature of these secreted killer-enzymes may make them appealing for study as novel antibiotics, but these enzymes alone are not enough for *M. xanthus* to prey on cells effectively; A motility is also required for this behavior[62]. Predator-prey interactions also affect fruiting body formations, as fruiting bodies are often observed in the regions immediately outside the footprint of a prey colony[48], indicating that the step down in nutrients from the prey colony to minimal media is likely an input into initiating fruiting body development[8].

1.3.2 Rippling

Another complex, possibly emergent behavior observed in *M. xanthus* biofilms or swarms, is the appearance of oscillating waves of cells called ripples[52]. Ripples are often observed between aggregates or fruiting bodies during fruiting body development[52] and during predation[50], both times when cells are actively moving in large numbers alongside others moving in a similar direction. Rippling waves of cells appear to move radially outward from the point of contact between an advancing *M. xanthus* swarm and a larger prey colony[51], as well as between fruiting bodies with sizes and positions still in flux[52]. Interestingly, these waves appear to pass easily through one another[49], which gives the appearance that each given wave is oscillating between its two neighbors.

1.3.3 Slime trail following

Smaller numbers of cells also exhibit interesting behavior. *M. xanthus* cells, as previously discussed, secrete EPS or slime as they move[34,38]. When cells in front of a swarm are moving on a naïve substrate, they deposit phase-bright slime trails which induce later cells that encounter them to re-orient and follow the same trajectory[5] as shown in Figure 1.3. While the production of slime is of clear importance to the motility of *M. xanthus*[37,40], several other species have also been observed depositing and following slime trails of their own[55,56]. Slime trail following may play an even larger role in pattern-formation and the genesis of other complex behaviors in *M. xanthus*, as model-based studies predict that slime trail following alone is sufficient for aggregation and fruiting body formation[57]. Though slime trails are thought to be of importance to a number of species[5,54,56], there has been considerable difficulty

in identifying or isolating which, if any, biological signal inherent in the slime is capable of altering the behavior of later cells that follow slime trails.

1.3.4 Elasticotaxis

Also observed in, but not unique to *M. xanthus*, is the response to substrate deformation known as elasticotaxis[14]. Initially recognized as a change in the distribution of fruiting bodies[14] elasticotaxis was thought to be a response to stress within the agar gel substrate it is typically cultured on. Later this response was thought to be utilized by *M. xanthus* during predation[59]. Eventually other species[60,61] were found to respond similarly to *M. xanthus*; they formed colonies which were elongated perpendicular to compression, rather than the more common circular

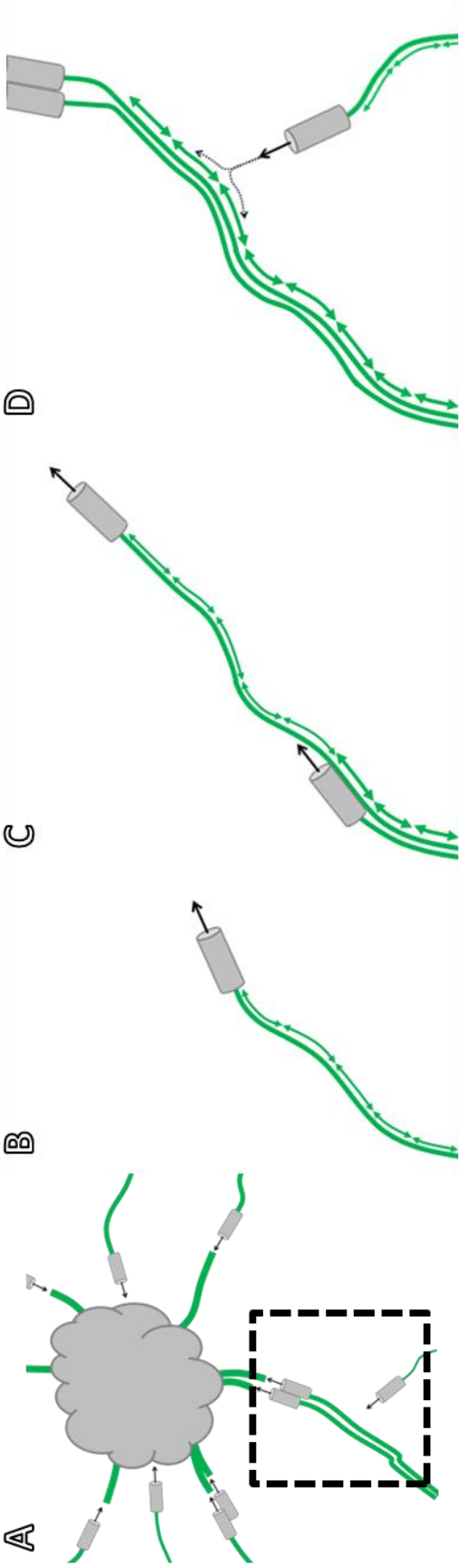

Figure 1.3. Slime trail following. Cells (grey cylinders) approaching a developing fruiting body (grey cloud) shown in A. Cells extrude exopolysaccharide, called slime (green), as they move over the surface, forming trails. Other cells which encounter these trails follow along them, reinforcing this effect in a positive feedback over time (B-D).

colonies found on uncompressed or unstressed substrates[58]. However, not unlike the case of slime trail following, while several distantly related species have been observed to respond to deformation or compression of their substrate, the precise nature of the stimulus which induces these responses remains elusive.

The characterization of the response to substrate compression and the identification of the stimuli causing this response are the focus of this work. Portions of this work have been or will be submitted for publication. Chapters 3 and 4 and parts of Chapter 5 have been submitted as "Polymertropism of rod-shaped bacteria: movement along aligned polysaccharide fibers" by David J. Lemon, Xingbo Yang, Pragya Srivastava, Yan-Yeung Luk, & Anthony G. Garza. Parts of Chapters 5 and 6 will be submitted as a manuscript by David J. Lemon, Derek A. Schutzman, & Anthony G. Garza.

1.4 References

1 Wireman, J. W. & Dworkin, M. Morphogenesis and developmental interactions in Myxobacteria. *Science* **189**, 516 - 523 (1975).

2 Berleman, J. E. & Kirby, J. R. Deciphering the hunting strategy of a bacterial wolfpack. *FEMS microbiology reviews* **33**, 942-957, doi:10.1111/j.1574-6976.2009.00185.x (2009).

3 Shi, W. & Zusman, D. R. The two motility systems of *Myxococcus xanthus* show different selective advantages on various surfaces. *PNAS* **90**, 3378 - 3382 (1993).

4 White, D., Dworkin, M. & Tipper, D. J. Peptidoglycan of *Myxococcus xanthus*: Structure and Relation to Morphogenesis. *J Bacteriol* **95**, 2186 - 2197 (1968).

5 Yu, R. & Kaiser, D. Gliding motility and polarized slime secretion. *Molecular microbiology* **63**, 454-467, doi:10.1111/j.1365-2958.2006.05536.x (2007).

6 Shimkets, L. J. Correlation of Energy-Dependent Cell Cohesion with Social Motility in *Myxococcus xanthus*. *Journal of Bacteriology* **166**, 837 - 841 (1986).

7 O'Toole, G. A., Kaplan, H. B. & Kolter, R. Biofilm Formation as Microbial Development. *Annu. Rev. Microbiol.* **54**, 49 - 97 (2000).

8 Dworkin, M. Nutritional Regulation of Morphogenesis in *Myxococcus xanthus*. *J Bacteriol* **86**, 67 - 72 (1963).

9 Rosenberg, E., Keller, K. H. & Dworkin, M. Cell Density-Dependent Growth of *Myxococcus xanthus* on Casein. *Journal of Bacteriology* **129**, 770 - 777 (1977).

10 Kaiser, D., Robinson, M. & Kroos, L. Myxobacteria, polarity, and multicellular morphogenesis. *Cold Spring Harbor perspectives in biology* **2**, a000380, doi:10.1101/cshperspect.a000380 (2010).

11 Wireman, J. W. Developmental induction of *Myxococcus xanthus* myxospores. *J Bacteriol* **140**, 147 - 153 (1979).

12 Starruss, J. *et al.* Pattern-formation mechanisms in motility mutants of *Myxococcus xanthus*. *Interface Focus* **2**, 774-785, doi:10.1098/rsfs.2012.0034 (2012).

13 Zhang, Y., Ducret, A., Shaevitz, J. & Mignot, T. From individual cell motility to collective behaviors: insights from a prokaryote, *Myxococcus xanthus*. *FEMS microbiology reviews* **36**, 149-164, doi:10.1111/j.1574-6976.2011.00307.x (2012).

14 Stanier, R. Y. A Note on Elasticotaxis in Myxobacteria. *J Bacteriol* **44**, 405 - 412 (1942).

15 Smith, B. A. & Dworkin, M. Adenylate Energy Charge During Fruiting Body Formation by *Myxococcus xanthus*. *Journal of Bacteriology* **142**, 1007 - 1009 (1980).

16 Licking, E., Gorski, L. & Kaiser, D. A common step for changing cell shape in fruiting body and starvation-independent sporulation of *Myxococcus xanthus*. *J Bacteriol* **182**, 3553 - 3558 (2000).

17 Voelz, H. & Dworkin, M. Fine Structure of *Myxococcus xanthus* During Morphogenesis. *J Bacteriol* **84**, 943 - 952 (1962).

18 Sozinova, O., Jiang, Y., Kaiser, D. & Alber, M. A three-dimensional model of myxobacterial fruiting-body formation. *Proceedings of the National Academy of Sciences of the United States of America* **103**, 17255-17259, doi:10.1073/pnas.0605555103 (2006).

19 Bahar, F., Pratt-Szeliga, P. C., Angus, S., Guo, J. & Welch, R. D. Describing *Myxococcus xanthus* aggregation using Ostwald ripening equations for thin liquid films. *Sci Rep* **4**, 6376, doi:10.1038/srep06376 (2014).

20 Mauriello, E. M., Mignot, T., Yang, Z. & Zusman, D. R. Gliding motility revisited: how do the myxobacteria move without flagella? *Microbiology and molecular biology reviews : MMBR* **74**, 229-249, doi:10.1128/MMBR.00043-09 (2010).

21 Dworkin, M. Fibrils as extracellular appendages of bacteria: their role in contact-mediated cell-cell interactions in *Myxococcus xanthus*. *BioEssays* **21**, 590 - 595 (1999).

22 Bischof, L. F., Friedrich, C., Harms, A., Sogaard-Andersen, L. & van der Does, C. The Tipe IV Pilus Assembly ATPase PilB of *Myxococcus xanthus* Interacts with the Inner

Membrane Platform Protein PilC and the Nucleotide-binding Protein PilM. *Journal of Biololgical Chemistry* **291**, 6946 - 6957 (2016).

23 Friedrich, C., Bulyha, I. & Sogaard-Andersen, L. Outside-In Assembly Pathway of the Type IV Pilus System in *Myxococcus xanthus*. *Journal of Bacteriology* **196**, 378 - 390 (2014).

24 Sun, H., Zusman, D. R. & Shi, W. Type IV pilus of *Myxococcus xanthus* is a motility apparatus controlled by the frz chemosensory system. *Curr Biol* **10**, 1143 - 1146 (2000).

25 Kaiser, D. Social gliding is correlated with the presence of pili in *Myxococcus xanthus*. *PNAS* **76**, 5952 - 5256 (1979).

26 Clausen, M., Jakovljevic, V., Sogaard-Andersen, L. & Maier, B. High-force generation is a conserved property of type IV pilus systems. *J Bacteriol* **191**, 4633-4638, doi:10.1128/JB.00396-09 (2009).

27 Sogaard-Andersen, L. Directional intracellular trafficking in bacteria. *Proceedings of the National Academy of Sciences of the United States of America* **108**, 7283-7284, doi:10.1073/pnas.1104616108 (2011).

28 Siewering, K. *et al.* Peptidoglycan-binding protein TsaP functions in surface assembly of type IV pili. *PNAS* **111**, E953 - E961 (2014).

29 Burrows, L. L. Weapons of mass retraction. *Molecular microbiology* **57**, 878 - 888 (2005).

30 Darzins, A. & Russel, M. A. Molecular genetic analysis of type-4 pilus biogenesis and twitching motility using *Pseudomonas aeruginosa* as a model system - a review. *Gene* **192**, 109 - 115 (1997).

31 Leighton, T. L., Buensuceso, R. N. C., Howell, P. L. & Burrows, L. L. Biogenesis of *Pseudomonas aeruginosa* type IV pili and regulation of their function. *Environmental Microbiology* **17**, 4148 - 4163 (2015).

32 Hager, A. J. *et al.* Type IV pili-mediated secretion modulates *Francisella* virulence. *Molecular microbiology* **62**, 227 - 237 (2006).

33 Burdman, S., Bahar, O., Parker, J. K. & De la Fuente, L. Involvement of Type IV Pili in Pathogenicity of Plant Pathogenic Bacteria. *Genes* **2**, 706 - 735 (2011).

34 Kaiser, D. Are there lateral as well as polar engines for A-motile gliding in myxobacteria? *J Bacteriol* **191**, 5336-5341, doi:10.1128/JB.00486-09 (2009).

35 Nan, B., McBride, M. J., Chen, J., Zusman, D. R. & Oster, G. Bacteria that glide with helical tracks. *Curr Biol* **24**, R169-173, doi:10.1016/j.cub.2013.12.034 (2014).

36 Mignot, T., Shaevitz, J. W., Hartzell, P. L. & Zusman, D. R. Evidence that focal adhesion complexes power bacterial gliding motility. *Science* **315**, 853-856, doi:10.1126/science.1137223 (2007).

37 Wolgemuth, C. W. Force and flexibility of flailing myxobacteria. *Biophys J* **89**, 945-950, doi:10.1529/biophysj.105.062513 (2005).

38 Wolgemuth, C. W., Hoicyk, E., Kaiser, D. & Oster, G. How myxobacteria glide. *Curr Biol* **12**, 369 - 377 (2002).

39 Dworkin, M., Keller, K. H. & Weisberg, D. Experimental Observations Consistent with a Surface Tension Model of Gliding Motility of *Myxococcus xanthus*. *J Bacteriol* **155**, 1367 - 1371 (1983).

40 Ducret, A., Valignant, M.-P., Mouhamar, F., Mignot, T. & Theodoly, O. Wet-surface-enhanced ellipsometric contrast microscopy identifies slime as a major adhesion factor during bacterial surface motility. *PNAS* **199** (2012).

41 Cabeen, M. T. & Jacobs-Wagner, C. The bacterial cytoskeleton. *Annual review of genetics* **44**, 365-392, doi:10.1146/annurev-genet-102108-134845 (2010).

42 Nan, B. *et al.* Myxobacteria gliding motility requires cytoskeleton rotation powered by proton motive force. *Proceedings of the National Academy of Sciences*, doi:10.1073/pnas.1018556108 (2011).

43 Balagam, R. *et al. Myxococcus xanthus* Gliding Motors Are Elastically Coupled to the Substrate as Predicted by the Focal Adhesion Model of Gliding Motility. *PLoS computational biology* **10** (2014).

44 Islam, S. T. & Mignot, T. The mysterious nature of bacterial surface (gliding) motility: A focal adhesion-based mechanism in *Myxococcus xanthus*. *Semin Cell Dev Biol* **46**, 143-154, doi:10.1016/j.semcdb.2015.10.033 (2015).

45 Faure, L. *et al.* The mechanism of force transmission at bacterial focal adhesion complexes. *Nature* **539**, 530 - 535 (2016).

46 Treuner-Lange, A. *et al.* The small G-protein MglA connects to the MreB actin cytoskeleton at bacterial focal adhesions. *J Cell Biol* **210**, 246 - 256 (2015).

47 Wartel, M. *et al.* A Versatile Class of Cell Surface Directional Motors Gives Rise to Gliding Motility and Sporulation in *Myxococcus xanthus*. *PLoS Biol* **11** (2013).

48 Berleman, J. E. & Kirby, J. R. Multicellular development in *Myxococcus xanthus* is stimulated by predator-prey interactions. *J Bacteriol* **189**, 5675-5682, doi:10.1128/JB.00544-07 (2007).

49 Berleman, J. E., Scott, J., Chumley, T. & Kirby, J. R. Predataxis behavior in *Myxococcus xanthus*. *Proceedings of the National Academy of Sciences of the United States of America* **105**, 17127-17132, doi:10.1073/pnas.0804387105 (2008).

50 Zhang, H. *et al.* The mechanistic basis of *Myxococcus xanthus* rippling behavior and its physiological role during predation. *PLoS computational biology* **8**, e1002715, doi:10.1371/journal.pcbi.1002715 (2012).

51 Berleman, J. E., Chumley, T., Cheung, P. & Kirby, J. R. Rippling is a predatory behavior in *Myxococcus xanthus*. *J Bacteriol* **188**, 5888-5895, doi:10.1128/JB.00559-06 (2006).

52 Shimkets, L. J. & Kaiser, D. Induction of coordinated movement of *Myxococcus xanthus* cells. *J Bacteriol* **152**, 451 - 461 (1982).

53 Sliusarenko, O., Neu, J., Zusman, D. R. & Oster, G. Accordion waves in *Myxococcus xanthus*. *Proceedings of the National Academy of Sciences of the United States of America* **103**, 1534-1539, doi:10.1073/pnas.0507720103 (2006).

54 Burchard, R. P. Trail following by gliding bacteria. *J Bacteriol* **152**, 495 - 501 (1982).

55 Kranz, W. T., Gelimson, A., Zhao, K., Wong, G. C. & Golestanian, R. Effective Dynamics of Microorganisms That Interact with Their Own Trail. *Phys Rev Lett* **117**, 038101, doi:10.1103/PhysRevLett.117.038101 (2016).

56 Zhao, K. *et al.* Psl trails guide exploration and microcolony formation in *Pseudomonas aeruginosa* biofilms. *Nature* **497**, 388-391, doi:10.1038/nature12155 (2013).

57 Balagam, R. & Igoshin, O. A. Mechanism for Collective Cell Alignment in *Myxococcus xanthus* Bacteria. *PLoS computational biology* **11**, e1004474, doi:10.1371/journal.pcbi.1004474 (2015).

58 Fontes, M. & Kaiser, D. Myxococcus cells respond to elastic forces in their substrate. *Proceedings of the National Academy of Sciences of the United States of America* **96**, 8052 - 8057 (1999).

59 Dworkin, M. Tactic behavior of *Myxococcus xanthus*. *J Bacteriol* **154**, 452 - 459 (1983).

60 Stratford, J. P., Woodley, M. A. & Park, S. Variation in the morphology of *Bacillus mycoides* due to applied force and substrate structure. *PloS one* **8**, e81549, doi:10.1371/journal.pone.0081549 (2013).

61 Polka, J. K. & Silver, P. A. Induced sensitivity of *Bacillus subtilis* colony morphology to mechanical media compression. *PeerJ* **2**, e597, doi:10.7717/peerj.597 (2014).

62 Pham, V. D., Shebelut, C. W., Diodati, M. E., Bull, C. T. & Singer, M. Mutations affecting predation ability of the soil bacterium *Myxococcus xanthus*. *Microbiology* **151**, 1865-1874, doi:10.1099/mic.0.27824-0 (2005).

Chapter 2 - History and context of elasticotaxis

A change in behavior in response to substrate compression or tension was first reported by R.Y. Stanier in 1942[1]. M. Dworkin expanded upon this observation in 1983 and posited that *Myxococcus xanthus* was able to leverage this response to stress on the substrate by tracking and swarming toward small groups of prey cells[2]. The first quantitative measure of the bacterial response to substrate compression came in 1999 when the Kaiser lab measured the aspect ratio, which they referred to as the "elasticotaxis coefficient", of elongated colonies on compressed substrates[3]. M. Fontes & D. Kaiser also characterized the response of single *M. xanthus* cells to compression of their substrate, noted that groups of cells emerging from the colony edge, called flares, also appeared to respond to substrate compression, and that *M. xanthus* was not unique in its response to compression[3]. J.P. Stratford, M.A. Woodley, and S. Park expanded the number of species responsive to substrate compression in 2013 when they characterized *Bacillus mycoides*' response to substrate manipulation[4], and another *Bacillus* species, *B. subtilis*, was added to this list by the Silver group in 2014[5].

2.1 Stanier 1942

The first observations which lead to our current understanding of the bacterial response to substrate compression was that fruiting bodies which formed around an indented inoculum on an agar plate appeared to be in concentric circles with said inoculum at their center[1]. To test the hypothesis that there was some physical change in the agar medium that the biofilm was sensing and responding to Stanier abutted two pieces of agar media directly up against each other so that one common biofilm could swarm across both. One of these pieces was

under stress, either tension or compression, while the other was not. After incubation the fruiting bodies on the unstressed gel appeared to be randomly distributed like those in Fig. 2.1 A, while the fruiting bodies on the stressed agar gel were aligned in roughly parallel lines like those in Figure 2.1 B.

To determine the difference, if any, between responses to tension and compression Stanier draped a rectangular slab of agar media over a glass rod and added a drop of *Myxococcus* cells at the top of the resulting peak. By again monitoring the distribution of fruiting bodies, which formed an "H" shape, a line across the peak and perpendicular lines at the base of the peak, Stanier concluded that fruiting bodies aligned parallel to tension and perpendicular to compression. To refer to this response to the compressive or tensile stress within the media he coined the term "elasticotaxis", though it does not meet the requirements of a true -taxis, namely a biological feedback loop, response to a gradient, and a capacity for desensitization to a constant degree of stimulation, it does capture the spirit of a biological response to the physical stimuli which results from substrate compression[1].

2.2 Dworkin 1983

The first suggested use for this response to substrate compression was put forth by Dworkin in 1983 when he suggested that *M. xanthus* was able to use the response to hunt small groups of prey cells without the need for a biochemical gradient, only a physical one[2]. To test this, small groups of prey cells were deposited tens of μm away from *M. xanthus* flares, then the *M. xanthus* flares were monitored via time-lapse microscopy for a perceived turn toward, movement to, and lingering at the location of the prey cells. To confirm that this was in fact

due to a physical signal, rather than some biochemical gradient he repeated the experiment with well-rinsed polystyrene and glass beads, and observed that again the *M. xanthus* flares moved toward and found these targets as well. For good measure, he then attempted to prove that the predator was finding the prey at a rate greater than what might be attributed to random chance alone by tracing the edge of a *M. xanthus* colony onto graph paper, picking random coordinates, and checking if this was within the perimeter of the colony or not[2]. While by this method it did appear that *M. xanthus* was tracking down targets with accuracy due only to the physical disruption of the agar substrate, these experiments were largely qualitative and subsequent contact mechanics calculation by Xingbo Yang, a collaborator in the Marchetti lab at Syracuse University reveals the depression caused by the weight of a few non-motile cells would have been vanishingly small. While it may be the case that an actively moving target may perturb the agar gel enough to present as a target to be found through this response, the weight alone of the provided targets is so negligible as to be unlikely to cause any response.

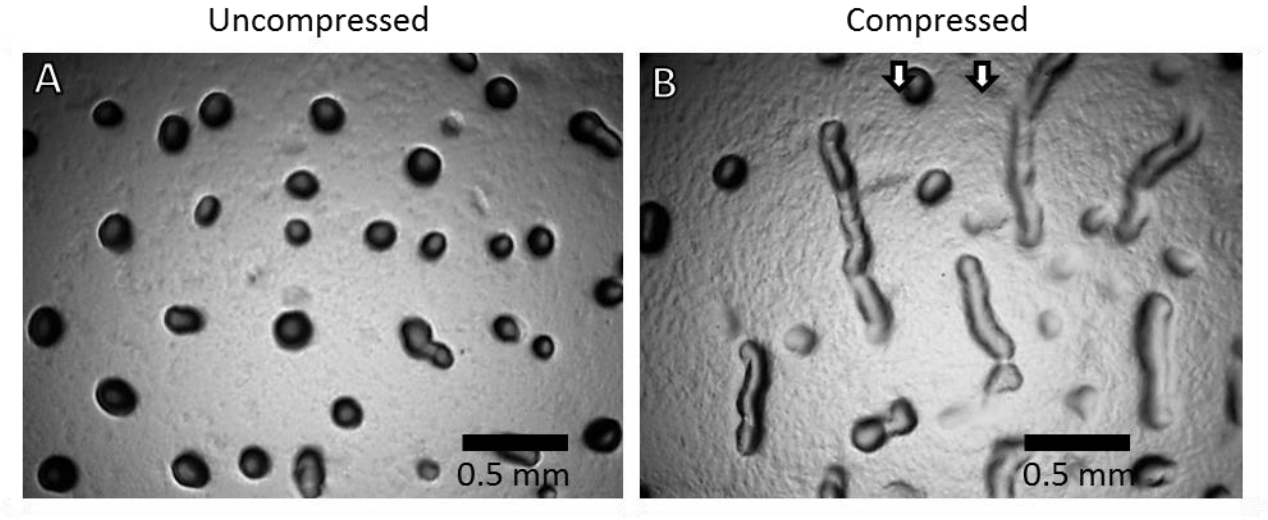

Figure 2.1. Fruiting body alignment. *M. xanthus* fruiting bodies on uncompressed (A) and compressed (B) 1.5% agar nutrient-poor media. White arrows in B represent the orientation of compression. This experiment was performed by David J. Lemon.

Perhaps it is the case that the act of depositing the targets was sufficient to induce this response, similar to Stanier's experiments[1] concerning the placement of an inoculum and subsequent response to the perturbation of the gel substrate.

2.3 Fontes & Kaiser 1999

While Dworkin's experiments were qualitative, Fontes & Kaiser in 1999 produced the first quantitative study of this response. By inserting a length of plastic tubing between the wall of a petri dish and the agar gel slab they compressed their cells' substrate and observed the shape of colonies which formed on these stressed substrates, which were elliptical[3]. In addition to investigating changes in colony morphology in response to what the authors termed "elastic forces" within the agar gel, they also showed that single cells reorient upon compression of their substrate such that their long axes are perpendicular to the axis of compression[3]. This study utilized both 9 cm square dishes and 8.5 cm round dishes, and showed that in the round geometry there is an effect on aspect ratio by distance away from the inserted tubing, while the same was not true for square plates. This indicates that the square plate set-up likely represents a relatively uniform, uniaxial compression while the round set-up does not. The authors also showed that, like many of *M. xanthus*' other behaviors[6-8], motility - in this case specifically Adventurous (A) motility - is required. While *M. xanthus*' response was the most comprehensively characterized in this study, several other species were also tested, and indeed *Flavobacterium johnsoniae* was also found to be responsive to substrate compression[3]. Unfortunately this study, like the others before it, did not address the precise nature of what

result or byproduct of substrate compression was being sensed and responded to by the biofilm-forming bacteria.

2.4 Stratford, Woodley, & Park 2013 and Polka & Silver 2014

After the Kaiser lab's investigation of this response in *M. xanthus* it was another 15 years before this response was re-examined, this time twice in relatively quick succession after a history of long gaps between studies. Stratford, Woodley, & Park applied compression to agar gel substrates in a similar manner to Fontes & Kaiser, and showed that *B. mycoides* which is evolutionarily distant from *M. xanthus*, also formed elongated colonies oriented perpendicular to the axis of compression on substrates that had been squeezed[4]. This group also showed that *B. mycoides* is sensitive to unusual deformations in uncompressed but poorly characterized substrates that had gelled around various glassware which was then removed prior to inoculation. Unfortunately these experiments did not resolve the question of precisely what the cells were responding to, though they were able to show that large-scale compression of the gel was not required to induce unusual colony morphologies.

The following year Polka & Silver observed that *B. subtilis* also responds to substrate compression in a similar manner[5]. Because this study also investigated the chemical content of media which appeared necessary to help trigger this response, it is difficult to parse any chemical effects, particularly those which alter cell length and flexibility, from the mysterious physical stimuli that this and other species may be responding to. All of these works however combine to clearly show that there is some physical change or stimuli in the agar gel media that

multiple, distantly related species are capable of sensing and responding to, though the stimulus itself is not clear from the results of these studies.

2.5 Theories of stress lines, surface tension, and topography or deformation

In dubbing the newly discovered response to substrate compression "elasticotaxis" in 1942, Stanier clearly shows his thinking that compression or tension has some telltale signature, by product, or after-effect on the gel, though he did not identify it[1]. Fontes & Kaiser also use the term and describe "elastic forces" at play in their compressed substrates, but too do not specifically identify what they suppose the cells are sensing[3]. However while Fontes & Kaiser did not specifically identify a stimulus, they describe "stress forces" and note that cells only capable of A motility display a stronger response to substrate compression than wild-type cells, and they note that Social (S) motility is not sufficient to reproduce a wild-type response[3]. This suggests that the downward-facing A motility motor[9-12] is somehow involved in sensing this novel stimulus. Changes in surface tension have been observed to correlate with changes in *M. xanthus* behavior[13,14]. This suggests that compressing the substrate, which results in water being squeezed out of the gel, may have an effect on surface tension that the cells are able to respond to.

It may also be the case that topographical changes in the substrate as a result of compression are driving the change in *M. xanthus*' behavior; such changes have previously been shown to alter cell and flare trajectories[15,16]. For this to be the case however these topographical features must be approximately the width of a cell, on the order of 1 μm wide, wide enough to allow a cell to fall into one, but not so wide that they dwarf the cell's width,

which would make them difficult or impossible for single cells to respond to at the low Reynolds number regimes typical of small, slow moving masses in a relatively viscous environment[17]. This narrow range of sizes is useful in potentially ruling out topography, as such a size feature would surely be detectable by techniques which readily visualize individual cells. Changes in substrate stiffness have also been identified to alter motility and behavior[18], though *M. xanthus* does not appear to be climbing up a gradient in stiffness, as it moves perpendicular to compression rather than towards it[3]. There are several biological responses to physical changes which have been observed and are well-characterized, including some that are also sensed by downward-facing motility apparatuses, in both eukaryotic and prokaryotic species. Closer examination of these may prove useful in the attempt to identify the precise stimulus which *M. xanthus* cells are responding to on compressed substrates.

2.6 Biophysical signals that can change cell behavior

While most research into bacterial responses to physical changes in their substrate are tailored around stopping the proliferation of biofilms or eliminating them altogether, there are a handful of examples of studies which investigated stiffness, topography, or surface tension as described above. Responses to similar physical changes are better understood in eukaryotic cell models, and these too should be explored.

2.6.1 Eukaryotic responses to biophysical signals

Some of the earliest examples of sensing and responding to physical signals have been observed not in animal cells, but in plant cells[19,20]. Sunflowers are aptly named because they track the sun's path across the sky, a behavior called heliotropism (movement in response to

the sun), a subset of phototropism (movement in response to light)[21,22]. Other plant processes such as orienting new growth up or down in response to acceleration, typically due to gravity and called gravitropism (movement in response to gravity)[19], can be overridden in roots by the response to water gradients known as hydrotropism (movement in response to water)[23].

Animal models are more relevant here however, as animal cells, like *M. xanthus* cells, are capable of movement in addition to bending and growth. Reponses to topography have been well-characterized, as they can alter cell morphologies[24,25] and branching patterns[26-30], and endogenous bone repair has been shown to be triggered by cracks in the bone's surface[31-33]. Motile animal cells have been shown to have the ability to climb up gradients in stiffness, a behavior dubbed durotaxis (movement in response to hardness or stiffness)[34-37], as has the nematode *C. elegans*[35]. The response to substrate stiffness has also repeatedly been shown to influence cell differentiation and cell fate[25,27,38-41]. Interestingly durotaxis has been shown to involve a focal adhesion system[42,43] which, while eukaryotic focal adhesions are distinct from those used in *M. xanthus*, are similar in nature as a downward-facing direct interaction with the gel media's component polymers. The forces generated during and involved in eukaryotic cell locomotion have also been examined in relative detail, and results of these studies may shed additional light on the mysterious nature at the root of what has historically been referred to as elasticotaxis[1].

Traction forces, the forces exerted on the substrate during locomotion[44-46], while they allow a cell to propel itself forward also have effects on the substrate[47]. It has been hypothesized that this pulling or pushing on the substrate can pull polymers within the

substrate into alignment[46,48,49] or enable the cells to communicate mechanically with each other over long distances[50-52]. Studies of gel substrates, similar to those used in everyday culturing of bacteria, have suggested that such pulling or pushing on the substrate may bring its components into alignment[53-55], which may have further effects on cell behavior and motility. Indeed the sum of traction forces exerted on the substrate has been observed to dictate the behavior of sheets of cells[56-59] and may even play a role in the prognosis of cancer[60].

2.6.2 Prokaryotic responses to biophysical signals

Like eukaryotic cells, prokaryotic cells have also been observed to respond to changes in topography[16,61-63], as well as stiffness[12]. *M. xanthus* motility specifically is sensitive to changes in surface tension[13,14], stiffness[64], and has, along with a handful of other species[3-5], been found to respond to substrate compression[1-3] though the precise nature of the physical stimuli inherent in these species' response to substrate compression has yet to be identified.

2.7 Our hypothesis

Substrate polymer alignment, as discussed earlier in the eukaryotic context of pushing and pulling during focal adhesion-based motility, is also likely occurring during compression of the agar gel media[65-67]. Such alignment has clearly demonstrated effects on eukaryotic cell behavior discussed above, we hypothesize that it may be underpinning the bacterial response to substrate compression that has been previously observed[1-5], but never understood. If this is indeed the case, then compression of a gel substrate must be forcing the gel's component polymers into alignment, and this alignment is then driving a change in the behaviors of biofilm-forming bacteria. Investigations into the stress and strain within the substrate, a more detailed

characterization of the bacterial response to substrate compression, and further examination of the gel itself, including its surface, may reveal that this is indeed the case - elasticotaxis may be a response to polymer alignment caused by substrate compression.

2.8 Materials & methods

To determine fruiting body arrangement 4 µL 5 x 10^9 cells / mL of wild-type DK1622 cells was spotted on nutrient-poor 1.5% agar dCTA[6] that was uncompressed or had been previously compressed by insertion of a length of 5.56 mm diameter Tygon tubing between the wall of the petri plate and the agar slab. Images were captured with a 3.0 megapixel AmScope USB ocular camera and Toupview image capture software after 5 days of incubation at 30 °C.

2.9 References

1 Stanier, R. Y. A Note on Elasticotaxis in Myxobacteria. *J Bacteriol* **44**, 405 - 412 (1942).

2 Dworkin, M. Tactic behavior of *Myxococcus xanthus*. *J Bacteriol* **154**, 452 - 459 (1983).

3 Fontes, M. & Kaiser, D. Myxococcus cells respond to elastic forces in their substrate. *Proceedings of the National Academy of Sciences of the United States of America* **96**, 8052 - 8057 (1999).

4 Stratford, J. P., Woodley, M. A. & Park, S. Variation in the morphology of *Bacillus mycoides* due to applied force and substrate structure. *PloS one* **8**, e81549, doi:10.1371/journal.pone.0081549 (2013).

5 Polka, J. K. & Silver, P. A. Induced sensitivity of *Bacillus subtilis* colony morphology to mechanical media compression. *PeerJ* **2**, e597, doi:10.7717/peerj.597 (2014).

6 Pham, V. D., Shebelut, C. W., Diodati, M. E., Bull, C. T. & Singer, M. Mutations affecting predation ability of the soil bacterium *Myxococcus xanthus*. *Microbiology* **151**, 1865-1874, doi:10.1099/mic.0.27824-0 (2005).

7 Kroos, L., Hartzell, P. L., Stephens, K. & Kaiser, A. D. A link between cell movement and gene expression argues that motility is required for cell-cell signaling during fruiting body development. *Genes and Development* **2**, 1677 - 1685 (1988).

8 Zhang, Y., Ducret, A., Shaevitz, J. & Mignot, T. From individual cell motility to collective behaviors: insights from a prokaryote, *Myxococcus xanthus*. *FEMS microbiology reviews* **36**, 149-164, doi:10.1111/j.1574-6976.2011.00307.x (2012).

9 Mignot, T. The elusive engine in *Myxococcus xanthus* gliding motility. *Cellular and molecular life sciences : CMLS* **64**, 2733-2745, doi:10.1007/s00018-007-7176-x (2007).

10 Ducret, A., Valignant, M.-P., Mouhamar, F., Mignot, T. & Theodoly, O. Wet-surface-enhanced ellipsometric contrast microscopy identifies slime as a major adhesion factor during bacterial surface motility. *PNAS* **199** (2012).

11 Islam, S. T. & Mignot, T. The mysterious nature of bacterial surface (gliding) motility: A focal adhesion-based mechanism in *Myxococcus xanthus*. *Semin Cell Dev Biol* **46**, 143-154, doi:10.1016/j.semcdb.2015.10.033 (2015).

12 Balagam, R. *et al. Myxococcus xanthus* Gliding Motors Are Elastically Coupled to the Substrate as Predicted by the Focal Adhesion Model of Gliding Motility. *PLoS computational biology* **10** (2014).

13 Dworkin, M., Keller, K. H. & Weisberg, D. Experimental Observations Consistent with a Surface Tension Model of Gliding Motility of *Myxococcus xanthus*. *J Bacteriol* **155**, 1367 - 1371 (1983).

14 Keller, K. H., Grady, M. & Dworkin, M. Surface Tension Gradients: Feasible Model for Gliding Motility of *Myxococcus xanthus*. *J Bacteriol* **155**, 1358 - 1366 (1983).

15 Meel, C., Kouzel, N., Oldewurtel, E. R. & Maier, B. Three-Dimensional Obstacles for Bacterial Surface Motility. *Small* **8**, 530 - 534 (2012).

16 Friedlander, R. S. *et al.* Bacterial flagella explore microscale hummocks and hollows to increase adhesion. *PNAS* **110**, 5624 - 5629 (2013).

17 Purcell, E. M. Life at low Reynolds number. *Am J Phys* **45**, 3 - 11 (1976).

18 Guegan, C. *et al.* Alteration of bacterial adhesion induced by the substrate stiffness. *Colloids Surf B Biointerfaces* **114**, 193-200, doi:10.1016/j.colsurfb.2013.10.010 (2014).

19 Bastien, R., Douady, S. & Moulia, B. A Unified Model of Shoot Tropism in Plants: Photo-, Gravi-, and Proprio-ception. *PLoS computational biology* **11** (2014).

20 Telewski, F. A unified hypothesis of mechanoperception in plants. *Am J Bot* **93**, 1466 - 1476 (2006).

21 Atamian, H. S. *et al.* Circadian regulation of sunflower heliotropism, floral orientation, and pollinator visits. *Science* **353**, 587 - 590 (2016).

22 Jekely, G. Evolution of phototaxis. *Philos Trans R Soc Lond B Biol Sci* **364**, 2795-2808, doi:10.1098/rstb.2009.0072 (2009).

23 Eapen, D., Barroso, M. L., Ponce, G., Campos, M. E. & Cassab, G. I. Hydrotropism: root growth responses to water. *Trends Plant Sci* **10**, 44-50, doi:10.1016/j.tplants.2004.11.004 (2005).

24 Bettadapur, A. *et al.* Prolonged Culture of Aligned Skeletal Myotubes on Micromolded Gelatin Hydrogels. *Sci Rep* **6**, 28855, doi:10.1038/srep28855 (2016).

25 Teo, B. K. K., Ankam, S., Chan, L. Y. & Yim, E. K. F. Nanotopography/Mechanical Induction of Stem-Cell Differentiation. *Methods in Cell Biology* **98**, 241-294, doi:10.1016/s0091-679x(10)98011-4 (2010).

26 Pelham, R. J. & Wang, Y. Cell locomotion and focal adhesions are regulated by substrate flexibility. *Proceedings of the National Academy of Sciences of the United States of America* **94**, 13661 - 13665 (1997).

27 Previtera, M. L., Langhammer, C. G. & Firestein, B. L. Effects of substrate stiffness and cell density on primary hippocampal cultures. *J Biosci Bioeng* **110**, 459-470, doi:10.1016/j.jbiosc.2010.04.004 (2010).

28 Previtera, M. L., Langhammer, C. G., Langrana, N. A. & Firestein, B. L. Regulation of dendrite arborization by substrate stiffness is mediated by glutamate receptors. *Ann Biomed Eng* **38**, 3733 - 3743 (2010).

29 Dunn, G. A. & Brown, F. Alignment of fibroblasts on grooved surfaces described by a simple geometric transformation. *Journal of cell science* **83**, 313 - 340 (1986).

30 Lawrence, B. D., Pan, Z. & Rosenblatt, M. I. Silk Film Topography Directs Collective Epithelial Cell Migration. *PloS one* **7**, doi:10.1371/ (2012).

31 Shu, Y. *et al.* Surface microcracks signal osteoblasts to regulate alignment and bone formation. *Mater Sci Eng C Mater Biol Appl* **44**, 191-200, doi:10.1016/j.msec.2014.08.036 (2014).

32 Frost, H. M. Wolff's Law and bone's structural adaptations to mechanical usage: an overview for clinicians. *Angle Ortho* **64**, 175 - 188 (1994).

33 Matsugaki, A., Isobe, Y., Saku, T. & Nakano, T. Quantitative regulation of bone-mimetic, oriented collagen/apatite matrix structure depends on the degree of osteoblast alignment on oriented collagen substrates. *Journal of biomedical materials research. Part A* **103**, 489-499, doi:10.1002/jbm.a.35189 (2015).

34 Lazopoulos, K. A. & Stamenovic, D. Durotaxis as an elastic stability phenomenon. *Journal of biomechanics* **41**, 1289-1294, doi:10.1016/j.jbiomech.2008.01.008 (2008).

35 Parida, L. & Padmanabhan, V. Durotaxis in Nematode *Caenorhabditis elegans*. *Biophys J* **111**, 666-674, doi:10.1016/j.bpj.2016.06.030 (2016).

36 Lo, C.-M., Wang, H.-B., Dembo, M. & Wang, Y. Cell Movement is Guided by the Rigidity of the Substrate. *Biophys J* **79**, 144 - 152 (2000).

37 Wormer, D. B., Davis, K. A., Henderson, J. H. & Turner, C. E. The focal adhesion-localized CdGAP regulates matrix rigidity sensing and durotaxis. *PloS one* **9**, e91815, doi:10.1371/journal.pone.0091815 (2014).

38 Dreier, B. *et al.* Early responses of vascular endothelial cells to topographic cues. *Am J Physiol Cell Physiol* **305**, C290-298, doi:10.1152/ajpcell.00264.2012 (2013).

39 Yeung, T. *et al.* Effects of substrate stiffness on cell morphology, cytoskeletal structure, and adhesion. *Cell motility and the cytoskeleton* **60**, 24-34, doi:10.1002/cm.20041 (2005).

40 Costa, P., Almeida, F. V. & Connelly, J. T. Biophysical signals controlling cell fate decisions: how do stem cells really feel? *Int J Biochem Cell Biol* **44**, 2233-2237, doi:10.1016/j.biocel.2012.09.003 (2012).

41 Gasiorowski, J. Z., Murphy, C. J. & Nealey, P. F. Biophysical cues and cell behavior: the big impact of little things. *Annu Rev Biomed Eng* **15**, 155-176, doi:10.1146/annurev-bioeng-071811-150021 (2013).

42 Prager-Khoutorsky, M. *et al.* Fibroblast polarization is a matrix-rigidity-dependent process controlled by focal adhesion mechanosensing. *Nat Cell Biol* **13**, 1457-1465, doi:10.1038/ncb2370 (2011).

43 Freyman, T. M., Yannas, I. V., Yokoo, R. & Gibson, L. J. Fibroblast contractile force is independent of the stiffness which resists the contraction. *Exp Cell Res* **272**, 153-162, doi:10.1006/excr.2001.5408 (2002).

44 Dubin-Thaler, B. J. *et al.* Quantification of cell edge velocities and traction forces reveals distinct motility modules during cell spreading. *PloS one* **3**, e3735, doi:10.1371/journal.pone.0003735 (2008).

45 Tanimoto, H. & Sano, M. Dynamics of traction stress field during cell division. *Phys Rev Lett* **109**, 248110, doi:10.1103/PhysRevLett.109.248110 (2012).

46 Feng, Z. *et al.* Analysis of the contraction of fibroblast collagen gels and the traction force of individual cells by a novel elementary structural model. *35th Annual International Conference of the IEEE EMBS*, 6232-6235 (2013).

47 Koch, T. M., Munster, S., Bonakdar, N., Butler, J. P. & Fabry, B. 3D Traction Forces in Cancer Cell Invasion. *PloS one* **7**, doi:10.1371/10.1371/journal.pone.0033476.g001 (2012).

48 Harris, A. K., Stopak, D. & Wild, P. Fibroblast traction as a mechanism for collagen morphogenesis. *Nature* **290**, 249-251 (1981).

49 Miron-Mendoza, M., Seemann, J. & Grinnel, F. Collagen fibril flow and tissue translocation coupled to fibroblast migration in 3d collagen matrices. *Molecular biology of the cell* **19**, doi:10.1091/mbc.E07-09-0930) (2008).

50 Reinhart-King, C. A., Dembo, M. & Hammer, D. A. Cell-cell mechanical communication through compliant substrates. *Biophys J* **95**, 6044-6051, doi:10.1529/biophysj.107.127662 (2008).

51 Ma, X. *et al.* Fibers in the extracellular matrix enable long-range stress transmission between cells. *Biophys J* **104**, 1410-1418, doi:10.1016/j.bpj.2013.02.017 (2013).

52 Winer, J. P., Oake, S. & Janmey, P. A. Non-linear elasticity of extracellular matrices enables contractile cells to communicate local position and orientation. *PloS one* **4**, e6382, doi:10.1371/journal.pone.0006382 (2009).

53 Mohammadi, H. & McCulloch, C. A. Impact of elastic and inelastic substrate behaviors on mechanosensation. *Soft Matter* **10**, 408-420, doi:10.1039/c3sm52729h (2014).

54 Wang, H., Abhilash, A. S., Chen, C. S., Wells, R. G. & Shenoy, V. B. Long-range force transmission in fibrous matrices enabled by tension-driven alignment of fibers. *Biophys J* **107**, 2592-2603, doi:10.1016/j.bpj.2014.09.044 (2014).

55 Stamenovic, D., Lazopoulos, K. A., Pirentis, A. & Suki, B. Mechanical Stability Determines Stress Fiber and Focal Adhesion Orientation. *Cellular and molecular bioengineering* **2**, 475-485, doi:10.1007/s12195-009-0093-3 (2009).

56 Angelini, T. E., Hannezo, E., Trepat, X., Fredberg, J. J. & Weitz, D. A. Cell migration driven by cooperative substrate deformation patterns. *Phys Rev Lett* **104**, 168104, doi:10.1103/PhysRevLett.104.168104 (2010).

57 Gov, N. Cell mechanics: moving under peer pressure. *Nat Mater* **10**, 412-414, doi:10.1038/nmat3036 (2011).

58 Trepat, X. & Fredberg, J. J. Plithotaxis and emergent dynamics in collective cellular migration. *Trends Cell Biol* **21**, 638-646, doi:10.1016/j.tcb.2011.06.006 (2011).

59 Tzlil, S. & Tirrell, D. A. Strain propagation in artificial extracellular matrix proteins can accelerate cell spreading and polarization. *Soft Matter* **9**, 5602, doi:10.1039/c3sm27137d (2013).

60 Conklin, M. W. *et al.* Aligned collagen is a prognostic signature for survival in human breast carcinoma. *Am J Pathol* **178**, 1221-1232, doi:10.1016/j.ajpath.2010.11.076 (2011).

61 Gu, H., Hou, S., Yongyat, C., De Tore, S. & Ren, D. Patterned Biofilm Formation Reveals a Mechanism for Structural Heterogeneity in Bacterial Biofilms. *Langmuir* **29**, 11145 - 11153 (2013).

62 Gu, H., Kolewe, K. W. & Ren, D. Conjugation in *Escherichia coli* Biofilms on Poly(dimethylsiloxane) Surfaces with Microtopographic Patterns. *Langmuir* **33**, 3142 - 3150 (2017).

63 Song, F., Koo, H. & Ren, D. Effects of Material Properties on Bacterial Adhesion and Biofilm Formation. *Oral Biology & Medicine* **94**, 1027 - 1034 (2015).

64 Shi, W. & Zusman, D. R. The two motility systems of *Myxococcus xanthus* show different selective advantages on various surfaces. *PNAS* **90**, 3378 - 3382 (1993).

65 Busby, G. A., Grant, M. H., Mackay, S. P. & Riches, P. E. Confined compression of collagen hydrogels. *Journal of biomechanics* **46**, 837-840, doi:10.1016/j.jbiomech.2012.11.048 (2013).

66 White, D., Bott, D. C. & Weatherhead, R. H. Direct evidence for chain orientation in poly(acetylene). *Polymer* **14**, 805 - 809 (1983).

67 Wu, Z. L. *et al.* Strain-Induced Molecular Reorientation and Birefringence Reversion of a Robust, Anisotropic Double-Network Hydrogel. *Macromolecules* **44**, 3542-3547, doi:10.1021/ma200123u (2011).

Chapter 3 - Characterization of the response to substrate compression

Previous work has shown that single *Myxococcus xanthus* cells respond to substrate compression by reorienting their long axes perpendicular to the direction of compression[1]. Outward movements of groups of cells from the edge of the colony, called flares, and the colonies themselves also reorient and respond to substrate compression. Single-cells, flares, and whole-colonies all require Adventurous (A) motility to respond to substrate compression[1], suggesting that the movements and responses result from an active biological process, rather than being a passive event.

3.1 Response to substrate compression

3.1.1 Whole-colony behavior

M. xanthus colonies which form on substrates which have been compressed (Fig. 3.1 A and B) form in ellipses with their long axes oriented perpendicular to the axis of compression. In contrast, colonies on unstressed agar substrates expand radially in all directions, which results in circular colonies (Figure 3.1 C and D). The strength of the whole-colony response can be inferred from how elliptical it is, dividing its length (long axis, perpendicular to compression) by its height (short axis, parallel to compression) yields the colony's aspect ratio, which was historically called its elasticotaxis coefficient[1]. While round colonies inherently have aspect ratios roughly equal to one, colonies with larger aspect ratios are relatively more elongated, which indicates a stronger response to substrate compression.

3.1.2 Flare behavior

M. xanthus flare behavior was also examined on compressed and uncompressed substrates. Still images reveal that flares at the edge of a colony on an unstressed substrate tend to move outward, but without any overarching directionality (Figure 3.1 D' and D''). Flares on compressed substrates appear qualitatively different. At the edge of the long axis of a colony on a compressed substrate (the edge closest to the inserted tubing) flares do not emerge often (Fig. 3.1 B'), and when they do emerge moving parallel to the axis of compression they do not appear to hold this

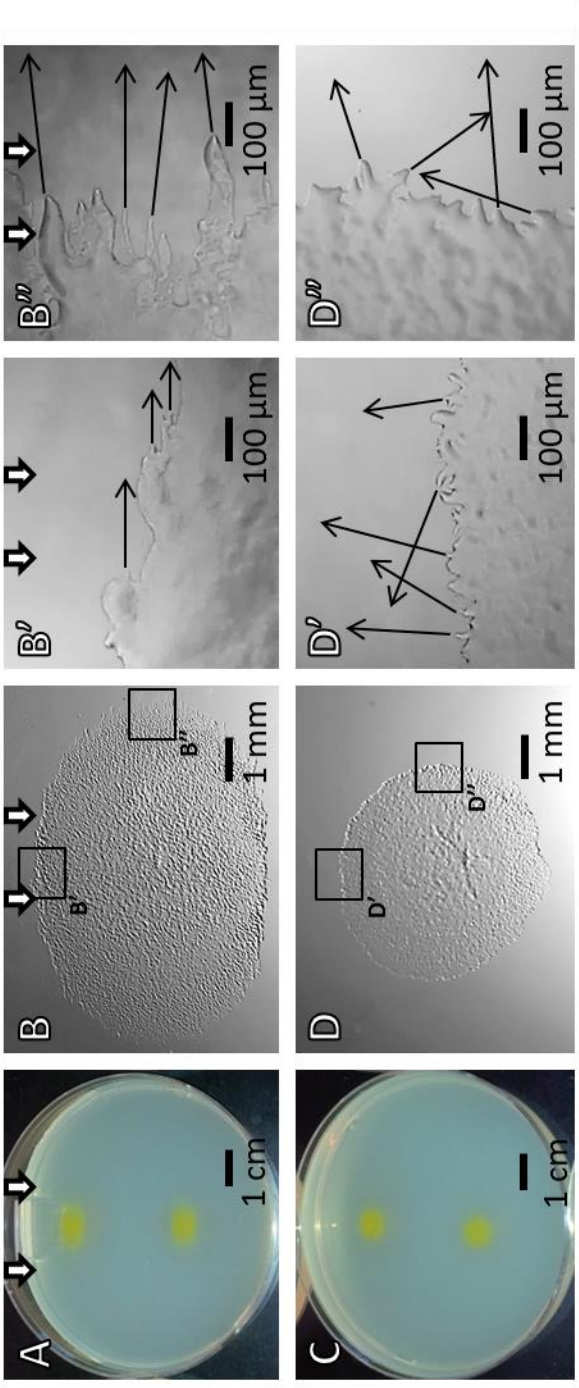

Figure 3.1. *M. xanthus* flares and colonies respond to substrate compression. Whole-colony morphologies on compressed (A and B) and uncompressed agar (C and D) are shown. The white arrows in panels A, B, B', and B'' indicate the direction of compression. The direction of movement of selected flares or groups of cells (black arrows) at one edge of the long axis and short axis of a colony on compressed agar is shown in B' and B'' respectively. The direction of movement of selected flares (black arrows) at the corresponding positions on uncompressed agar is shown in D' and D'', respectively. This experiment was performed by David J. Lemon.

trajectory for very long. At the end of the long axis however, many flares emerge oriented perpendicular to the axis of compression (Fig. 3.1 B'') and appear to hold this trajectory without encountering neighboring flares for extended times. Over time flare behavior appears similar to the behavior that can be deduced from still images. Time-lapse imaging of expanding *M. xanthus* colonies on compressed and uncompressed substrates allows for quantitative analysis of flare behavior, which will be discussed in later sections.

3.2 Aspect ratio vs. distance from inserted tubing

To quantify the effect of agar compression on the colony morphology I determined the aspect ratios of colonies as a function of the distance from the inserted tube and the tube diameter that controls the degree of compression. Eight drops of *M. xanthus* cells were placed in a column down the centerline of an agar slab, which is in a circular petri dish, using a multichannel pipettor. These agar slabs were compressed by inserting a length of tubing of varying diameter between the wall of the dish and the agar gel slab. The aspect ratios of colonies near the tube are relatively large and decrease as the distance between colonies and the tube increases. We find similar relationships between aspect ratio and distance from the tube when the tubes have different diameters, which keep the agar under different levels of compression (Figure 3.2). However, the larger the tube's diameter, the more exaggerated this relationship becomes; the larger diameter of the tube, the larger the aspect ratio of the colony closest to the tube and the greater the distances from the tube before the aspect ratios approach that of colonies on uncompressed agar. Together, these findings indicate that *M. xanthus* is able to detect and respond to different levels of agar compression. Interestingly, *M.*

xanthus responds to compression-induced changes in the agar over relatively large distances; the aspect ratio of colonies that are about 60 mm away from the inserted tubes are still greater than those of colonies at comparable locations on uncompressed agar (Figure 3.2, 3.3 A). These same trends hold up over a range of gels with varying concentrations of agar (Fig. 3.2), and stiffnesses from 100 kpa to 500 kpa, as agar gel stiffness is directly correlated to the

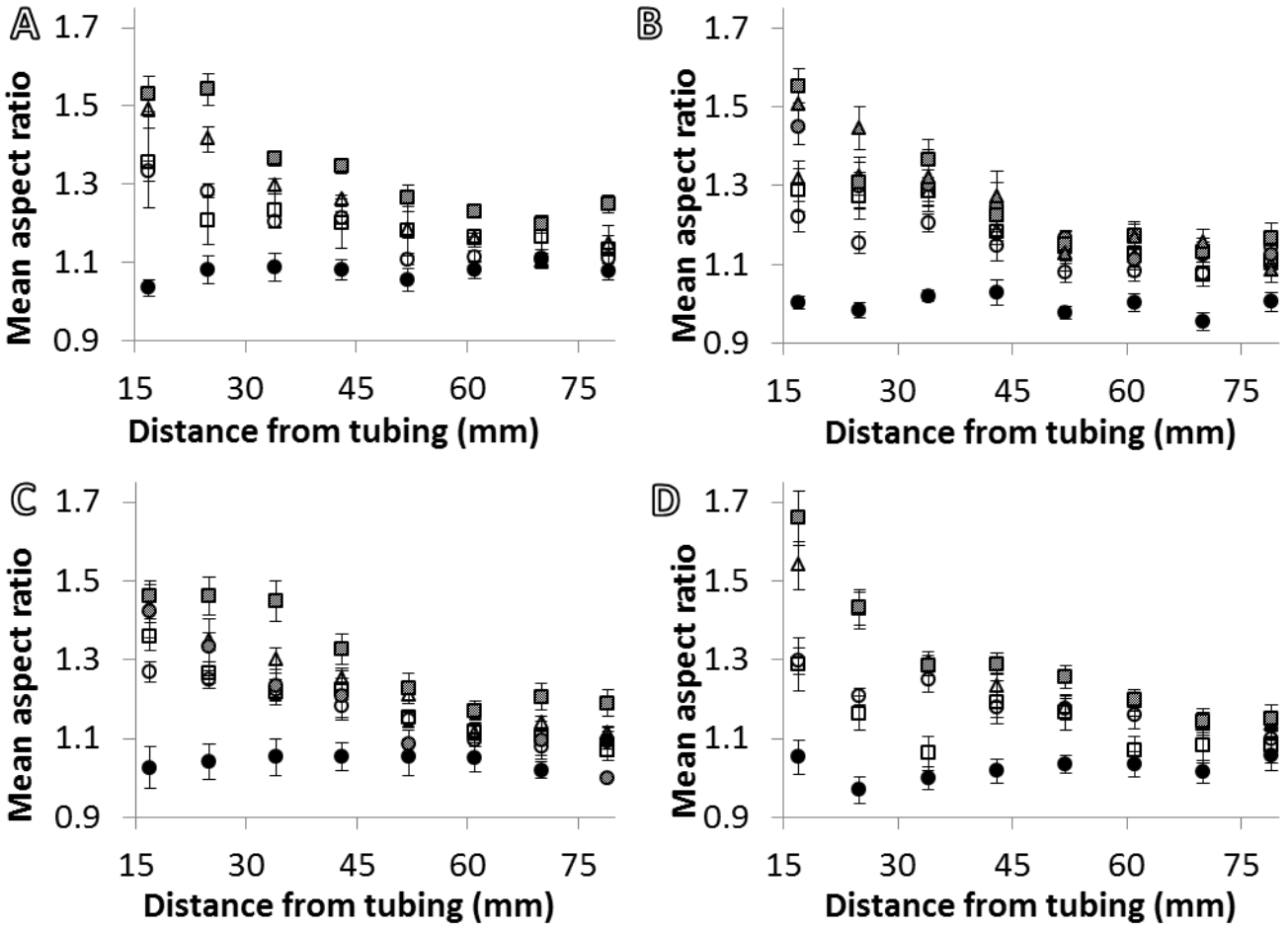

Figure 3.2. Aspect ratio vs. distance for varying stiffness substrates. A-D show the mean aspect ratios (± S.E.M.) of *M. xanthus* colonies at various distances from inserted tubing with different diameters. The mean number of colonies used to calculate each aspect ratio is approximately 31 for 1.25% agar (A), 16 for 1.75% agar (B), 20 for 2% agar (C), and 18 for 3% agar (D). Mean aspect ratios of colonies on uncompressed agar (black circles), and colonies on agar compressed with tubing with a diameter of 2.38 mm (white circles), 3.18 mm (white squares), 3.96 mm (white triangles), 4.77 mm (grey circles), 5.56 mm (grey squares), 6.35 mm (grey triangles) are shown. This experiment was performed by David J. Lemon.

concentration of agar[2].

3.3 Aspect ratio vs. predicted stress

Distance from the inserted tubing has a clear effect on the aspect ratio of a colony on a compressed substrate. The question then becomes one of "what varies with distance from the inserted tubing", the answer to which would then become a prime candidate for explaining *M. xanthus*[1,3,4] and other bacterial species'[1,5,6] responses to substrate compression. While a good candidate will vary proportionally with distance from the inserted tubing, these species are not likely responding to a gradient; they are likely responding across a gradient (if there is one), rather than along it.

The graph of aspect ratio as a function of distance from the inserted tubing for colonies

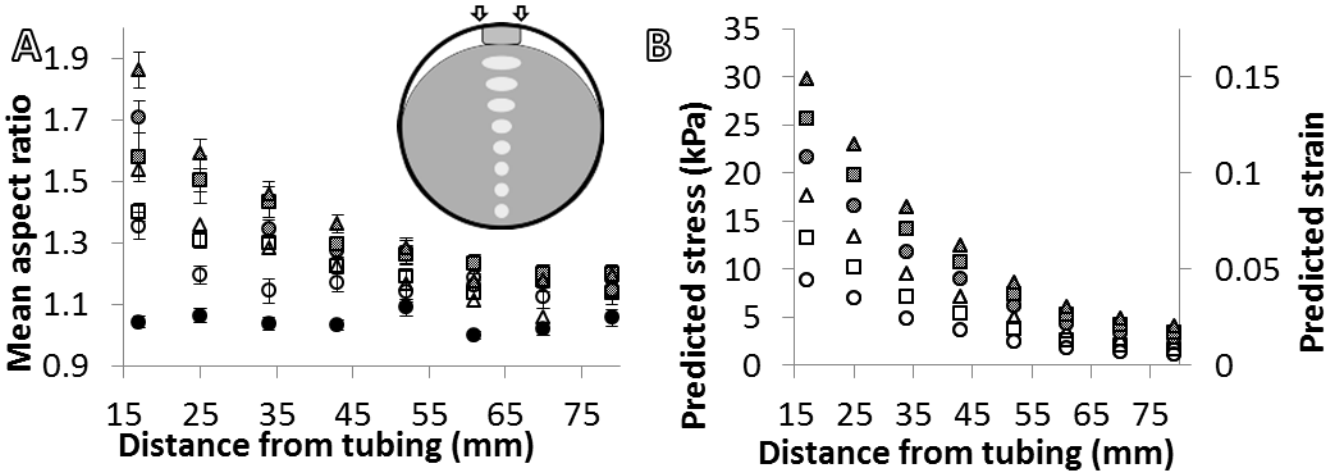

Figure 3.3. Effects of different levels of agar compression on aspect ratio, stress, and strain. Bacterial cells were spotted in a column down the centerline of compressed agar (inset in A) and the mean aspect ratios (± S.E.M.) of the colonies were determined (A). B shows the predicted stress and strain at various distances from the inserted tubes. Mean aspect ratios or predicted stress and strain on unstressed agar (black circles), and on agar compressed with tubing with a 2.38 mm (white circles), 3.18 mm (white squares), 3.96 mm (white triangles), 4.77 mm (grey circles), 5.56 mm (grey squares), or 6.35 mm (grey triangles) diameter are shown in A and B. An average of 23 colonies were included in average aspect ratios shown in A. This experiment was performed by David J. Lemon using predicted stress/strain values from simulations performed by Xingbo Yang.

on 1.5% agar under varying degrees of compression appears qualitatively similar to numerical predictions of stress as a function of distance (Figure 3.3 B). We examined the relationship between the stress and strain in compressed agar and changes in the aspect ratios of colonies. Specifically, we assumed that the agar slab behaves like a linear elastic medium, of known elastic constants, and used Comsol's solid mechanics module to calculate the stress and strain profiles of a circular agar slab compressed by a tube of a given diameter, in agreement with our previous experimental set up (Figure 3.3A). Since we operated under the assumption of linear elasticity, the predicted stress and strain within the agar are directly proportional to each other, and each can be converted to the other using the known elastic constant for each agar concentration[2]. The predicted stress and strain at positions on the agar that correspond to where the cells were spotted in previous experiments are shown in Figure 3.3 B. Similar to the colony aspect ratios (Fig. 3.2, 3.3 A), the predicted stress within the agar and predicted strain are largest in the regions closest to the inserted tubes and decrease with an increase in distance from the tubes. When predicted stress values were combined with the aspect ratio vs. distance data sets generated from substrates with different agar concentrations and hence varying stiffness[2] (Fig. 3.2) and the mean aspect ratios are plotted as a function of predicted stress, the data does not collapse onto a single line (Figure 3.4 A). Thus, stress is not the factor that best predicts the strength of the bacterial response to compression of the agar substrate.

3.4 Aspect ratio vs. predicted strain

While aspect ratio vs. predicted stress values for a given concentration of agar do fall along a linear distribution, these lines vary with each concentration of agar and corresponding

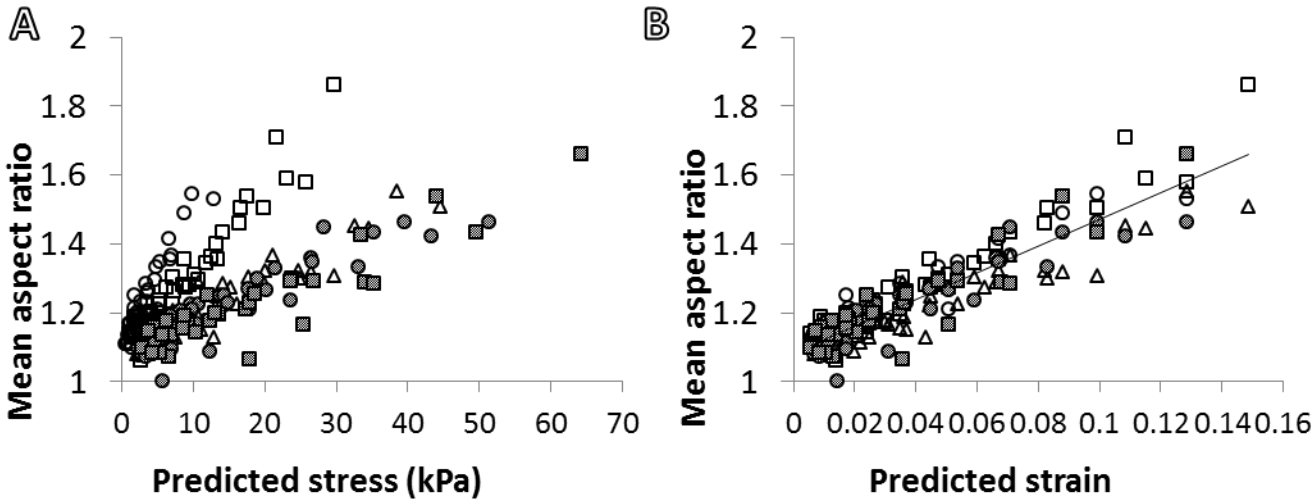

Figure 3.4. Aspect ratio as a function of predicted stress and predicted strain. A and B show mean aspect ratios as a function of stress or strain for different agar concentrations. Mean aspect ratios of colonies on 1.25% agar (white circles), 1.5% agar (white squares), 1.74% agar (white triangles), 2% agar (grey circles), or 3% agar (grey squares) are shown in A and B. This experiment was performed by David J. Lemon using stress and strain values from simulations performed by Xingbo Yang.

stiffness gel. However, because we have predicted values for stress, and the stiffness of agar gels have been measured experimentally[2], converting from values for stress, a measure of force per unit area, with strain, a measure of shape change as the result of said force, is a rudimentary calculation; stiffness is equal to stress divided by strain. By converting all predicted stress values to predicted strain values, and graphing aspect ratio as a function of these strain values, we observe that all values, across all stiffness gels tested (Fig. 3.2, 3.3 A), do collapse onto the same line (Figure 3.4 B). The clear linear relationship ($r = 0.915$, $r^2 = 0.838$) that emerges (Fig. 3.4 B) suggests that the deformation in the agar (strain), rather than the amount of stress within the agar, may dictate the previously observed changes in the orientation of individual bacterial cells, groups of cells, and colony spreading patterns[1] (Figure 3.1). The question then becomes "what varies according to the relative deformation of the substrate that the cells are responding to?"

3.5 Materials and methods

The bacterial response to substrate compression was assayed using a method similar to that previously described by Fontes and Kaiser[1]. Briefly, wild-type DK1622 *M. xanthus* was grown at 30 ^{o}C in CTTYE broth[7] or on plates containing CTTYE broth and 1.25%, 1.5%, 1.75%, 2% or 3% agar which was poured into petri dishes, allowed to solidify, and compressed using 1.5-cm pieces of Tygon tubing with a diameter of 2.38, 3.18, 3.96, 4.76, 5.56, 6.53, or 7.1 mm. Water squeezed out of the gels by compression was allowed to evaporate. Eight 4 µl drops of *M. xanthus* at density of 5 x 10^{9} cells/ml were placed in a column down the centerline of compressed gels using a multichannel pipettor such that the furthest spot was 1 cm from the edge of the petri dish. This was repeated multiple times, with the mean number of colonies used to calculate each aspect ratio being approximately 31 for 1.25% agar, 23 for 1.5% agar, 16 for 1.75% agar, 20 for 2% agar, and 18 for 3% agar.

Flares were examined with an Olympus CK2 inverted microscope and colonies were examined with a SMZ-168 Series Motic stereo zoom microscope. Images were captured with a 3.0 megapixel AmScope USB ocular camera and Toupview image capture software.

Agar compression was simulated under different loads for various agar concentrations to determine the mechanical and deformational state of the substrate characterized by stress and strain on the agar surface. The simulation was performed using the solid mechanics module provided by Comsol, which assumes the condition of linear elasticity. The assumption of linear elasticity for the range of deformations considered here is supported by experimental studies[2].

The geometrical representation of the simulation is in accordance with the experimental set up in Figure 3.3 A. The loading condition reduces to contact between two cylinders of cross-sectional diameters 10 cm and 1 cm, corresponding to the dimensions of the agar and the compressing tube, respectively. The simulation was performed with boundary conditions with the displacements (2.38 mm, 3.18 mm, 3.96 mm, 4.76 mm, 5.56 mm, 6.35 mm) induced by the tube at the contacting surface and zero displacement at the other end of the agar where it was bounded by the dish. The material properties of the agar were specified by a Poisson ratio $\nu = 0.4$ and a Young's modulus $E =$ 100 kpa, 200 kpa, 300 kpa, 400 kpa, 500 kpa for agar concentrations of 1.25%, 1.50%, 1.75%, 2.00% and 3.00%, respectively[2]. The Young's modulus of the Tygon tube was chosen to be 7 Gpa for practical purposes, whose presence was to provide the correct boundary conditions at the contacting surface under loading forces that induced the experimentally imposed boundary displacements.

The stress σ_{ij} and strain ϵ_{ij} tensors on the surface of the agar were computed by solving the force balance equation (1) $\partial_j \sigma_{ij} = 0$ together with the constitutive equation (2) $\epsilon_{ij} = \frac{1}{E}[(1+\nu)\sigma_{ij} - \nu\delta_{ij}\sigma_{kk}]$ under the imposed boundary conditions. While the stress and strain tensors completely specified the mechanical and deformational state of the substrate, the goal was to construct a scalar quantity from the tensors that is proportional to the response of the bacteria to the anisotropic substrate deformation measured by the aspect ratio of the colony. For this, we choose the Von Mises stress, which was defined by equation (3) $\sigma_{VM} = \sqrt{\frac{3}{2}\sigma'_{ij}\sigma'_{ij}}$, with equation (4) $\sigma'_{ij} = \sigma_{ij} - \frac{1}{3}\delta_{ij}\sigma_{kk}$, as the deviatoric part of the stress tensor. This scalar quantity was proportional to the magnitude of the deviatoric stress on the surface of the agar.

In parallel, we defined a scalar quantity that was proportional to the magnitude of the deviatoric strain as in equation (5) $\epsilon_{VM} = \sqrt{\frac{3}{2}\epsilon'_{ij}\epsilon'_{ij}}$, which we termed as Von Mises strain. Using the relationship in linear elasticity defined in equation (6) $\epsilon'_{ij} = \frac{1}{2G}\sigma'_{ij}$, where (7) $G = \frac{E}{2(1+\nu)}$, we have (8) $\epsilon_{VM} = \frac{\sigma_{VM}}{2G}$. We recorded Von Mises stress and Von Mises strain obtained from the simulation along the middle line on the surface of the compressed agar (Figure 3.3 B).

3.6 References

1 Fontes, M. & Kaiser, D. Myxococcus cells respond to elastic forces in their substrate. *Proceedings of the National Academy of Sciences of the United States of America* **96**, 8052 - 8057 (1999).

2 Nayar, V. T., Weiland, J. D., Nelson, C. S. & Hodge, A. M. Elastic and viscoelastic characterization of agar. *J Mech Behav Biomed Mater* **7**, 60-68, doi:10.1016/j.jmbbm.2011.05.027 (2012).

3 Stanier, R. Y. A Note on Elasticotaxis in Myxobacteria. *J Bacteriol* **44**, 405 - 412 (1942).

4 Dworkin, M. Tactic behavior of *Myxococcus xanthus*. *J Bacteriol* **154**, 452 - 459 (1983).

5 Stratford, J. P., Woodley, M. A. & Park, S. Variation in the morphology of *Bacillus mycoides* due to applied force and substrate structure. *PloS one* **8**, e81549, doi:10.1371/journal.pone.0081549 (2013).

6 Polka, J. K. & Silver, P. A. Induced sensitivity of *Bacillus subtilis* colony morphology to mechanical media compression. *PeerJ* **2**, e597, doi:10.7717/peerj.597 (2014).

7 Giglio, K. M., Zhu, C., Klunder, C., Kummer, S. & Garza, A. G. The enhancer binding protein Nla6 regulates developmental genes that are important for *Myxococcus xanthus* sporulation. *J Bacteriol* **197**, 1276-1287, doi:10.1128/JB.02408-14 (2015).

Chapter 4 - Strain induced polymer alignment

4.1 Mapping the substrate and response

Having determined that the strength of *M. xanthus*' response to substrate compression varies directly with the local substrate deformation or strain at a given location (Fig. 3.4 B), we were principally interested in what the effect of strain on the substrate that is detectable by bacterial cells could be. As previously discussed, bacteria have been found to be sensitive to changes in their substrate's surface tension[1,2], topography[3-6], and stiffness[7]. An ideal candidate for the stimulus which elicits the elasticotaxis[8-10] response will vary with strain or deformation, but not necessarily form a gradient which decreases with distance from the inserted tubing. Single-cell, flare, and whole-colony orientation all align perpendicular to the axis of compression, not parallel to it as would be expected if the cells were responding to a gradient.

4.1.1 Hydration

During the act of compressing the gel and inserting the length of tubing between it and the wall of the plate, water is squeezed out of the gel and pools on the surface, a process called syneresis[11,12]. While this byproduct of compression may be relevant, we observe no correlation between areas where water emerges onto the gel's surface and where the bacterial response to compression is observed. Though water is squeezed predominantly out of regions on the plate with high strain, it is allowed to evaporate overnight before the media is inoculated, and changes in hydration do not appear to be a good candidate for the stimulus which elicits the bacterial response to substrate compression.

4.1.2 Topography

Cells are known to be sensitive to changes in topography[3-6], and buckling or wrinkling which could occur would likely be perpendicular to the axis of compression, aligning with the bacterial response to compression, so topographical defects as a result of compression must be

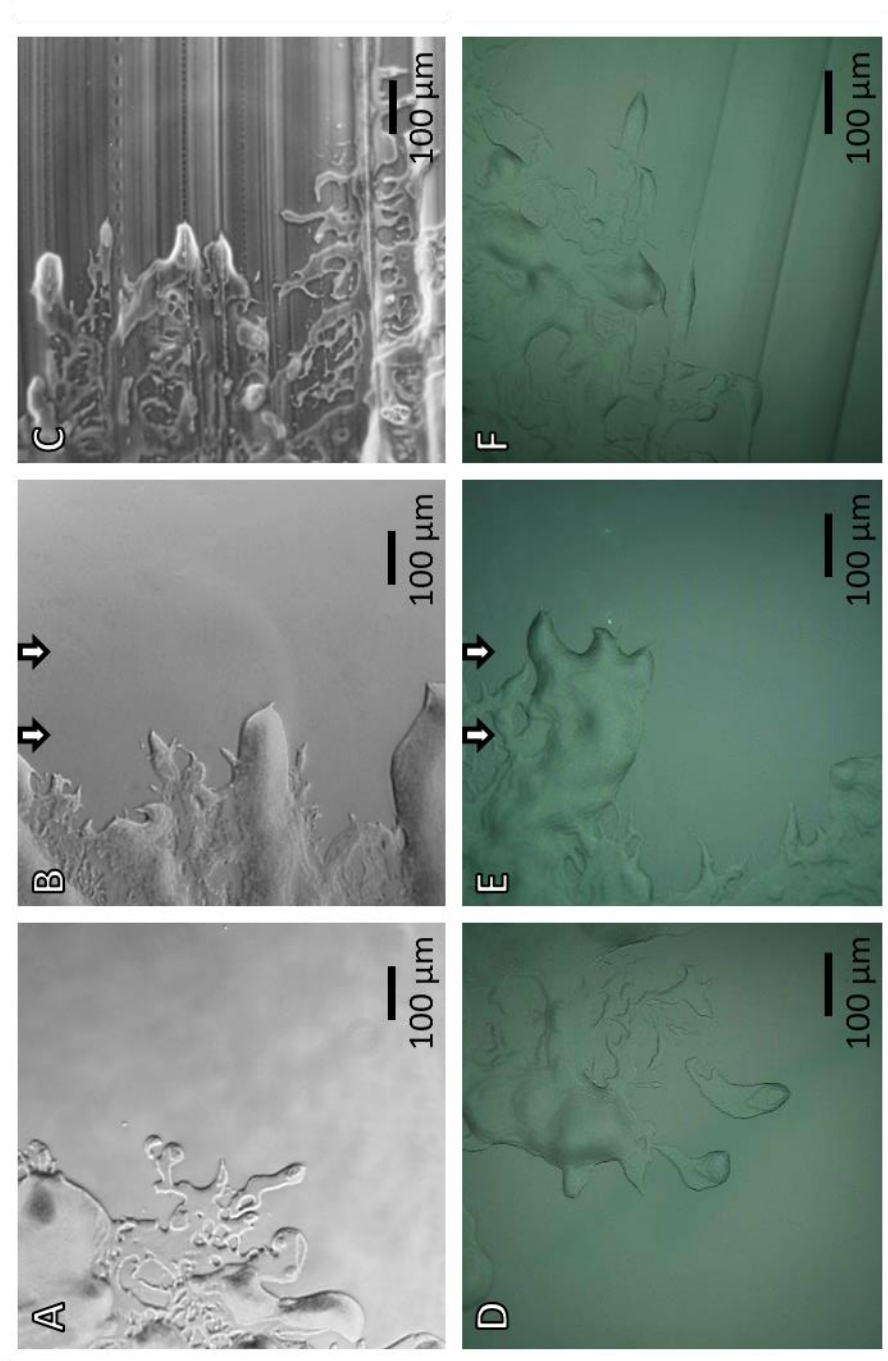

Figure 4.1. Examination of surface topography. Examination of the substrate surface at the *M. xanthus* colony edge on uncompressed (A), compressed (B), and uncompressed scored (C) substrates via phase-contrast microscopy. Examination of the substrate surface under identical conditions as the panels above via 3D digital microscopy (D-F). White arrows in B and E represent the axis of compression. Uncompressed substrates in C and F were scored with the grooved edge of a vinyl LP fragment. This experiment was performed by David J. Lemon.

ruled out. To that end we examined the agar surface near the edge of growing *M. xanthus* colonies with phase-contrast and 3D digital microscopy.

Our examination revealed no topographical defects on uncompressed substrates or on compressed substrates (Figure 4.1 A, B). As a positive control grooves were scored into the surface of an uncompressed gel, and these grooves were visualized by both phase-contrast (Fig. 4.1 C) and 3D digital microscopy methods (Figure 4.1 F). The grooves produced did appear to alter the behavior of the *M. xanthus* cells, both individuals and groups, as movements were directed parallel to the direction of the grooves (Figure 4.1 C, F). As both the grooves and single-cells could be resolved by these methods, but no such grooves or wrinkles were detected on compressed substrates (Fig. 4.1 B, E), we concluded that compression of the relatively thick agar gels used in our experimental set-up does not cause changes in the topography of the gel. While vanishingly small topographical changes cannot be ruled out, wrinkles on the same length scale as single cells, the most relevant length scale to our purposes, can be.

4.1.3 Predicted strain

Predicted strain down the centerline of the agar plate (Fig. 3.3 B) has been discussed previously, but our numerical simulations provide the distribution of strain in two dimensions, not just on the center line moving away from the inserted tubing. Mapping the predicted strain for the entire surface of the plate (Fig. 4.2) reveals that strain is greatest in regions closest to the inserted tubing and decreases with distance from the tubing in both dimensions. Larger diameter tubes hold the agar under greater degrees of compression and result in a relatively large maximum strain, as well as a larger region of the agar where at least some strain is

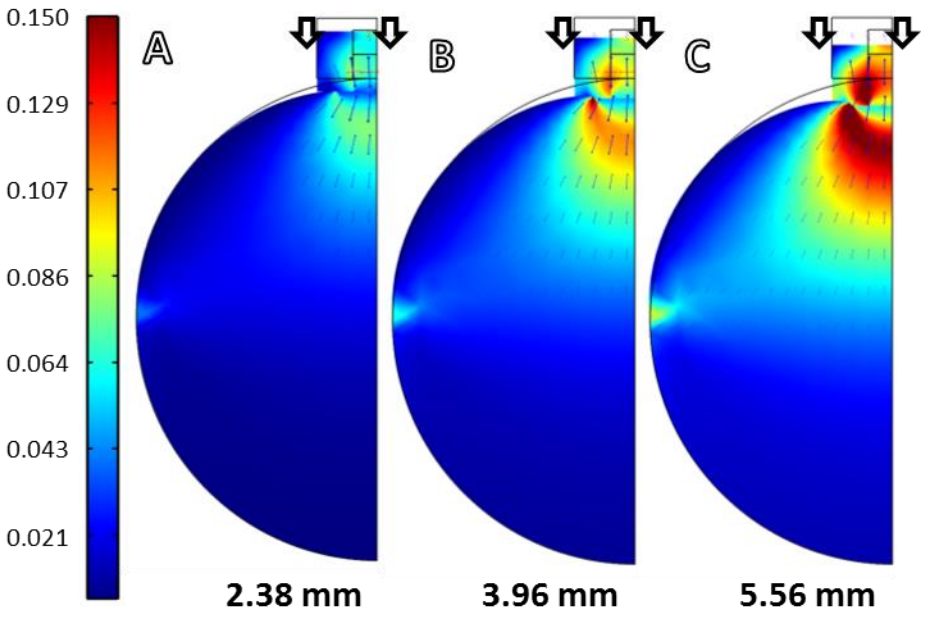

Figure 4.2. Predicted strain of compressed agar. A-C show heat maps of predicted strain due to compression of the 1.5% agar substrate. The scale bar on the left shows the magnitude of predicted strain. White arrows represent the axis of compression imposed by the tubing, modeled as a square being pushed into the half circle of the agar gel slab. Geometry of the set-up mimics experimental conditions, numbers below each map indicate the diameter of the tubing used for each model. Each map corresponds to one half of a plate. Stress and strain simulations were performed by Xingbo Yang.

predicted. As the diameter of the inserted tubes increases, the regions of the agar with predicted strain expand down the centerline moving away from the tube and across the axis perpendicular to the tube.

4.1.4 Birefringence

As previously discussed, one hypothesis which still remains is that strain induces the component polymers of the agar gel into alignment. While this would presumably leave the surface free from topographical defects, alignment is still detectable via microscopy. A chaotic sample, such as a gel with randomly oriented polymers, will not alter the polarization of light,

and when this sample is placed between polarized filters at 90° angles to each other (cross-polarized filters) and viewed the sample will appear dark. However, if the sample is somewhat structured, such as a gel with aligned polymers, it will rotate the polarization of light, and when viewed between the same cross-polarized filters it will appear brighter. By compressing agar gels with various diameter tubing, viewing them from between cross-polarized filters, and charting which samples appear bright rather than dark, a property called birefringence, we can investigate changes in the order or alignment of the polymers in the gel.

We marked a grid onto each plate to divide it into many sections, and checked each section for birefringence. As the diameter of the inserted tubing was increased we observed an

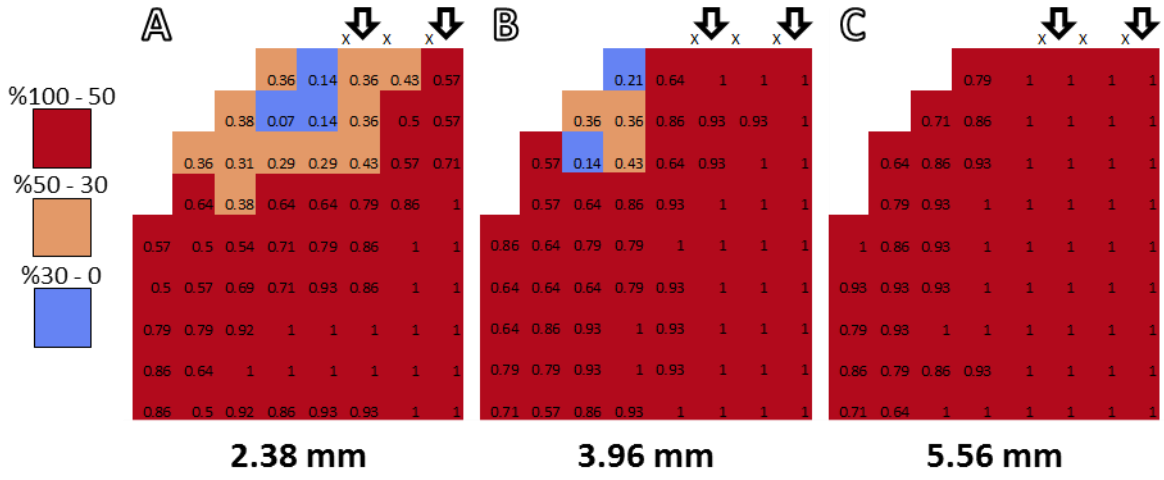

Figure 4.3. Birefringence of compressed agar. A-C show heat maps of birefringence in regions of compressed 1.5% agar with high levels of predicted strain. The heat maps were generated by dividing the agar into grids and determining whether each square in the grid was birefringent after compression. The heat maps show the percentage out of seven replicates that each square in the grid was birefringent after compression. The white arrows indicate where tubes were inserted and the axis of compression. The scale to the left indicates the percentage of samples that were birefringent at each location. The diameters of the tubing inserted between the agar and the petri dish are shown below the heat maps. Each map corresponds to roughly the top left quarter of a plate, or roughly the top half of the maps in Figure 4.2. This experiment was performed by David J. Lemon.

increase in the percentage of samples which were birefringent at each location (Figure 4.3). When compressed with the smallest diameter tubing the majority of locations on the agar are birefringent, but there is a region immediately below and to the left of the inserted tubing (Fig. 4.3 A) which remains dark when viewed between cross-polarized filters, indicating this region remains random or chaotic even after compression. As the size of the inserted tubing increases and the agar gel is placed under greater degrees of compression this disordered region becomes smaller (Fig. 4.3 B), and eventually becomes birefringent (Figure 4.3 C).

These changes in birefringence vary in step with the distribution of predicted strain (Fig. 4.2), indicating that the polymers of the gels are increasingly aligned by larger and larger degrees of compression. The pattern of birefringence appears qualitatively similar to the predicted distribution of strain (Fig. 4.2), and regions with relatively large predicted strain tend to be birefringent (Fig. 4.3), indicative of an increase in order through polymer alignment. Strain-induced polymer alignment appears to be the most promising candidate yet for the stimulus which elicits the bacterial response to substrate compression.

4.1.5 Bacterial response

As we can predict strain and measure birefringence in both dimensions, not just down the center line of the plate, we can also map the bacterial response. To examine whether the previously observed changes in colony aspect ratios are due to the orientation of the polysaccharide fibers within the compressed agar substrate, cells were spotted in regions of the agar that have moderate to high levels of predicted strain and polysaccharide fiber alignment. It is notable that the aspect ratios tend to be large in the regions with moderate to high levels

of predicted strain, and presumably some degree of polysaccharide fiber alignment, and similar to those on uncompressed agar in regions with little no predicted strain and polysaccharide fiber alignment (Figure 3.2, 3.3 A, 4.2, 4.3). In the regions of the agar with moderate to high levels of predicted strain, the long axes of the colonies are parallel to the predicted direction of polysaccharide fiber alignment and the short axes are perpendicular to the aligned polysaccharide fibers (Figure 4.4). As mentioned above, as the diameter of the inserted tube increases, the regions of the agar with predicted strain and polysaccharide fiber alignment expand down the centerline moving away from the tube and across the axis perpendicular to the tube. As shown in Fig. 4.4 B-C, the regions of the agar slab where biased colony elongation

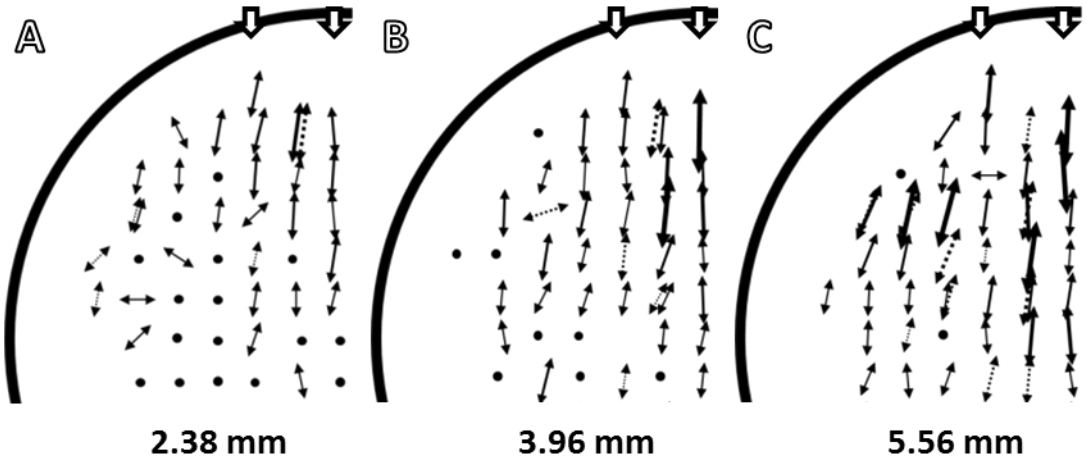

Figure 4.4. Surface spreading patterns at different locations on compressed agar. *M. xanthus* cells were spotted in regions of the agar that have moderate to high levels of predicted strain and aligned polysaccharide fibers. The arrows show the mean orientation of the short axes of 5-8 colonies (the long axes would be oriented 90° from the short axes) at each position and arrow length represents the relative mean aspect ratios. Dotted arrows represent data for colonies from comparable locations on the opposite side of the midline of the plate. Black circles represent mean aspect ratios below 1.1, similar to those observed on uncompressed agar. The diameters of the inserted tubing are noted below the diagrams. Each map corresponds to roughly one quarter of a plate, or roughly the top half of the maps in Figure 4.2. This experiment was performed by David J. Lemon.

is observed expands as the diameter of the inserted tube increases and the pattern of expansion is similar to that of predicted strain and polysaccharide fiber alignment.

4.2 Strain-induced alignment

Correlations of predicted strain with birefringence imply that strain-induced polymer alignment may well be the stimulus which elicits the bacterial response to substrate compression. We are most interested in polysaccharide substrates such as agar gels because of the previously discussed importance of exopolysaccharide matrix which surrounds cells in biofilms generally and because of the importance of slime in *M.*

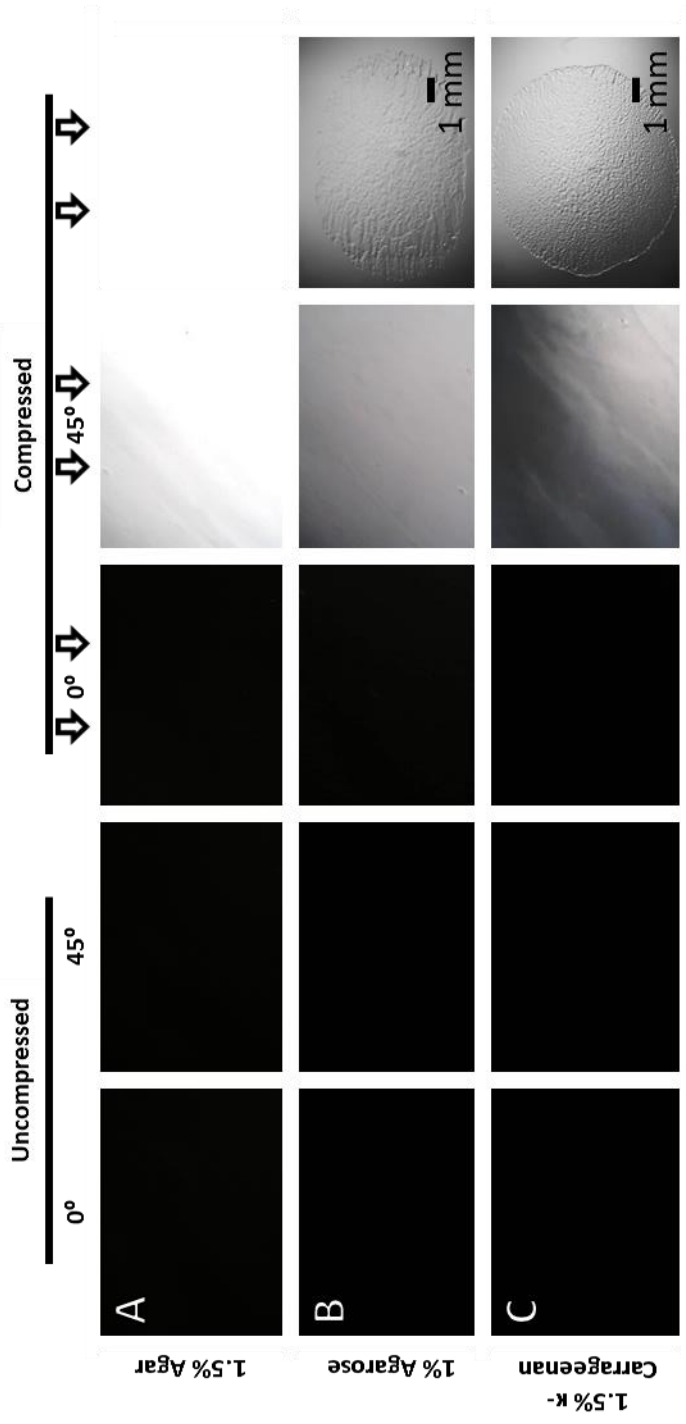

Figure 4.5. Birefringence of agar, agarose, and κ-carrageenan. Birefringence of 1.5% agar (A), 1% agarose (B), and 1.5% κ-carrageenan (C) gels before and after compression. The *M. xanthus* colony morphologies on compressed agarose and κ-carrageenan gels are shown in the right-most column. This experiment was performed by David J. Lemon.

xanthus behavior specifically. In addition to polysaccharide substrates, protein-based gels may also be useful if they behave similarly under compression. Collagen is a common substrate for eukaryotic, mammalian cell culture and may yield additional insight into the response of human cells to mechanical loads and aligned substrate in the future if it responds comparably to the polysaccharide substrates tested.

4.2.1 Polysaccharide hydrogels

4.2.1a Agar/agarose

Polymer alignment in response to compression has previously been discussed[13-15], though direct responses to such alignment have not been well characterized. We are most interested in polysaccharide substrates and their alignment upon compression due to the previously discussed importance of exopolysaccharide or slime to *M. xanthus* in particular and biofilm-forming species in general. Agar, produced by algae and composed chiefly of the linear polymer agarose, is the most common substrate for studies of microbiology and the substrate used for the majority of our experiments. Agarose gels are relatively stiffer and drier than agar gels of comparable concentration, but as agarose is a more refined product it is comparably more expensive and seldom used for large-scale microbiology experiments. Both agar (Fig. 4.5 A) and agarose (Fig. 4.5 B) gels become birefringent immediately upon compression by the insertion of a length of tubing between the wall of the plate and the gel slab, and indeed both produce similar effects on *M. xanthus* colony morphology (Figure 3.1 B, 4.5 B).

4.2.1b κ-Carrageenan

κ-Carrageenan is similarly produced by algae, and is also a linear polymer. Both agar/agarose[16-18] and κ-carrageenan[19] polysaccharides form entangled-polymer hydrogels when dissolved in water and heated above melting. Anecdotally, κ-carrageenan gels are much less prone to breaking than are agar gels of comparable concentration, κ-carrageenan gels are able to recover back to their original shape when compression is removed, and κ-carrageenan gels are optically clear. All of these properties make κ-carrageenan a useful stand-in or proxy for agar/agarose, as it is compressed it also elicits *M. xanthus* to form elongated colonies (Figure 4. 5 C). κ-Carrageenan gels also hold up to compression while still providing a softer, wetter surface for culturing species which are not as motile on agar gels. κ-Carrageenan gels, as mentioned previously, become birefringent immediately upon compression, however unlike agar κ-carrageenan gels can be made to partially

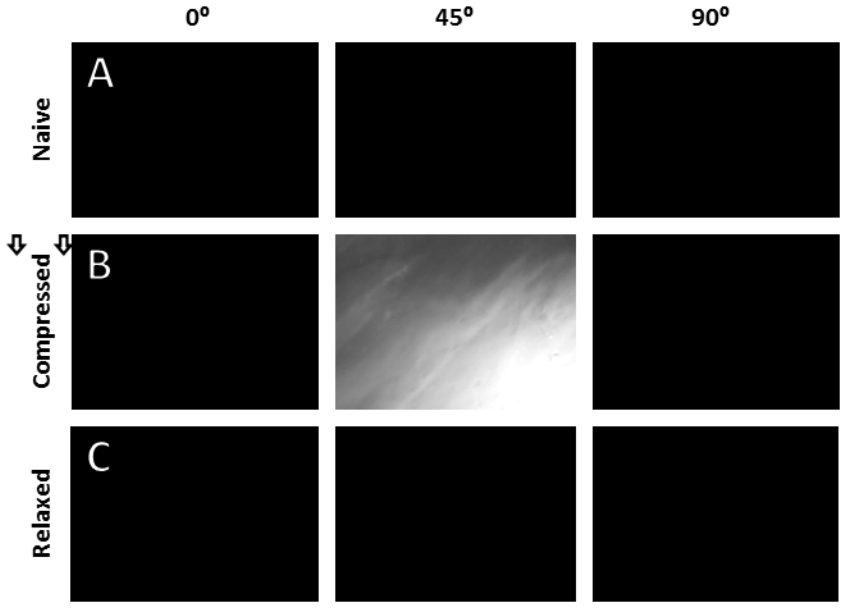

Figure 4.6. Reversible birefringence of 1.5% κ-carrageenan. Lack of birefringence in undisturbed 1.5% κ-carrageenan gel when rotated between cross-polarized filters shown in A. When compressed κ-carrageenan immediately becomes birefringent (B). When compression is removed the gel assumes its pre-compression shape and immediately loses its birefringence (C). Angles above the columns indicate the rotation of the sample between cross-polarized filters. White arrows indicate the axis of compression. This experiment was performed by David J. Lemon.

and reversibly compress themselves under their own weight. In these gels, also unlike agar, pre-compression shapes are recovered when compression is removed, and the gel immediately loses its birefringent properties as well (Figure 4.6).

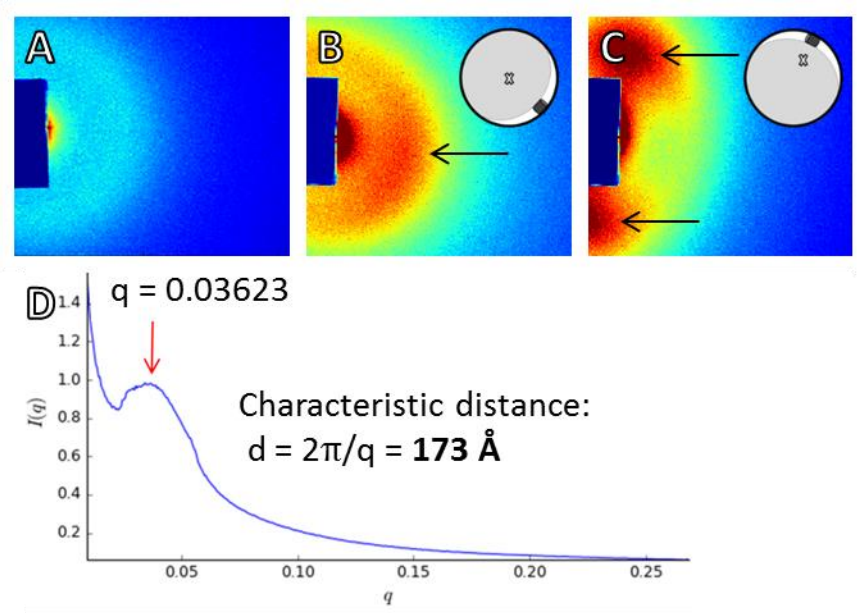

Figure 4.7. Small angle X-ray scattering (SAXS) analysis. The radially symmetric SAXS pattern before compression of the κ-carrageenan gel is shown in A. The initial incidence of the X-ray beam and the corresponding SAXS pattern for the compressed κ-carrageenan gel are shown in B. When the sample is rotated approximately 90°, as shown in C, the SAXS pattern has two lobes of greater intensity (C). The black arrows in B and C point to the lobes in the SAXS pattern. The plot of I(q) versus q shown in D has a peak at q=0.03623 (red arrow), which indicates a characteristic distance between adjacent, parallel long axes of polymer bundles of 173 Å. The values in D are representative of the pattern in C. This experiment and analysis was performed by Yan-Yeung Luk.

Birefringence is easily detected in real-time, and useful for our purposes with directly mapping the bulk alignment of polymers in a gel, but small-angle X-ray scattering (SAXS) experiments give more precise data regarding the arrangement of polymers within a gel. SAXS analysis measures the scattering of an X-ray beam by a sample. The beam passes through the sample and is deflected by it before hitting a two-dimensional detector. The intensity of the detected radiation, when combined with the degree of deflection, allows the user to calculate the anisotropy of the scattering and the characteristic distance between the polymers[18,20,21].

The graph of deflected radiation intensity, I(q), vs the magnitude of the scattering, q, from which the characteristic distance of 173 Å between parallel polymers is shown in Figure 4.6.

By examining the two-dimensional pattern of the SAXS analysis as the beam is moved around the κ-carrageenan sample, shown in Fig. 4.7, we observe that like strain, birefringence, and the *M. xanthus* response, polymer alignment is also relatively high in the regions closest to the inserted tubing. The two lobes of greater intensity in the SAXS pattern (Fig. 4.6 B-C, 4.7 C-D) are characteristic of nematic - head to tail alignment along the long axis - order, and indicate that the κ-carrageenan polymers in the compressed gel are aligned.

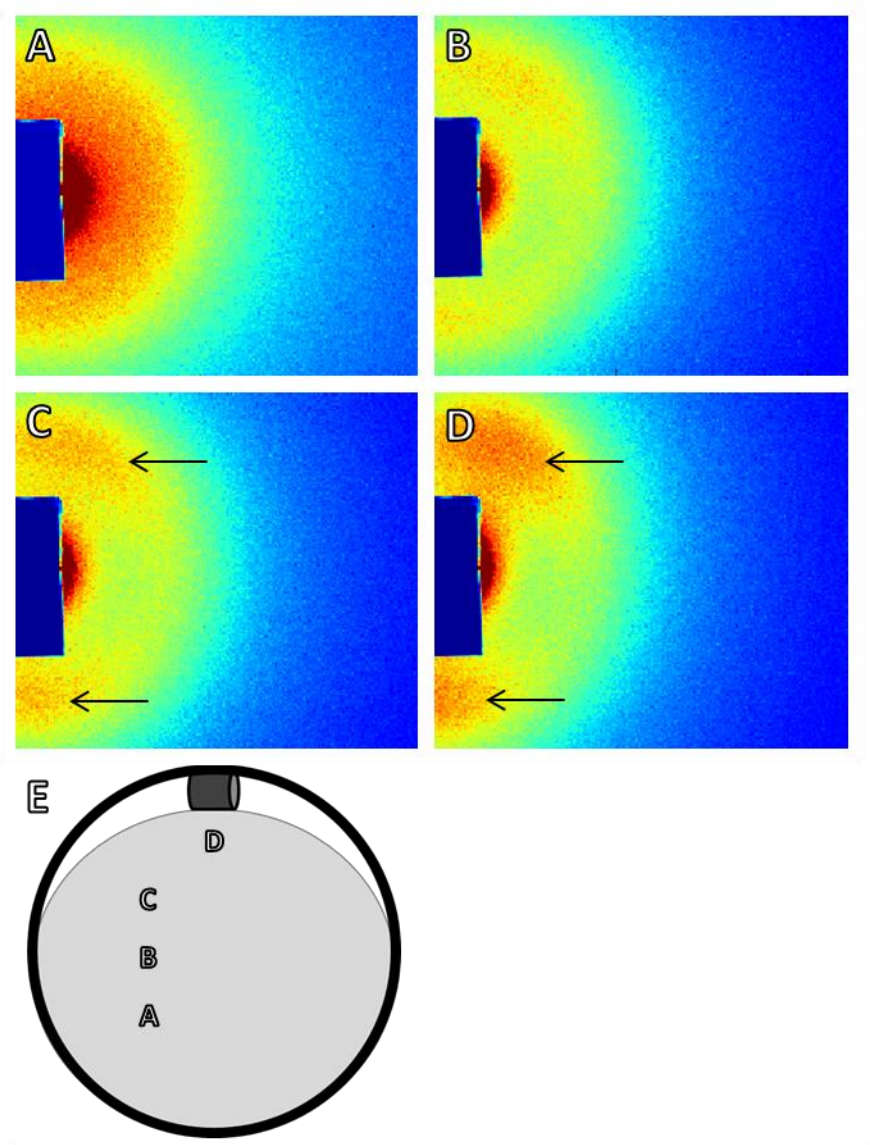

Figure 4.8. Small angle X-ray scattering (SAXS) analysis at different locations on compressed κ-carrageenan. A-D show the SAXS pattern when the incidence of the X-ray beam is shifted to different locations (shown in E) on the compressed κ-carrageenan gel. Black arrows point to the two lobes in the SAXS pattern. This experiment was performed by Yan-Yeung Luk.

Because of the similarities between agarose and κ-carrageenan, we take this result to mean that the tangled polymers in an agar gel would be comparably aligned by compression.

Based upon these findings, specifically the birefringence of agar and κ-carrageenan gels after compression, the alignment of the component polymers of compressed κ-carrageenan gels, and the correlations between predicted strain & aspect ratio (Fig. 3.4 B), predicted strain & birefringence (Fig. 4.2 and 4.3), and predicted strain & the orientation of the bacterial response to substrate compression (Fig. 4.4), we propose that compression of a polysaccharide hydrogel forces its component polymers into nematic (head to tail) alignment, and these aligned polymers elicit the bacterial response to substrate compression. With these new findings and conclusions we then suggest that "elasticotaxis"[8] is an incorrect term. "Inelasticotaxis" may be more precise, as the compression of agar is typically not reversible, though the term -taxis in microbiology settings typically requires additional experiments to confirm that, among other things, there is a gradient that is being sensed and responded to. We propose that there is no such gradient, as noted earlier even if there is indeed some gradient caused by the compression of the substrate that decays moving away from the inserted tubing, the bacteria would be moving across said gradient, rather than up it. The ending -tropism, more widely associated with plant behavior[22-25] than microbe behavior, is more appropriate. -tropism identifies a moving or bending in response to a stimulus, in this case the stimulus is polymer alignment. Therefore, we propose "polymertropism" to be a more precise and correct term than "elasticotaxis"[8], and use it in the remainder of this work accordingly.

4.2.2 Protein hydrogels

Though beyond the scope of this work, protein gels should also be tested for strain-induced polymer alignment and the capacity to elicit the polymertropism response, especially since these will be of further use in eukaryotic models, the findings from which are more readily applied to human biology and medicine. While protein-based substrates may be of less relevance to prokaryotic microbiology, some protein-based or protein functionalized substrates and scaffolds are widely used in eukaryotic and mammalian cell culture.

The least expensive protein-based gelling agent is gelatin. Commonly found in American kitchens, it is widely used to make gel-based desserts, however it does not readily form stable gels which can persist at room temperature, much less body temperature. This may be addressed with the addition of transglutaminase, an enzyme which cross-links proteins to proteins, though this adds a layer of complexity that is less than ideal. In the last decade this strategy has begun to take hold[26-28], though is still far from widespread.

The second, and more widely utilized protein-based gelling agent is collagen. 2D (collagen lined or coated surfaces) and 3D collagen gels are widely used in mammalian cell culture and experimental models[29-36]. Collagen has several advantages which offset its high cost: its component polymers can be visualized via light microscopy making direct and real-time characterization of its response to compression straightforward[32,33], it is found endogenously in the body and its response to mechanical loading or deformation is relatively well understood[31,37], and it is of relevance in disease prognostics[36]. Greater understanding of

mammalian cells' responses to compressed, aligned collagen may well yield an increased clinical understanding or improved techniques for tissue and organ culture or engineering.

4.3 Materials & methods

Substrate surfaces were examined with a Hirox KH-8700 3D digital microscope and with an AmScope T390A-PCS compound microscope. Grooved substrates in Fig. 4.1 were scored with the edge of a grooved fragment of a vinyl LP record.

For assays characterizing colony orientation and aspect ratio at various locations on the gels, the gels were divided into grids and 4 µl drops of *M*. *xanthus* at a density of 5 x 10^9 cells/ml were placed in each square on the grid. The same grid locations were used for birefringence assays. Cultures were incubated for 1 day at 30 °C, and the colony length (perpendicular to the direction of compression) and width (parallel to the direction of compression) were measured. 10-14 colony aspect ratios were determined for each position on the surface of the gels.

CTTYE broth with 1.5% agar was compressed using 1.5-cm pieces of Tygon tubing with a diameter of 2.38, 3.96, or 5.56 mm. Water that was squeezed out was allowed to evaporate. Gels in glass dishes were divided into grids and each square in the grid was examined between cross-polarized filters with an Olympus BX51 microscope fitted with a U-AN360P filter. Changes in birefringence were monitored visually as the sample was rotated between cross-polarized filters. The proportion of 7 replicates that were birefringent at each square on the grid was subsequently determined. Only the presence or absence of birefringence at each location was

noted; the magnitude of changes in birefringence was not determined. Strain was predicted as described in previous chapters.

SAXS data was collected on the G1 line at Cornell High Energy Synchrotron Source (CHESS). Briefly, a sheet of isotropic 25-um thick polystyrene (Goodfellow Cambridge Limited, England; model number LS437323 L O; ST311025/1) was taped onto a polyacrylic block with a circular hole such that the isotropic polystyrene was covering the hole. A black O-ring (outside diameter: 16.25 mm; inner diameter: 13.64 mm; thickness: 1.77 mm) was placed on top of the polystyrene sheet (Figure 4.8). The liquid 1.5% κ-carrageenan solution was kept from gelling with a heated water bath before being transferred to the O-ring with a Pasteur pipet. Any air bubbles were removed via a pipette. To compress the gel, a piece of cut O-ring was inserted

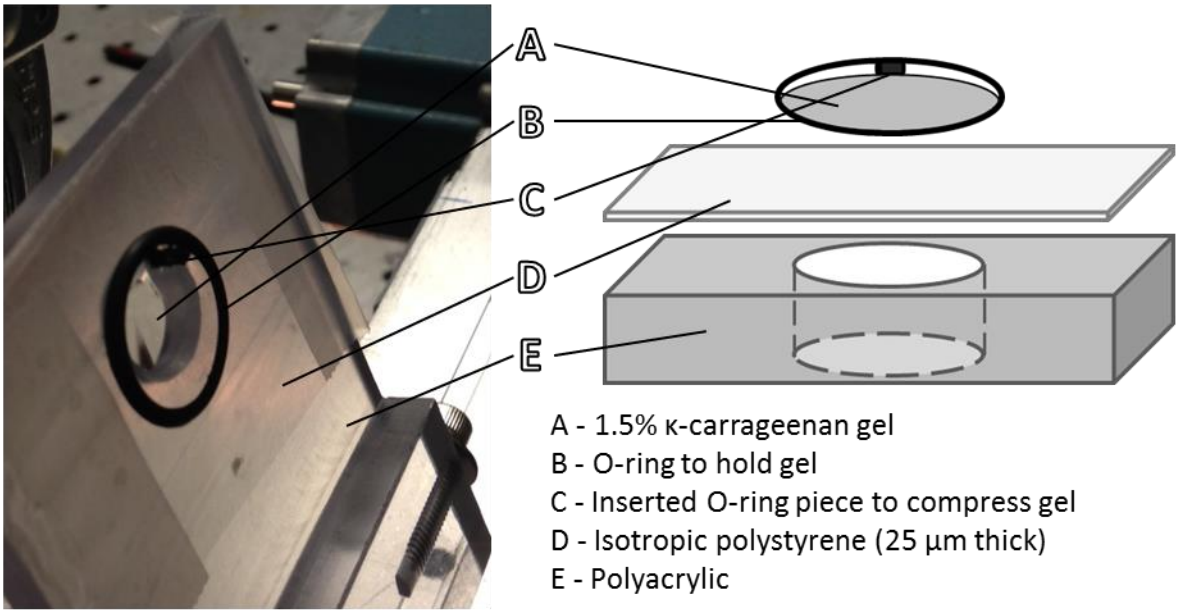

Figure 4.9. Experimental set-up of the small angle X-ray scattering (SAXS) analysis. The 1.5% κ-carrageenan gel (A) is held in position by an O-ring (B) and compressed by a piece of cut O-ring (C). The gel was placed on a 25 µm thick polystyrene plate (D), which was in turn placed over the hole in the polyacrylic support (E) such that the X-ray beam passed through the gel and the isotropic polystyrene, but not the polyacrylic support. This experiment was performed by Yan-Yeung Luk.

between the κ-carrageenan gel and the O-ring surrounding the gel, similar to the experimental set-up used in our earlier aspect ratio vs. distance experiments (Figure 3.3 A).

4.4 References

1 Keller, K. H., Grady, M. & Dworkin, M. Surface Tension Gradients: Feasible Model for Gliding Motility of *Myxococcus xanthus*. *J Bacteriol* **155**, 1358 - 1366 (1983).

2 Dworkin, M., Keller, K. H. & Weisberg, D. Experimental Observations Consistent with a Surface Tension Model of Gliding Motility of *Myxococcus xanthus*. *J Bacteriol* **155**, 1367 - 1371 (1983).

3 Friedlander, R. S. *et al.* Bacterial flagella explore microscale hummocks and hollows to increase adhesion. *PNAS* **110**, 5624 - 5629 (2013).

4 Meel, C., Kouzel, N., Oldewurtel, E. R. & Maier, B. Three-Dimensional Obstacles for Bacterial Surface Motility. *Small* **8**, 530 - 534 (2012).

5 Gu, H., Kolewe, K. W. & Ren, D. Conjugation in *Escherichia coli* Biofilms on Poly(dimethylsiloxane) Surfaces with Microtopographic Patterns. *Langmuir* **33**, 3142 - 3150 (2017).

6 Song, F., Koo, H. & Ren, D. Effects of Material Properties on Bacterial Adhesion and Biofilm Formation. *Oral Biology & Medicine* **94**, 1027 - 1034 (2015).

7 Shi, W. & Zusman, D. R. The two motility systems of *Myxococcus xanthus* show different selective advantages on various surfaces. *PNAS* **90**, 3378 - 3382 (1993).

8 Stanier, R. Y. A Note on Elasticotaxis in Myxobacteria. *J Bacteriol* **44**, 405 - 412 (1942).

9 Dworkin, M. Tactic behavior of *Myxococcus xanthus*. *J Bacteriol* **154**, 452 - 459 (1983).

10 Fontes, M. & Kaiser, D. Myxococcus cells respond to elastic forces in their substrate. *Proceedings of the National Academy of Sciences of the United States of America* **96**, 8052 - 8057 (1999).

11 Boral, S., Saxena, A. & Bohidar, H. B. Syneresis in agar hydrogels. *Int J Biol Macromol* **46**, 232-236, doi:10.1016/j.ijbiomac.2009.12.008 (2010).

12 Divoux, T., Mao, B. & Snabre, P. Syneresis and delayed detachment in agar plates. *Soft Matter* **11**, 3677 - 3685 (2015).

13 Osorio-Madrazo, A. *et al.* Reorientation of cellulose nanowhiskers in agarose hydrogels under tensile loading. *Biomacromolecules* **13**, 850-856, doi:10.1021/bm201764y (2012).

14 Wu, Z. L. *et al.* Strain-Induced Molecular Reorientation and Birefringence Reversion of a Robust, Anisotropic Double-Network Hydrogel. *Macromolecules* **44**, 3542-3547, doi:10.1021/ma200123u (2011).

15 White, D., Bott, D. C. & Weatherhead, R. H. Direct evidence for chain orientation in poly(acetylene). *Polymer* **14**, 805 - 809 (1983).

16 Roberts, J. J., Earnshaw, A., Ferguson, V. L. & Bryant, S. J. Comparative study of the viscoelastic mechanical behavior of agarose and poly(ethylene glycol) hydrogels. *J Biomed Mater Res B Appl Biomater* **99**, 158-169, doi:10.1002/jbm.b.31883 (2011).

17 Nayar, V. T., Weiland, J. D., Nelson, C. S. & Hodge, A. M. Elastic and viscoelastic characterization of agar. *J Mech Behav Biomed Mater* **7**, 60-68, doi:10.1016/j.jmbbm.2011.05.027 (2012).

18 Clarke, A. H., Rowlands, D. W. & Ross-Murphy, S. B. Small-angle X-ray Scattering Characterization of Agarose Sols and Gels. *Macromolecules* **22**, 180 - 188 (1989).

19 Michel, G. *et al.* The kappa-garrageenase of *P. carrageenovora* Features a Tunnel-Shaped Active Site: A Novel Insight in the Evolution of Clan-B Glycoside Hydrolases. *Structure* **9**, 513 - 525 (2001).

20 Martinez-Sanz, M., Gidley, M. J. & Gilbert, E. P. Application of X-ray and neutron small angle scattering techniques to study the hierarchical structure of plant cell walls: A review. *Carbohydrate Polymers* **125**, 120 - 134 (2015).

21 Trewhella, J. Small-angle scattering and 3D structure interpretation. *Curr Op Struct Biol* **40**, 1-7 (2016).

22 Bastien, R., Douady, S. & Moulia, B. A Unified Model of Shoot Tropism in Plants: Photo-, Gravi-, and Proprio-ception. *PLoS computational biology* **11** (2014).

23 Telewski, F. A unified hypothesis of mechanoperception in plants. *Am J Bot* **93**, 1466 - 1476 (2006).

24 Atamian, H. S. *et al.* Circadian regulation of sunflower heliotropism, floral orientation, and pollinator visits. *Science* **353**, 587 - 590 (2016).

25 Eapen, D., Barroso, M. L., Ponce, G., Campos, M. E. & Cassab, G. I. Hydrotropism: root growth responses to water. *Trends Plant Sci* **10**, 44-50, doi:10.1016/j.tplants.2004.11.004 (2005).

26 Paguirigan, A. L. & Beebe, D. J. Protocol for the fabrication of enzymatically crosslinked gelatin microchannels for microfluidic cell culture. *Nature Protocols* **2**, 1782 - 1788 (2007).

27 Fang, J. Y., Tan, S.-J., Yang, Z., Tayag, C. & Han, B. Tumor Bioengineering Using a Transglutaminase Crosslinked Hydrogel. *PloS one* **9** (2013).

28 Bettadapur, A. *et al.* Prolonged Culture of Aligned Skeletal Myotubes on Micromolded Gelatin Hydrogels. *Sci Rep* **6**, 28855, doi:10.1038/srep28855 (2016).

29 Leong, W. S. *et al.* Thickness sensing of hMSCs on collagen gel directs stem cell fate. *Biochem Biophys Res Commun* **401**, 287-292, doi:10.1016/j.bbrc.2010.09.052 (2010).

30 Matsugaki, A., Isobe, Y., Saku, T. & Nakano, T. Quantitative regulation of bone-mimetic, oriented collagen/apatite matrix structure depends on the degree of osteoblast alignment on oriented collagen substrates. *Journal of biomedical materials research. Part A* **103**, 489-499, doi:10.1002/jbm.a.35189 (2015).

31 Braziulis, E. *et al.* Modified plastic compression of collagen hydrogels provides an ideal matrix for clinically applicable skin substitutes. *Tissue Eng Part C Methods* **18**, 464-474, doi:10.1089/ten.TEC.2011.0561 (2012).

32 Harris, A. K., Stopak, D. & Wild, P. Fibroblast traction as a mechanism for collagen morphogenesis. *Nature* **290**, 249-251 (1981).

33 Miron-Mendoza, M., Seemann, J. & Grinnel, F. Collagen fibril flow and tissue translocation coupled to fibroblast migration in 3d collagen matrices. *Molecular biology of the cell* **19**, doi:10.1091/mbc.E07-09-0930) (2008).

34 Feng, Z. *et al.* Analysis of the contraction of fibroblast collagen gels and the traction force of individual cells by a novel elementary structural model. *35th Annual International Conference of the IEEE EMBS*, 6232-6235 (2013).

35 Keely, P. J., Fong, A. M., Zutter, M. M. & Santoro, S. A. Alteration of collagen-dependent adhesion, motility, and morphogenesis by the expression of antisense alpha 2 integrin mRNA in mammary cells. *Journal of cell science* **108**, 595 - 607 (1995).

36 Conklin, M. W. *et al.* Aligned collagen is a prognostic signature for survival in human breast carcinoma. *Am J Pathol* **178**, 1221-1232, doi:10.1016/j.ajpath.2010.11.076 (2011).

37 Busby, G. A., Grant, M. H., Mackay, S. P. & Riches, P. E. Confined compression of collagen hydrogels. *Journal of biomechanics* **46**, 837-840, doi:10.1016/j.jbiomech.2012.11.048 (2013).

Chapter 5 - Conservation of polymertropism

5.1 Universality of polymertropism

What we now identify as polymertropism has been observed previously in a handful of different, evolutionarily distant bacterial species[1-5]. We screened a number of additional bacterial species on both agar and κ-carrageenan gels with a variety of media compositions for the polymertropism response, and found it to be a relatively common trait (Table 5.1). While some of the strains identified as polymertropism-positive have been thought to be non-motile, the vast majority of polymertropism responders were rod-shaped, motile biofilm-forming bacteria, and the majority of rod-shaped, motile species tested displayed polymertropism on compressed substrates (Table 5.1). This screen was far from exhaustive. I tested a handful of different media compositions with both agar and carrageenan, but did produce noteworthy results.

5.1.1 Conservation across evolutionary time

Bacteria from four phyla were tested in either our screen or previous work by other groups[1-5]. The two phyla with the largest number of polymertropism positive species were the firmicutes, which include the *Bacillus* and *Paenibacillus* species and the proteobacteria, which include *M. xanthus*, *Pseudomonas*, *Proteus*, *Salmonella*, and *Shigella* species (Table 5.1). Interestingly, these two phyla are very evolutionarily distant from one another in the bacterial phylogenetic tree[6], only one other phylum is more distant from the proteobacteria than the firmicutes are. Of note, only rod-shaped cells were found to display the polymertropism response, and though these cells are often motile while spherical cells are not, it may also be

Species name	Phylum	Shape	Motile	Polymertropism	Reference	Source[a]	Gelling agent	Media	Temperature
Alcaligenes faecalis	Proteobacteria	Rod	Yes	Yes	This study	CBSC 154835A	1% κ-carrageenan	CTTYE	37 °C
Bacillus cereus	Firmicute	Rod	Yes	Yes	This study	CBSC 154870A	1.5% agar	CTTYE	30 °C
Bacillus megaterium	Firmicute	Rod	Yes	Not observed	This study	NRRL B-14308	1.5% agar	CTTYE	30 °C
Bacillus mycoides	Firmicute	Rod	No	Yes, previously observed	This study, Stratford *et al.* 2013[4]	NRRL B-14811	1.5% agar	CTTYE	30 °C
Bacillus subtilis	Firmicute	Rod	Yes	Yes	This study, Polka & Silver 2014[5]	NRRL B-354	1.5% agar	CTTYE	30 °C
Corallococcus exiguus	Proteobacteria	Rod	Yes	Previously observed	Stanier 1942[1]	-	2% agar	Dung[1]	Not provided
Enterococcus faecalis	Firmicute	Sphere	No	Not observed	This study	CBSC 155600A	-	-	-
Escherichia coli K12	Proteobacteria	Rod	Yes	Not observed	This study	NRRL B-3707	-	-	-
Escherichia coli RP437/pRSH103	Proteobacteria	Rod	Variable	Inconclusive[b]	This study	D. Ren[23]	-	-	-
Flavobacterium johnsoniae	Bacteriodetes	Rod	Yes	Previously observed	Fontes & Kaiser 1999[2]	-	1.5% agar	PY2[24]	27 °C
Klebsiella pneumoniae	Proteobacteria	Rod	No	Not observed	This study	CBSC 155095A	-	-	-
Lactococcus lactis	Firmicute	Sphere	No	Not observed	This study	CBSC 155610A	-	-	-
Micrococcus luteus	Actinobacteria	Sphere	No	Not observed	This study	CBSC 155155A	-	-	-
Micrococcus roseus	Actinobacteria	Sphere	No	Not observed	This study	CBSC 155160	-	-	-
Mycobacterium phlei	Actinobacteria	Rod	No	Not observed	This study	CBSC 155170A	-	-	-
Myxococcus xanthus	Proteobacteria	Rod	Yes	Yes	This study, Fontes & Kaiser 1999[2]	-	1.5% agar	CTTYE	30 °C
Paenibacillus alvei	Firmicute	Rod	Yes	Yes	This study	NRRL B-383	0.5% κ-carrageenan	CTTYE	37 °C
Paenibacillus dendritiformis	Firmicute	Rod	Yes	Yes	This study	NRRL B-23299	1.5% agar	CTTYE	30 °C
Paenibacillus phoenicis	Firmicute	Rod	Yes	Yes	This study	NRRL B-59348	1.25% κ-carrageenan	ECM[25]	37 °C
Proteus mirabilis	Proteobacteria	Rod	Yes	Yes	This study	CBSC 155239A	0.5% κ-carrageenan	CTTYE	37 °C
Proteus vulgaris	Proteobacteria	Rod	Yes	Not observed	This study	CBSC 155240A	-	-	-
Pseudomonas aeruginosa	Proteobacteria	Rod	Yes	Yes	This study	CBSC 155250A	0.5% κ-carrageenan	CTTYE	37 °C
Pseudomonas fluorescens	Proteobacteria	Rod	Yes	Not observed	This study	CBSC 155255A	-	-	-
Salmonella enteritidis	Proteobacteria	Rod	Yes	Yes	This study	CBSC 155350A	1% κ-carrageenan	CTTYE	37 °C
Salmonella typhimurium	Proteobacteria	Rod	Yes	Yes	This study	CBSC 155351A	0.5% κ-carrageenan	CTTYE	37 °C
Serratia marcescens	Proteobacteria	Rod	Yes	Yes	This study	NRRL B-23389	1.5% agar	CTTYE	25 °C
Shigella flexneri	Proteobacteria	Rod	No[c]	Yes	This study	CBSC 155470A	0.5% κ-carrageenan	CTTYE	37 °C
Staphylococcus epidermis	Firmicute	Sphere	No	Not observed	This study	CBSC 155556A	-	-	-

[a]Carolina Biological Supply Co. (CBSC) or USDA Northern Regional Research Lab Culture Collection (NRRL) catalog numbers.
[b]The colonies did not show anisotropic spreading on 1.5% agar. On 1% and 1.25% κ-carrageenan anisotropic spreading was observed for some experiments and not others.
[c]*Shigella flexneri* colonies had a slow expansion rate and did not show anisotropic spreading on 1.5% agar. On 0.5% and 1.25% κ-carrageenan the colonies expanded more rapidly and the colony expansion was anisotropic.

Table 5.1. Polymertropism species screen.

the case

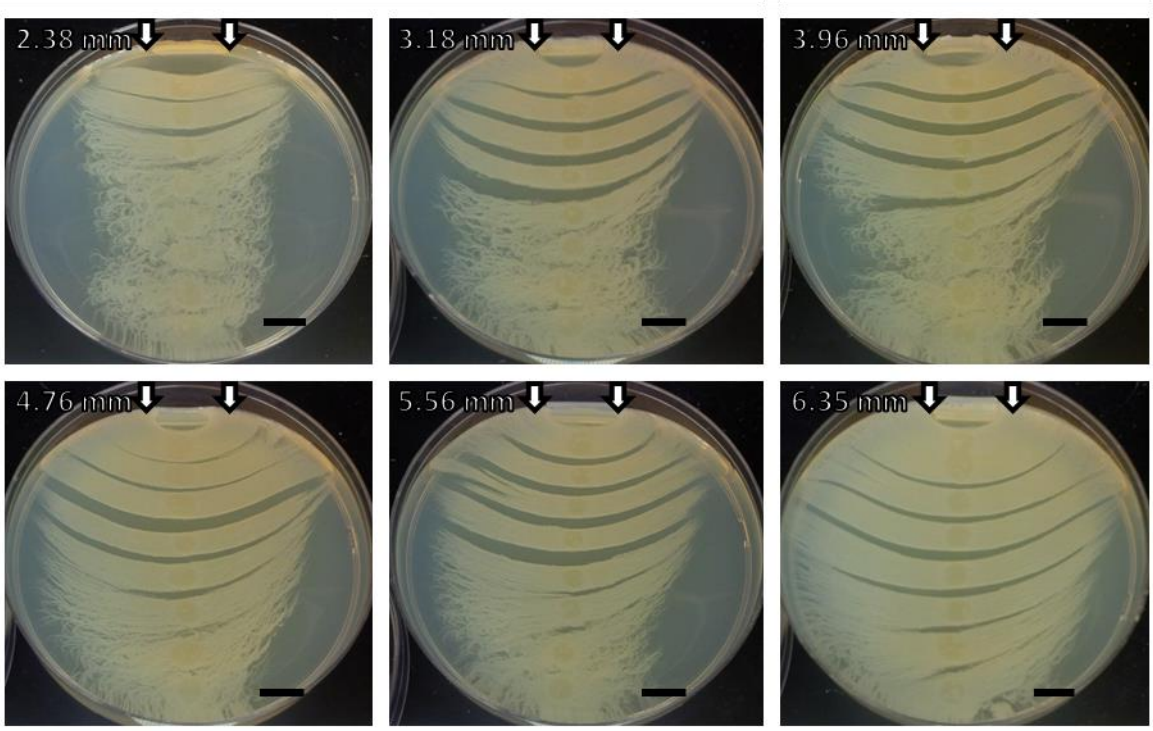

Figure 5.1. Polymertropism response of *Bacillus mycoides* . 24 hour *B. mycoides* colonies on compressed 1.5% agar nutrient-rich substrates. White arrows indicate axis of compression. Size of inserted tubing for each image listed in upper left. Scale bars represent 1 cm. This experiment was performed by David J. Lemon.

that the nature of self-propelled rods[7-11] has something to do with this response to nematic polymer arrangements, as logs floating on a river or wires on a vibrating plate display similar capacity for alignment[12-14].

That such a wide expanse of evolutionary time separates these two groups, which both include a large fraction of the species identified to be positive for polymertropism, seems to imply that the response to aligned polymers plays some larger role in the lifecycles of these species to their benefit, or at least is a neutral behavior which neither helps nor hurts the fitness of the cells which respond to aligned polymers.

5.1.2 Conservation across motility systems

In addition to being conserved across evolutionary time, the polymertropism response is also conserved across a variety of motility apparatuses (Table 5.1). Interestingly, the strongest response we observed occurred in *Bacillus mycoides* (Fig. 5.1), a species categorized as non-motile. *B. mycoides*' response is both rapid and strong, in 24 hours it is able to spread across the width of the plate while maintaining separation from the colonies immediately adjacent to it on substrates with relatively higher degrees of compression (Figure 5.1). *B. mycoides* is not the only species characterized as non-motile to possess the polymertropism response; *Shigella flexneri* also displays elliptical growth and spreading patterns, though *S. flexneri* only does so on compressed κ-carrageenan substrates (Table 5.1)

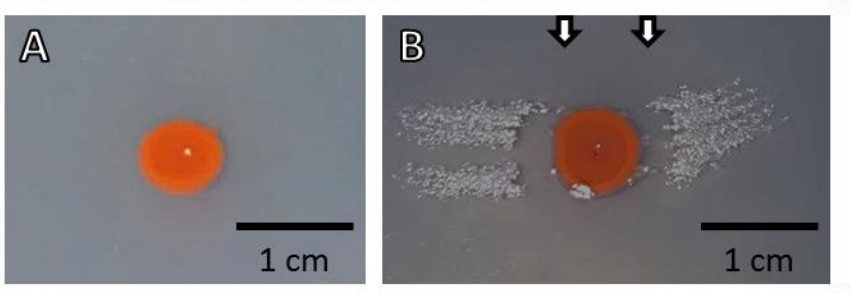

C

	25% *B. mycoides*, 75% *S. marcescens*	
	B. mycoides	*S. marcescens*
Mean # of colonies (0 mm)	0	116.5 ± 12.3
Mean # of colonies (5.56 mm)	20 ± 2.4	175.5 ± 8.9
	50% *B. mycoides*, 50% *S. marcescens*	
	B. mycoides	*S. marcescens*
Mean # of colonies (0 mm)	0	188.75 ± 9.6
Mean # of colonies (5.56 mm)	44.75 ± 5.0	223.75 ± 4.2
	75% *B. mycoides*, 25% *S. marcescens*	
	B. mycoides	*S. marcescens*
Mean # of colonies (0 mm)	8.25 ± 1.1	159.75 ± 7.7
Mean # of colonies (5.56 mm)	20.75 ± 2.6	185.5 ± 11.8

Figure 5.2. Survival in mixed-species biofilms. *S. marcescens* (red) survives in greater number than *B. mycoides* (white) after 24 hours on uncompressed media as shown in A. *B. mysoices* escapes and survives on compressed substrates, shown in B. *B. mycoides* survives in greater numbers on compressed substrates regardless of initial concentrations in mixed-species biofilms with *S. marcescens*, C. White arrows in B indicate the axis of compression. Means in C are ± S.E.M. Calculated from 3 technical replicates. Lengths in C represent degree of compression. This experiment was performed by David J. Lemon and Derek A. Schutzman.

and appears non-motile on agar.

While the mechanism which produces the directional spreading of *B. mycoides* and *S. flexneri* is unknown, many of the species we observe to produce the polymertropism response

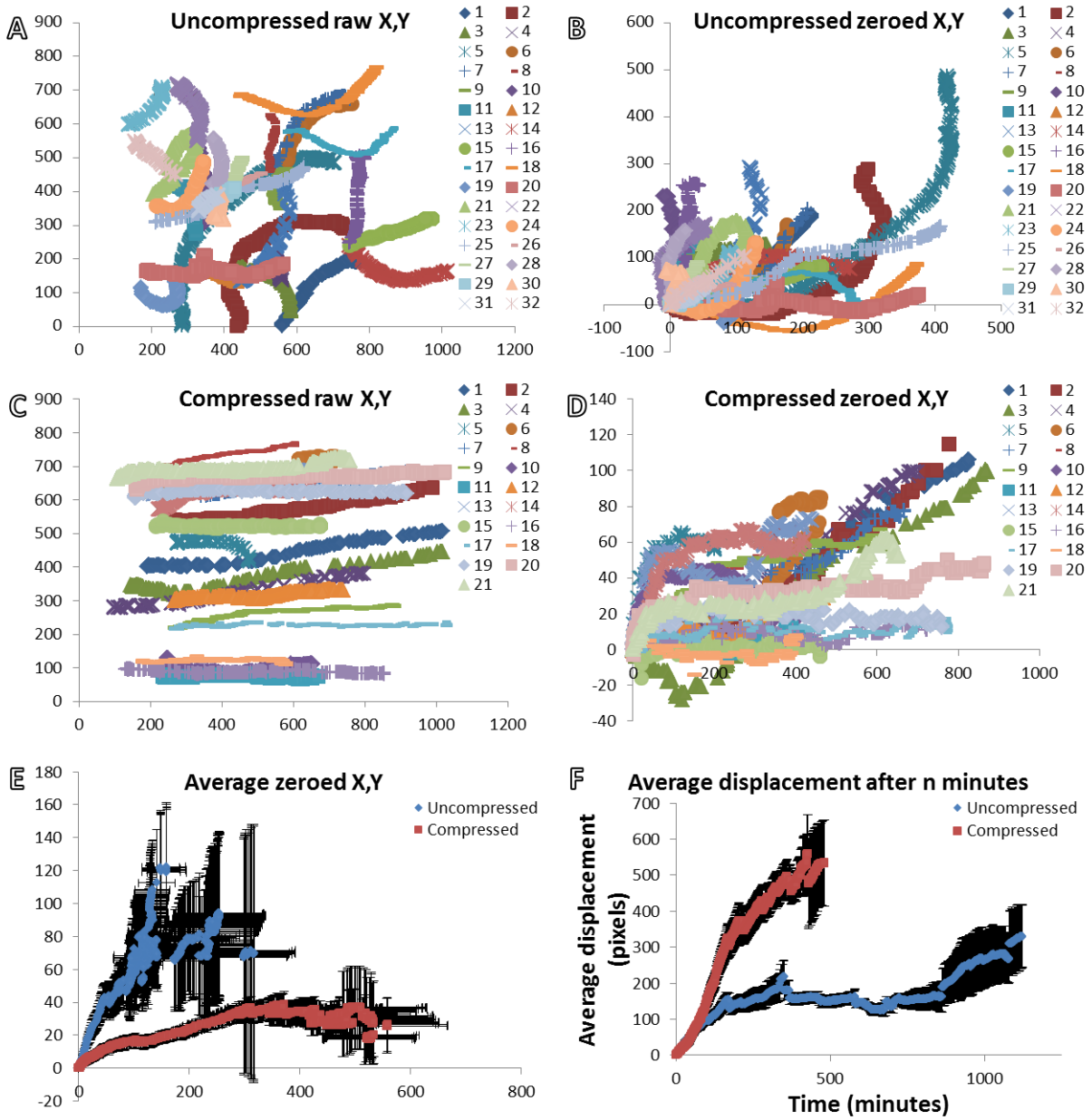

Figure 5.3. *B. mycoides* tracking data and analysis. Tracks extracted from time-lapse video results in raw X,Y position data over time as shown in A. Starting X,Y value subtracted from each track's raw X,Y such that all tracks start at 0,0, called zeroed X,Y, shown in B. Raw and zeroed data for compressed substrates shown under uncompressed data (C and D). Zeroed X,Y data averaged for each time interval to generate average zeroed X,Y (+/- S.E.M.) as shown in E. Displacement after each minute pooled to calculate average displacement after n minutes shown in F. This experiment was performed by David J. Lemon and Derek A. Schutzman.

on compressed substrates have mechanisms of surface motility which have been identified. Flagella-based, type IV pili or twitching based, and gliding or focal adhesion-based motility mechanisms have all, in at least one species, proved effective at polymertropism. The use of κ-carrageenan gels in addition to agar gels enabled us to test species which are not usually motile on harder, drier surfaces such as 1.5% agar. Species motile on 0.4% or lower agar may be better suited to culturing on κ-carrageenan gels, which are wetter than agar gels of the same concentration, but hold up to compression where soft-agar gels cannot.

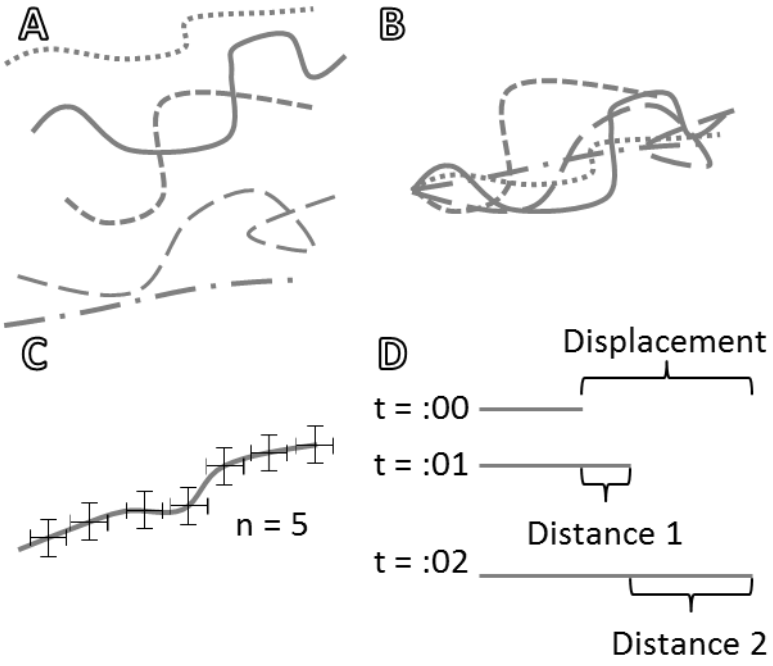

Figure 5.4. Schematic of tracking data analysis. Tracks extracted from time-lapse video results in raw X,Y position data over time as shown in A. Starting X,Y value subtracted from each track's raw X,Y such that all tracks start at 0,0, called zeroed X,Y, shown in B. Zeroed X,Y data averaged for each time interval to generate average zeroed X,Y (+/- S.E.M.) as shown in C. Minute-to-minute distance for each time interval calculated as shown in D were pooled to calculate average speed. Displacement at track end calculated as shown in D were pooled to calculate average displacement at track end. This analysis was performed by David J. Lemon.

5.2 Fitness benefits from polymertropism

That polymertropism is observed in species from widely divergent phyla, and which utilize a variety of motility apparatuses seems to imply that it is somehow either important to,

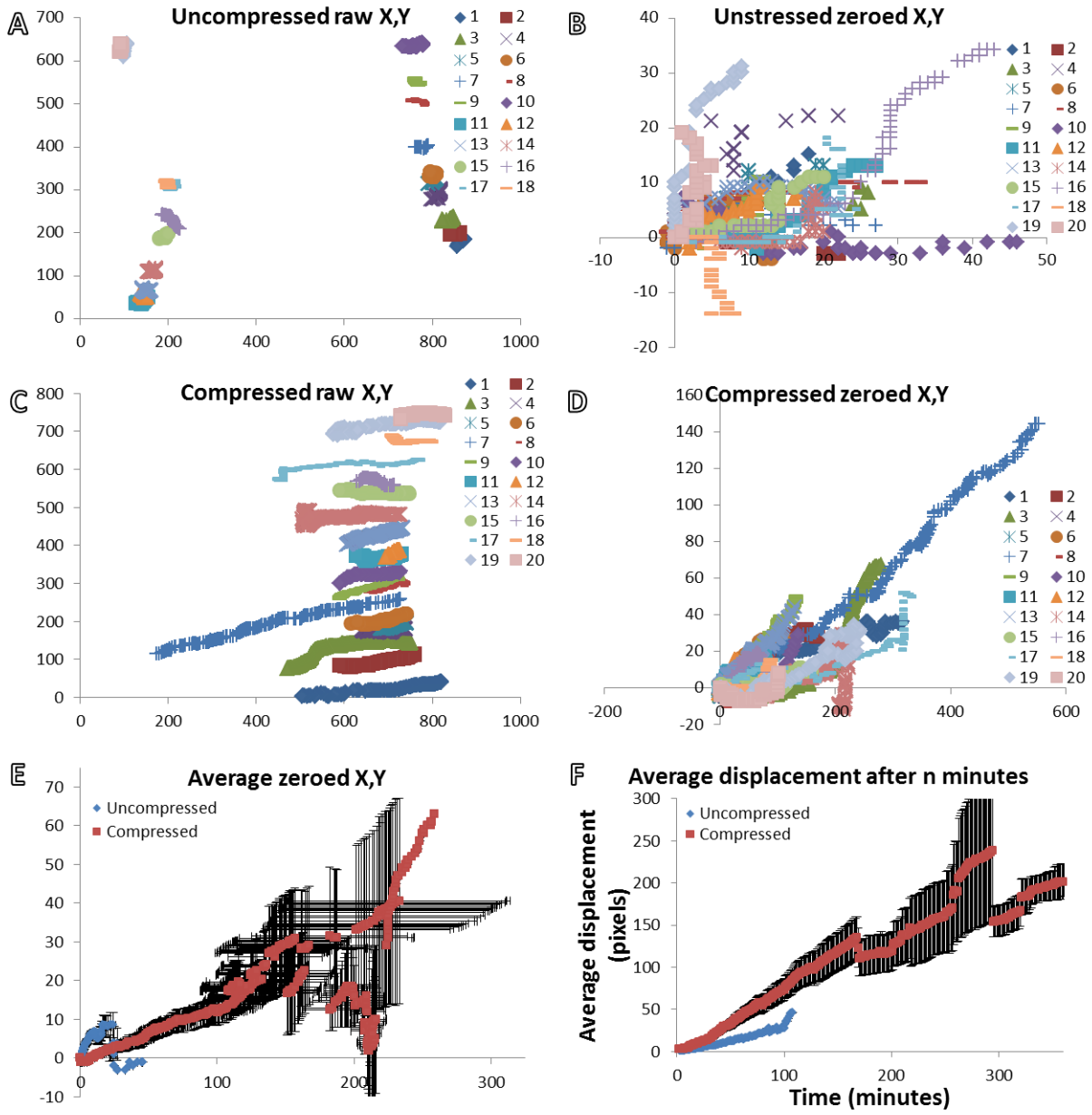

Figure 5.5. *B. subtilis* tracking data and analysis. Tracks extracted from time-lapse video results in raw X,Y position data over time as shown in A. Starting X,Y value subtracted from each track's raw X,Y such that all tracks start at 0,0, called zeroed X,Y, shown in B. Raw and zeroed data for compressed substrates shown under uncompressed data (C and D). Zeroed X,Y data averaged for each time interval to generate average zeroed X,Y (+/- S.E.M.) as shown in E. Displacement after each minute pooled to calculate average displacement after n minutes shown in F. This experiment was performed by David J. Lemon and Derek A. Schutzman.

or at least indifferent to, the lifecycle of biofilm-forming bacteria. The advantage of altered behavior on aligned polymers may present as the ability to escape from the presence of other species, move faster in the direction of polymer alignment, or impact biofilm formation at the earliest stages of aggregation and biofilm development.

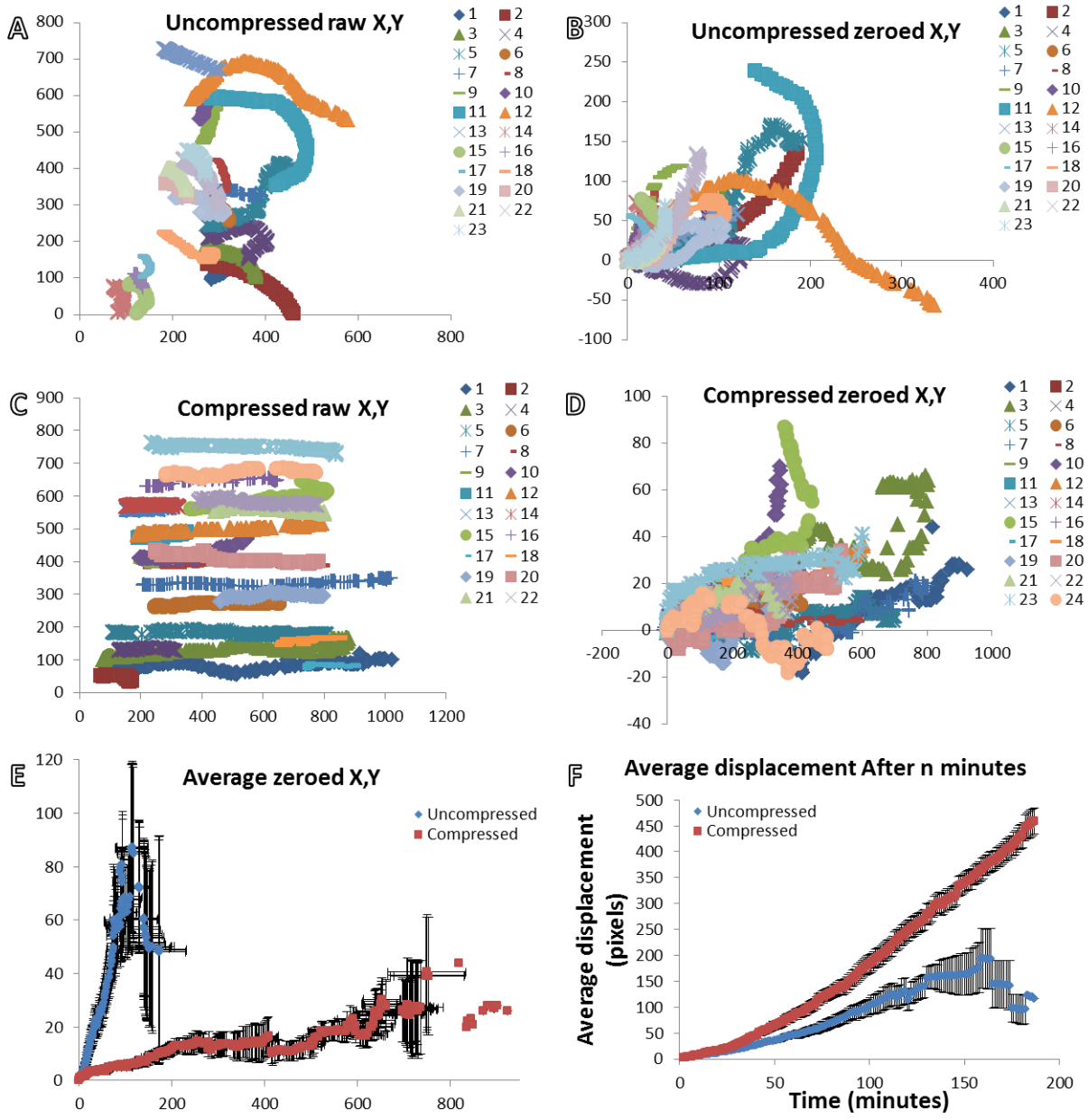

Figure 5.6. *B. cereus* tracking data and analysis. Tracks extracted from time-lapse video results in raw X,Y position data over time as shown in A. Starting X,Y value subtracted from each track's raw X,Y such that all tracks start at 0,0, called zeroed X,Y, shown in B. Raw and zeroed data for compressed substrates shown under uncompressed data (C and D). Zeroed X,Y data averaged for each time interval to generate average zeroed X,Y (+/- S.E.M.) as shown in E. Displacement after each minute pooled to calculate average displacement after n minutes shown in F. This experiment was performed by David J. Lemon and Derek A. Schutzman.

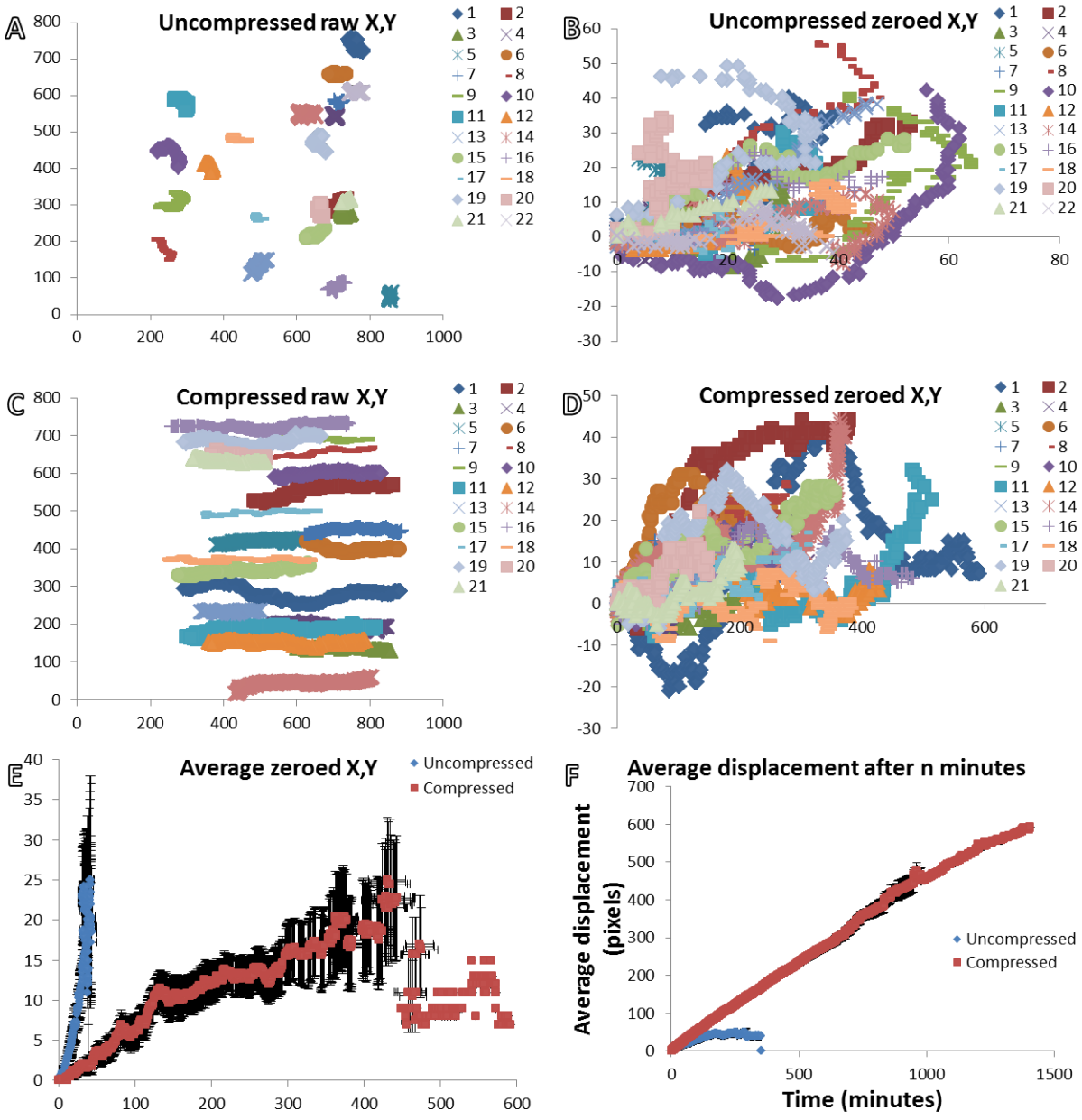

Figure 5.7. *M, xanthus* tracking data and analysis. Tracks extracted from time-lapse video results in raw X,Y position data over time as shown in A. Starting X,Y value subtracted from each track's raw X,Y such that all tracks start at 0,0, called zeroed X,Y, shown in B. Raw and zeroed data for compressed substrates shown under uncompressed data (C and D). Zeroed X,Y data averaged for each time interval to generate average zeroed X,Y (+/- S.E.M.) as shown in E. Displacement after each minute pooled to calculate average displacement after n minutes shown in F. This experiment was performed by David J. Lemon and Derek A. Schutzman.

5.2.1 Competition and survival

To test if a strong polymertropism response might confer a fitness or survival advantage on an artificially aligned substrate over a species which does not have a similarly strong response, but is otherwise able to out-compete the polymertropism positive species, we mixed liquid cultures of two species together and spotted this mixture on compressed and uncompressed substrates. *B. mycoides*, which has the strong polymertropism response as discussed above (Fig. 5.1), is typically unable to compete with *Serratia marcescens*, a species which has a much weaker polymertropism response, however when these two species are inoculated together on a compressed substrate the *B. mycoides* is able to escape the footprint of *S. marcescens* and survive in greater numbers to 24 hours (Figure 5.2). In three different proportions - 3:1 in favor of *S. marcescens*, 1:1, and 3:1 in favor of *B. mycoides* - *B. mycoides* survives in greater numbers on compressed substrates than on uncompressed substrates

	Flare speed (pixels / minute)		Flare duration (minutes)		Final displacement (pixels)	
	Uncompressed	Compressed	Uncompressed	Compressed	Uncompressed	Compressed
B. mycoides	1.22 +/- 0.027	2.18 +/- 0.052	272.0 +/- 29.7	327.8 +/- 23.9	197.3 +/- 24.3	581.2 +/- 43.1
B. subtilis	0.49 +/- 0.022	1.01 +/- 0.027	96.9 +/- 7.3	236.2 +/- 24.3	26.2 +/- 2.7	171.2 +/- 28.0
B. cereus	1.62 +/- 0.040	2.90 +/- 0.074	112.7 +/- 8.5	184.9 +/- 16.0	119.8 +/- 16.5	400.4 +/- 48.8
M. xanthus	0.71 +/- 0.018	0.82 +/- 0.013	179.0 +/- 16.8	745.5 +/- 51.2	41.4 +/- 3.6	324.9 +/- 24.5

	Speed (x increase)	Duration (x increase)	Displacement (x increase)
B. mycoides	1.781148338	1.205043626	2.945459536
B. subtilis	2.074293507	2.437048504	6.523350217
B. cereus	1.790399056	1.640850051	3.341441737
M. xanthus	1.147134967	4.165729284	7.840056231

Table 5.2. Flare speed, duration, and displacement. Average values for flare speed, flare duration, and displacement at track end from Fig. 5.3, 5.5, 5.6, and 5.7 are presented +/- S.E.M. Fold increases in bottom portion represent the gain in speed, duration, or displacement for each species on compressed relative to uncompressed substrates. This analysis was performed by David J. Lemon.

(Figure 5.2). While this is an admittedly best-case scenario for polymertropism; the strongest response to compression observed paired with a compressed substrate, it is an example nonetheless of polymertropism conferring a fitness, survival, or competitive benefit on the species which has a strong polymertropism response.

5.2.2 Increased speed, displacement, and duration of flares

While the mixed-species biofilm experiment and species screen described above are certainly useful, they do not yield insight into what the polymertropism response looks like in

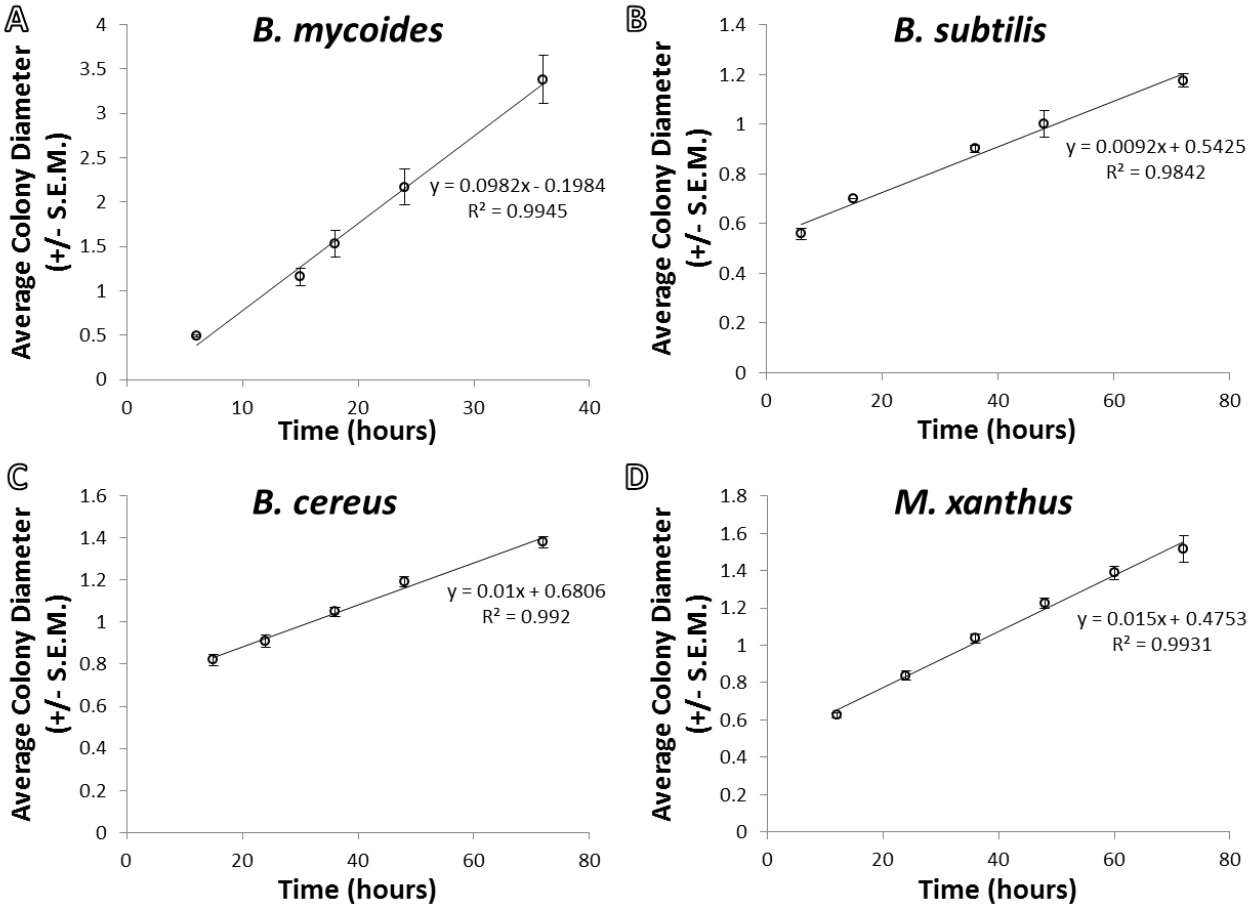

Figure 5.8. Motility over time. Average colony diameter +/- S.E.M. on 1.5% agar nutrient-rich media for *B. mycoides* (A), *B. subtilis* (B), *B. cereus* (C), and *M. xanthus* (D). Line of best fit calculated and displayed with its equation. Slope of the line of best fit represents the species' average rate of motility. This experiment was performed by David J. Lemon.

real-time as it is occurring. To bridge this gap we used time-lapse microscopy, capturing one frame every minute at low magnification for up to 24 hours, to examine how flare behavior is altered during the polymertropism response of four species: *Bacillus mycoides*, *Bacillus subtilis*, *Bacillus cereus*, and *Myxococcus xanthus*.

B. mycoides, which has the most pronounced polymertropism response (Fig. 5.1) of those we tested, displays generally curving flares on uncompressed substrates (Fig. 5.3 A-B), but relatively straight flares on compressed substrates (Figure 5.3 C-D). While *B. mycoides*' colonies are evidently curved over long distances (Fig. 5.1), over the short distance of the 35x

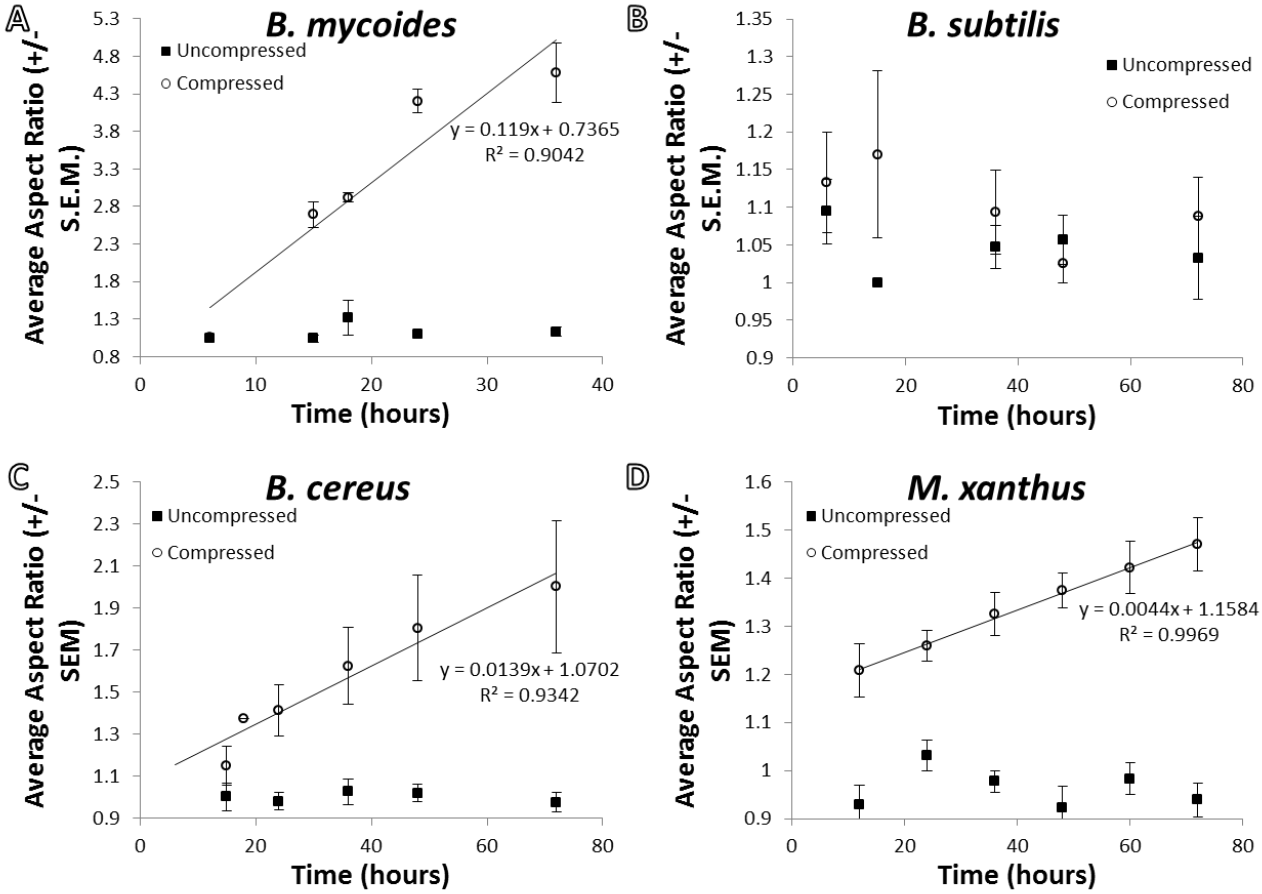

Figure 5.9. Aspect ratio over time. Average colony aspect ratio +/- S.E.M. on 1.5% agar nutrient-rich media for *B. mycoides* (A), *B. subtilis* (B), *B. cereus* (C), and *M. xanthus* (D). Line of best fit calculated and displayed with its equation. Slope of the line of best fit represents the species' average whole-colony rate of polymertropism. This experiment was performed by David J. Lemon.

field of view they appear to be nearly perpendicular to the axis of compression (Figure 5.3 C-D). When the raw X,Y data from these flares are converted to zeroed X,Y data such that all flares begin at 0,0 and move predominantly into quadrant I as demonstrated in Fig. 5.4, and the zeroed X,Y data are averaged to compare flare shape or trajectory, quantitative differences in flare trajectory emerge (Figure 5.3 E). On compressed substrates flares move much more in the X axis than the Y axis, while the opposite is true on uncompressed substrates (Figure 5.3 E). These differences in trajectory quickly add up to differences in average displacement from the flares' beginning. It takes no more than a few hours for the flares on compressed substrates to move further away from their origin than flares on uncompressed substrates do (Figure 5.3 F). These differences continue to pile up over time such that, on average, flares undergoing polymertropism reach nearly twice as far away from their origin than comparable flares on uncompressed substrates do (Figure 5.3 F).

These same general trends observed in *B. mycoides* also appear when flare behavior in the other three species are analyzed (Figure 5.5, 5.6, 5.7). While *B. mycoides* is not the fastest species we tested on compressed substrates, *B. cereus* is, *B. mycoides*' flares persist approximately twice as long (Table 5.2), which implies that while flare speed is surely important in the polymertropism response, speed alone may not be sufficient to cause the drastically elongated colonies characteristic of the strongest polymertropism responses. It is important to note however, a weakness in this kind of analysis: quantifying flare duration for quickly moving flares will result in an artificially lower average duration, as flares which cross the entire field of view rapidly may persist for much longer, though only their time within the field of view can be counted. Average flare duration on compressed substrates in Table 5.2 should therefore be

treated as the bottom of a range, the flares' true average duration will not be lower than calculated average duration, but may in fact be much greater. For relatively slower species this problem is less severe, as fast-moving flares can move directly across the field of view in a short period of time.

B. subtilis (Fig. 5.5) and *B. cereus* (Fig. 5.6) behave similarly to *B. mycoides*; their flare speed, duration, and final displacement are all increased on compressed substrates, though unlike *B. mycoides*, these two species have characterized motility systems; they move with flagella[15,16]. *M. xanthus* (Fig. 5.7) also has a well-characterized motility system, as discussed previously, which does not involve flagella[17]. In *M. xanthus* the motor which is most relevant to the polymertropism response is the focal adhesion gliding motor[2,18-22]. It does not appear that one particular motility apparatus is more well-suited to the polymertropism response, the greatest fold increase in flare duration and displacement was observed in *M. xanthus*, while the greatest fold speed increase was observed in *B. subtilis* (Table 5.2). It is interesting to note that the fold increases measured in *B. cereus* and *B. mycoides* are nearly identical (Table 5.2), if *B. mycoides* is truly non-motile it seems unlikely that its spreading speed should be increased in the same fashion as a known flagellar species. *B. mycoides* colonies spread quickly, more rapidly than any other species we tested (Fig. 5.8), which is also surprising for a canonically non-motile species.

	Motility (slope)	Polymertropism (slope)
B. mycoides	0.0982	0.1190
B. subtilis	0.0092	-
B. cereus	0.0100	0.0139
M. xanthus	0.0150	0.0044

Table 5.3. Colony motility and polymertropism. Slope of the line of best fit for average colony diameter (Fig. 5.6) and aspect ratio over time (Fig. 5.7). Aspect ratio of *B. subtilis* colonies too widely varied for a good fit. This analysis was performed by David J. Lemon.

The change in the aspect ratio of the colony over time allows us to quantify the rate of the polymertropism response (Figure 5.9). *B. subtilis*' whole-colony response is highly variable (Fig. 5.9 B), and *B. cereus*' becomes increasingly so over time (Figure 5.9 C). *B. mycoides* (Fig. 5.9 A) and *M. xanthus* (Fig. 5.9 D) have relatively consistent responses, though *B. mycoides* spans the width of the plate after 36 hours. That *B. cereus* and *B. subtilis* have similar rates of motility (Fig. 5.8), but differ in their polymertropism responses is also interesting, as *B. cereus*' flares moved more than three times the as fast as *B. subtilis*' on uncompressed substrates (Table 5.3), which reinforces the notion that speed change alone is insufficient for producing the polymertropism response of elongated colonies. That changes in flare speed are not recapitulated at the whole-colony level suggests that polymertropism is an emergent behavior, and may vary wildly at differing temporal scales and cell number or concentration.

5.3 Materials & methods

Wild-type DK1622 *M. xanthus* grown at 30° in CTTYE broth containing 1% casitone, 0.2% yeast extract, 1mM KH_2PO_4, 10mM Tris-HCl (pH 8.0), and 8mM $MgSO_4$ or on plates containing CTTYE broth and 1.5% agar. Other species[23] were tested on both agar and κ-carrageenan gels, with nutrient media[24,25] that yielded the most pronounced polymertaxis response to compression by 5.56 mm diameter Tygon tubing, as indicated on Table 5.1. Additional species tested obtained as noted on Table 5.1. For this and all tests 5.56 mm diameter Tygon tubing was used for compressing the substrates.

Mixed culture assays were performed with single species cultures were adjusted to $1x10^5$ cells / mL and mixed together in the prescribed ratios immediately prior to being spotted

in 4 µL drops and incubated at 30°C. After 24 hours the cells were scraped up, resuspended, briefly sonicated, diluted, and spread onto a plate of 3% agar CTTYE broth for counting colonies 18 hours later.

For the response to substrate compression over time assays colony perimeters were marked 24 hours after inoculation and periodically until 72 hours after inoculation. From these perimeters colony width and height measured by hand. Aspect ratios were calculated by dividing colony width by colony height for each colony at each time point, these values for each colony at each time point were combined to generate an average aspect ratio for each combination of species and time. The slope of a line of best fit for each species' aspect ratio vs. time function could then be compared to the speed increase a species derives from the polymertaxis response calculated as described above.

Time-lapse videos were obtained with an Olympus CK2 inverted microscope with 3.0 megapixel AmScope USB ocular camera and Toupview image capture software. One image was captured each minute for 1440 minutes or until the field of view became overgrown. Flares were tracked using ImageJ's[26] Manual Tracking plug-in, from when they initially emerged from the bulk of the colony until they merged with another, merged with the colony, or moved off the screen. Tracking was done before any slices were removed from the videos to decrease file size for publishing, such that every 1 minute interval, or slice, was represented in the analysis. After tracking was completed X,Y values from the results table were exported to Excel for analysis.

Maximal values for X,Y for each given track were subtracted from the raw X,Y data and were multiplied by -1 as needed such that all flare trajectories reached their largest deflection from the X and Y axes in quadrant I and each flare started at 0,0, which we refer to as zeroed X,Y. The value of these zeroed X,Y for each slice number was averaged, which enabled comparison between average flare shape across conditions. Slice-to-slice distance was calculated for each pair of successive images, and averaged across all intervals for all tracks of each condition, to measure the average distance which a flare covered in one minute, which we refer to as speed. A similar calculation was performed when determining displacement, distance between 0,0 and the ultimate zeroed X,Y for the final location of each track was calculated for each track and averaged across all tracks for a given condition, which we refer to as displacement as shown in Figure 5.4.

5.4 References

1 Stanier, R. Y. A Note on Elasticotaxis in Myxobacteria. *J Bacteriol* **44**, 405 - 412 (1942).

2 Fontes, M. & Kaiser, D. Myxococcus cells respond to elastic forces in their substrate. *Proceedings of the National Academy of Sciences of the United States of America* **96**, 8052 - 8057 (1999).

3 Dworkin, M. Tactic behavior of *Myxococcus xanthus*. *J Bacteriol* **154**, 452 - 459 (1983).

4 Stratford, J. P., Woodley, M. A. & Park, S. Variation in the morphology of *Bacillus mycoides* due to applied force and substrate structure. *PloS one* **8**, e81549, doi:10.1371/journal.pone.0081549 (2013).

5 Polka, J. K. & Silver, P. A. Induced sensitivity of *Bacillus subtilis* colony morphology to mechanical media compression. *PeerJ* **2**, e597, doi:10.7717/peerj.597 (2014).

6 Hug, L. A. *et al.* A new view of the tree of life. *Nat Microbiol* **1**, 16048, doi:10.1038/nmicrobiol.2016.48 (2016).

7 Volfson, D., Cookson, S., Hasty, J. & Tsimring, L. S. Biomechanical ordering of dense cell populations. *Proceedings of the National Academy of Sciences of the United States of America* **105**, 15346-15351, doi:10.1073/pnas.0706805105 (2008).

8 Lushi, E., Wioland, H. & Goldstein, R. E. Fluid flows created by swimming bacteria drive self-organization in confined suspensions. *Proceedings of the National Academy of Sciences of the United States of America* **111**, 9733-9738, doi:10.1073/pnas.1405698111 (2014).

9 Ginelli, F., Peruani, F., Bar, M. & Chate, H. Large-scale collective properties of self-propelled rods. *Phys Rev Lett* **104**, 184502, doi:10.1103/PhysRevLett.104.184502 (2010).

10 Peshkov, A., Aranson, I. S., Bertin, E., Chate, H. & Ginelli, F. Nonlinear field equations for aligning self-propelled rods. *Phys Rev Lett* **109**, 268701, doi:10.1103/PhysRevLett.109.268701 (2012).

11 Janulevicius, A., van Loosdrecht, M. C., Simone, A. & Picioreanu, C. Cell flexibility affects the alignment of model myxobacteria. *Biophys J* **99**, 3129-3138, doi:10.1016/j.bpj.2010.08.075 (2010).

12 Abkenar, M., Marx, K., Auth, T. & Gompper, G. Collective behavior of penetrable self-propelled rods in two dimensions. *Phys Rev E Stat Nonlin Soft Matter Phys* **88**, 062314, doi:10.1103/PhysRevE.88.062314 (2013).

13 Gokhale, S. & Gore, J. Biophysics: Life in a jam. *Nature Physics* **12**, 726-727, doi:10.1038/nphys3777 (2016).

14 Yang, P. Wires on water. *Nature* **425**, 243 - 244 (2003).

15 Senesi, S. *et al.* Surface-Associated Flagellum Formation and Swarming Differentiation in *Bacillus subtilis* Are Controlled by the ifm Locus. *Journal of Bacteriology* **186**, 1158-1164, doi:10.1128/jb.186.4.1158-1164.2004 (2004).

16 Houry, A., Briandet, R., Aymerich, S. & Gohar, M. Involvement of motility and flagella in *Bacillus cereus* biofilm formation. *Microbiology* **156**, 1009-1018, doi:10.1099/mic.0.034827-0 (2010).

17 Shi, W. & Zusman, D. R. The two motility systems of *Myxococcus xanthus* show different selective advantages on various surfaces. *PNAS* **90**, 3378 - 3382 (1993).

18 Mignot, T. The elusive engine in *Myxococcus xanthus* gliding motility. *Cellular and molecular life sciences : CMLS* **64**, 2733-2745, doi:10.1007/s00018-007-7176-x (2007).

19 Mignot, T., Shaevitz, J. W., Hartzell, P. L. & Zusman, D. R. Evidence that focal adhesion complexes power bacterial gliding motility. *Science* **315**, 853-856, doi:10.1126/science.1137223 (2007).

20 Mauriello, E. M., Mignot, T., Yang, Z. & Zusman, D. R. Gliding motility revisited: how do the myxobacteria move without flagella? *Microbiology and molecular biology reviews : MMBR* **74**, 229-249, doi:10.1128/MMBR.00043-09 (2010).

21 Faure, L. *et al.* The mechanism of force transmission at bacterial focal adhesion complexes. *Nature* **539**, 530 - 535 (2016).

22 Islam, S. T. & Mignot, T. The mysterious nature of bacterial surface (gliding) motility: A focal adhesion-based mechanism in *Myxococcus xanthus*. *Semin Cell Dev Biol* **46**, 143-154, doi:10.1016/j.semcdb.2015.10.033 (2015).

23 Hou, S., Gu, H., Smith, C. & Ren, D. Microtopographic patterns affect *Escherichia coli* biofilm formation on poly(dimethylsiloxane) surfaces. *Langmuir* **27**, 2686-2691, doi:10.1021/la1046194 (2011).

24 Agarwal, S., JHunnicutt, D. W. & McBride, M. J. Cloning and characterization of the *Flavobacterium johnsoniae* gliding motility gene gldA. *Proceedings of the National Academy of Sciences of the United States of America* **94** (1997).

25 Sperandio, V., Toggers, A. G. & Kaper, J. B. Quorum sensing *Escherichia coli* regulators B and C (QseBC): a novel two-component regulatory system involved in the regulation of flagella and motility by quorum sensing in E. coli. *Molecular microbiology* **43** (2002).

26 ImageJ (U. S. National Institutes of Health, Bethesda, Maryland, USA, 1997-2016).

Chapter 6 - Implications for bacterial behavior and organization

6.1 Possible mechanism

In *M. xanthus* it is known that Adventurous (A) motility is required for the polymertropism response[1]. From the results presented and discussed in previous sections we now know that during its response to compression-induced alignment of polymers *M. xanthus* flares move faster and in a different overall direction during this polymertropism response than do flares on uncompressed and unaligned substrates (Figure 5.7, Table 5.2). These effects should be unpacked separately.

Perhaps *M. xanthus* flares move more rapidly on compressed, aligned substrates because their motility apparatus is somehow more efficient. This seems plausible, as nutrient content is held constant between compressed and uncompressed substrates during these experiments, and previous work has shown *M. xanthus* motility to be sensitive to physical changes in the substrate, especially stiffness[2-5]. As stiffness in agar/agarose gels is principally a function of the concentration of agarose polymers[6-8], cells are known to be sensitive to changes in stiffness, and compression likely causes an increase in polymer packing, it seems logical then that this increase in polymer packing may be related to the increased speed. If focal adhesion complexes are more or more stable on stiffer substrates, which has been reported, or if the focal adhesions generally form or stabilize at locations of relatively high local polymer density, perhaps then their number, effectiveness, or stability is enhanced on the tightly packed polymers present during the polymertropism response. In this case the packing of the

polymers would be responsible for the speed increase, could the orientation of their alignment give rise to the changes in flare behavior we have observed?

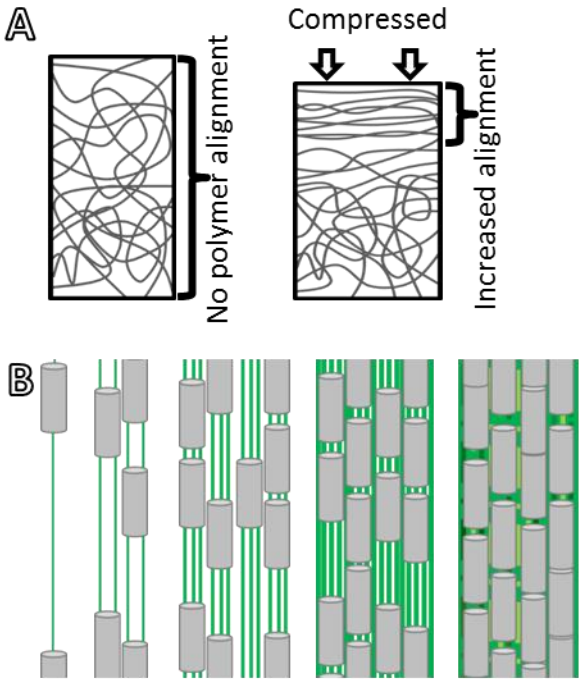

Figure 6.1. Strain-induced alignment and slime trail following lead to aggregation. Initially random, unaligned polymers become relatively aligned due to compression of the gel shown in A. Cells (grey) lay down slime trails (green) which induce other cells to follow the same path, reinforcing the trail shown in B. Over time (left to right in B) this feed-forward loop leads to increased cell density and alignment.

If, as demonstrated earlier, we assume that the alignment of polymers is indeed increased due to compression, and this alignment is perpendicular to the axis of compression, then both the polymers which prompt the polymertropism response and the cells which are undergoing it are both aligned perpendicular to the axis of compression. If we again think of the focal adhesion complexes which link the cell to its underlying substrate[2,3,9,10], it may be the case that these focal adhesions are better able to push off against and move along the long axes of these polymers, rather than across them. This would be somewhat akin to climbing along a rope rather than climbing across a net of them.

If a given input on the focal adhesion complex gives a greater return on a network of aligned polymers in one direction than another, and these complexes tend to form where polymers or groups of polymers are relatively highly packed, this may explain how the first cells

to respond to polymer alignment alter their orientation and motility; purely through the physical interaction with their substrate. These cells then will lay down slime trails, which will reinforce the change in direction, influencing later cells to follow their lead (Figure 6.1).

6.1.1 Adventurous motility

Previous work has shown that, in general, A motiliy is required for polymertropism[1]. In collaboration with the Tâm Mignot lab in Marseilles, France, we have tested mutants defective for single genes in the putative focal adhesion complex. Preliminary results show that each protein in the focal adhesion core[3] is required for polymertropism, a complete and functional AglRQS motor complex to power the movement of these focal adhesions down the length of the cell is required, and every other component protein, with the possible exception of AglH, is necessary for the polymertropism response.

6.1.2 Screening knock-out mutants

In addition to the mutants defective for portions of the A motility apparatus described above, we also tested a handful of genes known to be important to early biofilm development[11-13] (Figure 6.2). While these results did not reveal any fully defective mutants, the techniques involved in such a screen are easily scalable, and though a purely physical mechanism for polymertropism may make a larger scale screen unnecessary the techniques involved are readily scalable. Future screens for genetic mutants defective for polymertropism should focus on loci related to motility, especially the focal adhesion complex, slime production and secretion, stretch-sensitive ion channels which may help the cell perceive its physical surroundings, and signal transduction pathways which may leverage the polymertropism

response or be involved in pathways most relevant to the portions of the *M. xanthus* lifecycle most relevant (especially early development and fruiting body formation). While a purely physical model for polymertropism may eliminate the need for a biological feedback loop to sense and respond to aligned polymers, that is not to say that the cells' biological processes may not have evolved to leverage this response in some way.

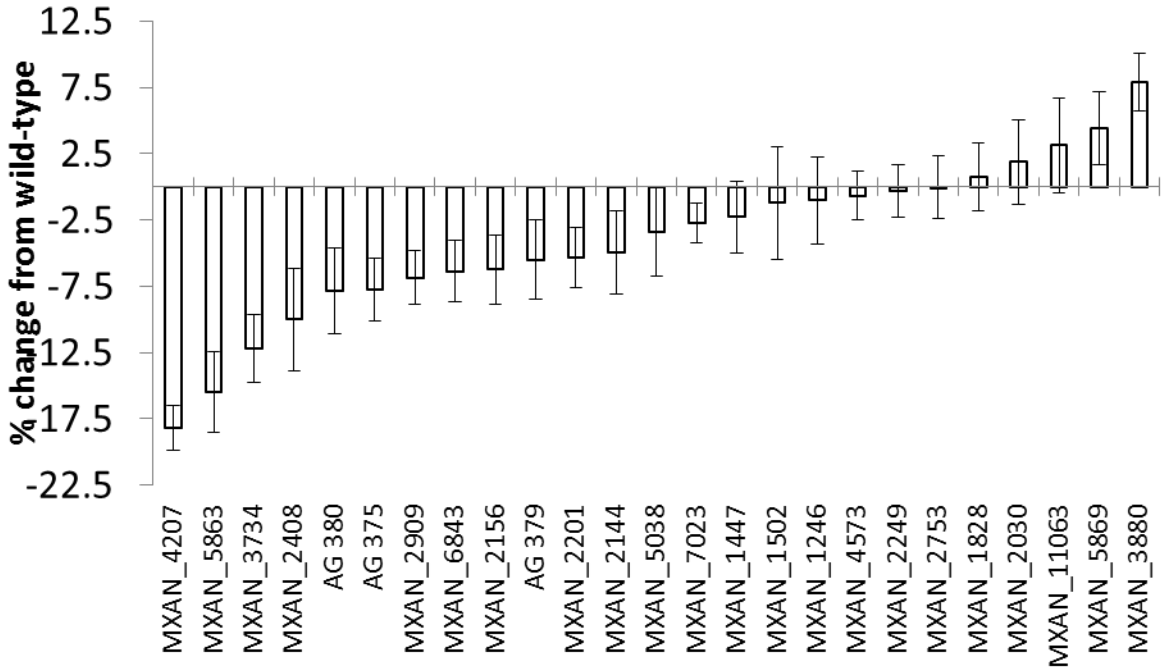

Figure 6.2. Polymertropism defects in *M. xanthus* mutants. A handful of *M. xanthus* single gene mutants were screened for defects in polymertropism and their % difference in average aspect ratio from wild-type graphed ±S.E.M. (n = 3-6). The genes targeted were genes known to be involved in early development and gene expression regulation. This experiment was performed by David J. Lemon.

6.2 Proposed model for polymertropism

On uncompressed, randomly oriented substrates the initial movements of cells will leave behind slime trails as discussed previously[14,15]. These slime trails, being composed of polysaccharides and extruded through relatively small nozzles in the cell's surface[16-18], may be themselves composed of aligned polymers. In this case, initially random movements of cells

will form the characteristics patterns observed in denser swarms of *M. xanthus* cells through slime trail following alone[14] by way of polymertropism. This effect would be reinforced over time, as additional cells following existing slime trails will continue to deposit slime along these trails in a feedforward loop. This condition may be even more pronounced on polymer substrates which are already aligned, as compressed gels are, which may explain the anisotropic colony spreading patterns characteristic of the polymertropism response; underlying aligned polymers with aligned slime trails on their surface may be elicit the most potent polymertropism response, but the aligned polymers found in nature as slime trails also have effects on cell and flare behavior[14,19].

6.3 What these results mean for *M. xanthus* and microbiology

6.3.1 Early biofilm development

The response to aligned polymers can sufficiently explain bacterial cells' tendency toward following slime trails deposited by cells which have moved over an area before them without a need for a biochemical, diffusible signal[14,17,20-22]. At the earliest stages of biofilm formation, when a small number of cells are dispersed and distant from each other, the polymertropism response to aligned polysaccharide slime trails will help cells find each other (Figure 6.1). Encountering a slime trail oriented perpendicular to a cell's present direction represents a 50% chance to head toward the cell which deposited that trail if it is followed. This could explain how dispersed cells aggregate initially before diffusible gradients of biochemical, rather than physical, signals can spread or indeed even be produced. The purely physical nature of the polymertropism response to slime trail following may also explain why there has

been considerable difficulty in identifying a biological signal in *Pseudomonas aeruginosa* slime[20]; it may be a physical signal rather than a biological one.

6.3.2 Aggregation and fruiting body development

The same processes described above may also enable cells in a loosely organized biofilm find common centers to initiate fruiting body formation during development or starvation[23-26]. By working in concert with diffusible gradients emanating from these highly dense fruiting bodies, slime trail following through polymertropism will cause the initial trickle of cells into or toward a common center to become a flood. The cells nearest to a fruiting body can be drawn into it in response to biological or physical signals, which will feedforward, again reinforcing the effect as cells even further away follow the diffusible gradient or slime trails toward the fruiting body, over and over again until fruiting body locations become static and development ceases. This dovetails nicely with the observation that slime trails alone are sufficient to induce organization in *M. xanthus*[14] and with a coarsening model that predicts large fruiting bodies will grow at the expense of smaller nearby fruiting bodies[27].

6.3.3 Clinical & eukaryotic microbiology

Motile eukaryotic cells should be investigated for responses to aligned polymers, as they have previously been shown to actively cause said alignment[28-31], communicate through the substrate[28,32-35], are sensitive to changes in the stiffness and orientation of the substrate[36-43], and substrate alignment has been implicated in disease progression[44-46]. Additionally, it may be possible, if these cells do have some response to substrate alignment as predicted, to leverage this response to induce cells into alignment, culture tissues with appropriate mechanical

properties for grafting, or guide cells into 3D scaffolds for implantation. Physical models of focal adhesion stability and force transduction, experimental observation that motile mammalian cells are sensitive to changes in the concentration of polymers (durotaxis), and simulations which suggest actively moving cells can pull their substrates into alignment, possibly even use this to communicate with their distant neighbors all point to a plausible likelihood that motile mammalian cells may also respond to alignment of their substrate's component polymers.

Perhaps the simplest example of a clinical application that may be possible through greater understanding of the biological response to aligned polymers is an improvement to the indwelling urinary catheter. These catheters are problematic, as they are associated with a staggering number of hospital-acquired infections[47] due to the infiltration of bacteria from outside the body to the inside via the catheter's lumen. There is a presently understood need for improvements in catheter design[48], perhaps the extrusion process of manufacturing or the tensile strain on an indwelling catheter causes its component polymers to become relatively aligned, which could present a metaphorical highway into the body to any bacterial species which could leverage this polymer arrangement. Indeed *Proteus mirabilis*, a common cause of complicated urinary tract infections[49], does respond to polymer alignment (Table 5.1). Perhaps a subtle change to the manufacturing process, for example adding an element of rotation to the extrusion process so that the polymers of the catheter form a helical screw rather than a straight line, can dramatically slow down the species' advance through the catheter and reduce nosocomial infections. That the production of slime is also known to be related to the emergence of pathogenicity[50,51] and the previously discussed importance of polymertropism to

interactions between bacterial cells and slime or slime trails also lends credence to the notion that there may be clinical relevance to understanding the polymertropism response.

Taken together, these results and their potential application to both prokaryotic and eukaryotic microbiology should encourage future study of physical interactions between cells and substrates, especially on substrates which have been aligned due to compression. Compression of hydrogels, as described in this work, represents an inexpensive, easy, and fast way to produce aligned polymer substrates, and the biological responses these substrates elicit from the cells moving on their surfaces may well be leveraged in novel ways to examine even more complex or relevant behaviors going forward.

6.4 Materials & methods

4 µL drops of *M. xanthus* liquid culture at 10^5 cells/mL were spotted on 1.5% agar CTTYE media compressed with 5.56 mm diameter Tygon tubing as described previously. After 24 hours aspect ratios were calculated for mutants and wild-type colonies, average aspect ratio ± S.E.M. presented as a percentage of comparable values for wild-type colonies.

Gene-deletion mutants from the Tâm Mignot lab were grown overnight and inoculated onto compressed agar media as described above. Colony perimeters were marked every 24 hours for 120 hours. Mutants with average aspect ratios which increased linearly over time, as wild-type does, were classified as polymertropism positive, while mutants with aspect ratio vs. time graphs that did not increase were categorized as defective.

6.5 References

1 Fontes, M. & Kaiser, D. Myxococcus cells respond to elastic forces in their substrate. *Proceedings of the National Academy of Sciences of the United States of America* **96**, 8052 - 8057 (1999).

2 Faure, L. *et al.* The mechanism of force transmission at bacterial focal adhesion complexes. *Nature* **539**, 530 - 535 (2016).

3 Islam, S. T. & Mignot, T. The mysterious nature of bacterial surface (gliding) motility: A focal adhesion-based mechanism in *Myxococcus xanthus*. *Semin Cell Dev Biol* **46**, 143-154, doi:10.1016/j.semcdb.2015.10.033 (2015).

4 Guegan, C. *et al.* Alteration of bacterial adhesion induced by the substrate stiffness. *Colloids Surf B Biointerfaces* **114**, 193-200, doi:10.1016/j.colsurfb.2013.10.010 (2014).

5 Song, F., Koo, H. & Ren, D. Effects of Material Properties on Bacterial Adhesion and Biofilm Formation. *Oral Biology & Medicine* **94**, 1027 - 1034 (2015).

6 Arnott, S., Fulmer, A. & Scott, W. E. The agarose double helix and its function in agarose gel structure. *J. Mol. Biol.* **90**, 269-284 (1974).

7 Roberts, J. J., Earnshaw, A., Ferguson, V. L. & Bryant, S. J. Comparative study of the viscoelastic mechanical behavior of agarose and poly(ethylene glycol) hydrogels. *J Biomed Mater Res B Appl Biomater* **99**, 158-169, doi:10.1002/jbm.b.31883 (2011).

8 Nayar, V. T., Weiland, J. D., Nelson, C. S. & Hodge, A. M. Elastic and viscoelastic characterization of agar. *J Mech Behav Biomed Mater* **7**, 60-68, doi:10.1016/j.jmbbm.2011.05.027 (2012).

9 Mignot, T., Shaevitz, J. W., Hartzell, P. L. & Zusman, D. R. Evidence that focal adhesion complexes power bacterial gliding motility. *Science* **315**, 853-856, doi:10.1126/science.1137223 (2007).

10 Shi, W. & Lux, R. Focal adhesion: getting a grasp on myxobacterial gliding. *Nat Chem Biol* **3**, 205 - 206 (2007).

11 Giglio, K. M., Caberoy, N., Suen, G., Kaiser, D. & Garza, A. G. A cascade of coregulating enhancer binding proteins initiates and propagates a multicellular developmental program. *Proceedings of the National Academy of Sciences of the United States of America* **108**, E431-439, doi:10.1073/pnas.1105876108 (2011).

12 Giglio, K. M., Zhu, C., Klunder, C., Kummer, S. & Garza, A. G. The enhancer binding protein Nla6 regulates developmental genes that are important for *Myxococcus xanthus* sporulation. *J Bacteriol* **197**, 1276-1287, doi:10.1128/JB.02408-14 (2015).

13 Caberoy, N. B., Welch, R. D., Jakobsen, J. S., Slater, S. C. & Garza, A. G. Global Mutational Analysis of NtrC-Like Activators in *Myxococcus xanthus*: Identifying Activator Mutants Defective for Motility and Fruiting Body Development. *Journal of Bacteriology* **185**, 6083-6094, doi:10.1128/jb.185.20.6083-6094.2003 (2003).

14 Balagam, R. & Igoshin, O. A. Mechanism for Collective Cell Alignment in *Myxococcus xanthus* Bacteria. *PLoS computational biology* **11**, e1004474, doi:10.1371/journal.pcbi.1004474 (2015).

15 Ducret, A., Valignant, M.-P., Mouhamar, F., Mignot, T. & Theodoly, O. Wet-surface-enhanced ellipsometric contrast microscopy identifies slime as a major adhesion factor during bacterial surface motility. *PNAS* **199** (2012).

16 Koch, M. K. & Hoiczyk, E. Characterization of myxobacterial A-motility: insights from microcinematographic observations. *J Basic Microbiol* **53**, 785-791, doi:10.1002/jobm.201200307 (2013).

17 Yu, R. & Kaiser, D. Gliding motility and polarized slime secretion. *Molecular microbiology* **63**, 454-467, doi:10.1111/j.1365-2958.2006.05536.x (2007).

18 Nan, B. & Zusman, D. R. Uncovering the mystery of gliding motility in the myxobacteria. *Annual review of genetics* **45**, 21-39, doi:10.1146/annurev-genet-110410-132547 (2011).

19 Burchard, R. P. Trail following by gliding bacteria. *J Bacteriol* **152**, 495 - 501 (1982).

20 Zhao, K. *et al.* Psl trails guide exploration and microcolony formation in *Pseudomonas aeruginosa* biofilms. *Nature* **497**, 388-391, doi:10.1038/nature12155 (2013).

21 Gelimson, A. *et al.* Multicellular Self-Organization of *P. aeruginosa* due to Interactions with Secreted Trails. *Phys Rev Lett* **117**, 178102, doi:10.1103/PhysRevLett.117.178102 (2016).

22 Starruss, J. *et al.* Pattern-formation mechanisms in motility mutants of Myxococcus xanthus. *Interface Focus* **2**, 774-785, doi:10.1098/rsfs.2012.0034 (2012).

23 Smith, B. A. & Dworkin, M. Adenylate Energy Charge During Fruiting Body Formation by *Myxococcus xanthus*. *Journal of Bacteriology* **142**, 1007 - 1009 (1980).

24 Skotnicka, D. *et al.* A Minimal Threshold of c-di-GMP Is Essential for Fruiting Body Formation and Sporulation in *Myxococcus xanthus*. *PLoS Genet* **12**, e1006080, doi:10.1371/journal.pgen.1006080 (2016).

25 Sozinova, O., Jiang, Y., Kaiser, D. & Alber, M. A three-dimensional model of myxobacterial fruiting-body formation. *Proceedings of the National Academy of Sciences*

of the United States of America **103**, 17255-17259, doi:10.1073/pnas.0605555103 (2006).

26 Sozinova, O., Jiang, Y., Kaiser, D. & Alber, M. A three-dimensional model of myxobacterial aggregation by contact-mediated interactions. *Proceedings of the National Academy of Sciences of the United States of America* **102**, 11308-11312, doi:10.1073/pnas.0504259102 (2005).

27 Bahar, F., Pratt-Szeliga, P. C., Angus, S., Guo, J. & Welch, R. D. Describing *Myxococcus xanthus* aggregation using Ostwald ripening equations for thin liquid films. *Sci Rep* **4**, 6376, doi:10.1038/srep06376 (2014).

28 Wang, H., Abhilash, A. S., Chen, C. S., Wells, R. G. & Shenoy, V. B. Long-range force transmission in fibrous matrices enabled by tension-driven alignment of fibers. *Biophys J* **107**, 2592-2603, doi:10.1016/j.bpj.2014.09.044 (2014).

29 Angelini, T. E., Hannezo, E., Trepat, X., Fredberg, J. J. & Weitz, D. A. Cell migration driven by cooperative substrate deformation patterns. *Phys Rev Lett* **104**, 168104, doi:10.1103/PhysRevLett.104.168104 (2010).

30 Feng, Z. *et al.* Analysis of the contraction of fibroblast collagen gels and the traction force of individual cells by a novel elementary structural model. *35th Annual International Conference of the IEEE EMBS*, 6232-6235 (2013).

31 Harris, A. K., Stopak, D. & Wild, P. Fibroblast traction as a mechanism for collagen morphogenesis. *Nature* **290**, 249-251 (1981).

32 Ma, X. *et al.* Fibers in the extracellular matrix enable long-range stress transmission between cells. *Biophys J* **104**, 1410-1418, doi:10.1016/j.bpj.2013.02.017 (2013).

33 Winer, J. P., Oake, S. & Janmey, P. A. Non-linear elasticity of extracellular matrices enables contractile cells to communicate local position and orientation. *PloS one* **4**, e6382, doi:10.1371/journal.pone.0006382 (2009).

34 Reinhart-King, C. A., Dembo, M. & Hammer, D. A. Cell-cell mechanical communication through compliant substrates. *Biophys J* **95**, 6044-6051, doi:10.1529/biophysj.107.127662 (2008).

35 Rudnicki, M. S. *et al.* Nonlinear strain stiffening is not sufficient to explain how far cells can feel on fibrous protein gels. *Biophys J* **105**, 11-20, doi:10.1016/j.bpj.2013.05.032 (2013).

36 Harland, B., Walcott, S. & Sun, S. X. Adhesion dynamics and durotaxis in migrating cells. *Physical biology* **8**, 015011, doi:10.1088/1478-3975/8/1/015011 (2011).

37 Lazopoulos, K. A. & Stamenovic, D. Durotaxis as an elastic stability phenomenon. *Journal of biomechanics* **41**, 1289-1294, doi:10.1016/j.jbiomech.2008.01.008 (2008).

38 Previtera, M. L., Langhammer, C. G. & Firestein, B. L. Effects of substrate stiffness and cell density on primary hippocampal cultures. *J Biosci Bioeng* **110**, 459-470, doi:10.1016/j.jbiosc.2010.04.004 (2010).

39 Leong, W. S. *et al.* Thickness sensing of hMSCs on collagen gel directs stem cell fate. *Biochem Biophys Res Commun* **401**, 287-292, doi:10.1016/j.bbrc.2010.09.052 (2010).

40 Pelham, R. J. & Wang, Y. Cell locomotion and focal adhesions are regulated by substrate flexibility. *Proceedings of the National Academy of Sciences of the United States of America* **94**, 13661 - 13665 (1997).

41 Previtera, M. L., Langhammer, C. G., Langrana, N. A. & Firestein, B. L. Regulation of dendrite arborization by substrate stiffness is mediated by glutamate receptors. *Ann Biomed Eng* **38**, 3733 - 3743 (2010).

42 Parida, L. & Padmanabhan, V. Durotaxis in Nematode *Caenorhabditis elegans*. *Biophys J* **111**, 666-674, doi:10.1016/j.bpj.2016.06.030 (2016).

43 Lo, C.-M., Wang, H.-B., Dembo, M. & Wang, Y. Cell Movement is Guided by the Rigidity of the Substrate. *Biophys J* **79**, 144 - 152 (2000).

44 Matsugaki, A., Isobe, Y., Saku, T. & Nakano, T. Quantitative regulation of bone-mimetic, oriented collagen/apatite matrix structure depends on the degree of osteoblast alignment on oriented collagen substrates. *Journal of biomedical materials research. Part A* **103**, 489-499, doi:10.1002/jbm.a.35189 (2015).

45 Tzlil, S. & Tirrell, D. A. Strain propagation in artificial extracellular matrix proteins can accelerate cell spreading and polarization. *Soft Matter* **9**, 5602, doi:10.1039/c3sm27137d (2013).

46 Conklin, M. W. *et al.* Aligned collagen is a prognostic signature for survival in human breast carcinoma. *Am J Pathol* **178**, 1221-1232, doi:10.1016/j.ajpath.2010.11.076 (2011).

47 Nicolle, L. E. Catheter associated urinary tract infections. *Antimicrobial Resistance & Infection Control* **3** (2014).

48 Pascual, A. Pathogenesis of catheter-related infections: lessons for new designs. *Clin Microbiol Infect* **8**, 256 - 264 (2002).

49 Chen, C.-Y. *et al. Proteus mirabilis* urinary tract infection and bacteremia: Risk factors, clinical presentation, and outcomes. *Journal of Microbiology, Immunology, and Infection* **45**, 228 - 236 (2012).

50 Ishak, M. A., Groschel, D. H. M., Mandell, G. L. & Wenzel, R. P. Association of Slime with Pathogenicity of Coagulase-Negative Saphylococci Causing Nosocomial Septicemia. *Journal of Clinical Microbiology* **22**, 1025 - 1029 (1985).

51 Christensen, G. D., Simpson, W. A., Bisno, A. L. & Beachey, E. H. Adherence of Slime-Producing Strains of *Staphylococcus epidermis* to Smooth Surfaces. *Infection and Immunity* **37**, 318 - 326 (1982).

VITA

David James Lemon was born in Rochester NY, and in 2006 graduated from McQuaid Jesuit High School there. After high school he attended Saint Joseph's University in Philadelphia PA and earned his Bachelor of Science degree in Biology before moving on to Rutgers, The State University of New Jersey in Camden NJ. At Rutgers he worked in Dr. Nir Yakoby's *D. melanogaster* lab, studying the role of *division abnormally delayed* (*dally*) on bone morphogenetic protein signaling in the developing fruit fly eggshell and was awarded Thesis with Distinction upon defense of thesis "The glypican Dally is a target and mediator of BMP signaling in eggshell patterning" for his Master of Science degree in Biology. In August 2012 he matriculated into the Department of Biology at Syracuse University in the inaugural cohort of SU's interdisciplinary National Science Foundation's Integrative Graduate Education and Research Traineeship Program in Soft Interfaces, was a University Fellow in the Department of Biology, a member of Dr. Anthony Garza's *M. xanthus* microbiology lab, and was awarded his Doctor of Philosophy in Biology in the summer of 2017.